Inverse Problems and the Nonlinear Fourier Transform

Samuli Siltanen

Department of Mathematics and Statistics
University of Helsinki, Finland
samuli.siltanen@helsinki.fi
www.siltanen-research.net

Finnish Mathematical Society
Mathematical Days 2020
Oulu, Finland, January 3, 2020

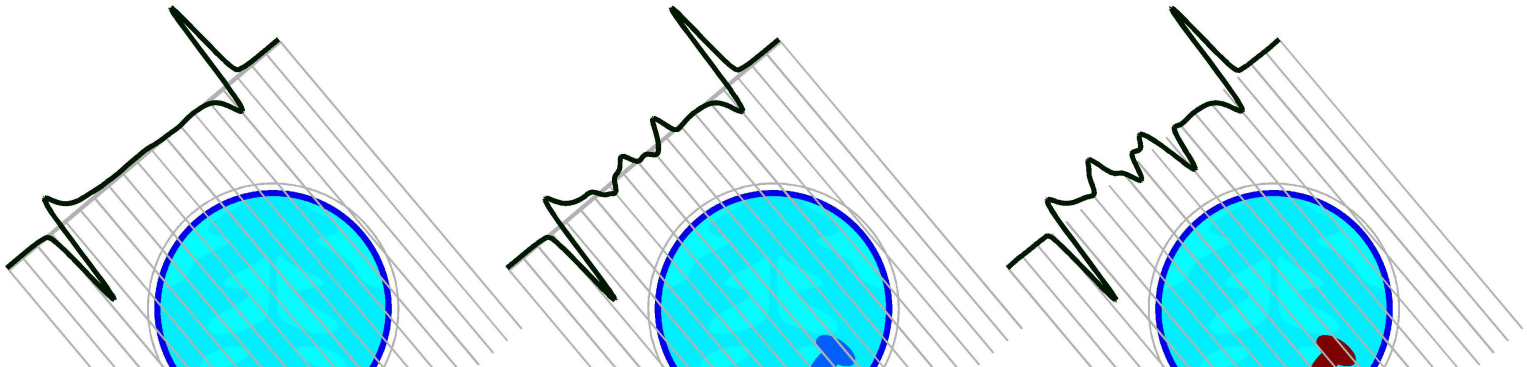

Finnish Centre of Excellence in Inverse Modelling and Imaging

2018-2025

ACADEMY OF FINLAND

OULUN YLIOPISTO / UNIVERSITY of OULU

UNIVERSITY OF EASTERN FINLAND

LUT University

UNIVERSITY OF JYVÄSKYLÄ

UNIVERSITY OF HELSINKI

TAMPERE UNIVERSITY OF TECHNOLOGY

FINNISH METEOROLOGICAL INSTITUTE

Aalto University

Samun tiedekanava

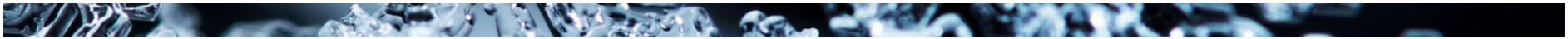

Samun tiedekanava

2.63K subscribers

CUSTOMIZE CHANNEL | YOUTUBE STUDIO

HOME | VIDEOS | PLAYLISTS | COMMUNITY | CHANNELS | ABOUT

Uploads PLAY ALL

SORT BY

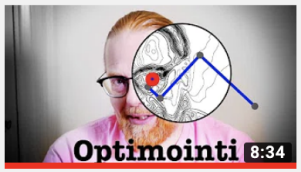

Samun tiedepläjäys: Optimointi

623 views • 2 weeks ago

CC

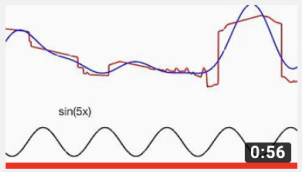

Illustration of Fourier series

689 views • 1 month ago

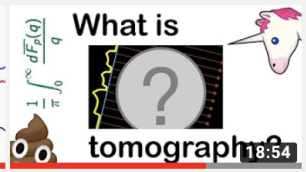

What is tomography?

1K views • 1 month ago

CC

Matematiikan ihmeitä: Gaussin kellokäyrä

1.2K views • 2 months ago

CC

Voimistelun fysiikkaa

1.3K views • 2 months ago

Introduction to inversion 1: the instability of predicting...

970 views • 3 months ago

CC

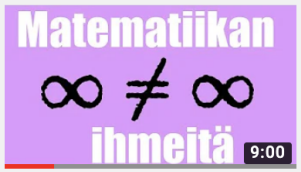

Wonders of mathematics:

Microphotography

Kirjani "Astu matematiikan

Kukkaravukki

Harvestman's adventures in

Ampiainen syö muroa

SAMULI SILTANEN

ASTU MATEMATIIKAN MAAILMAAN

MATEMATIIKKA ON KAUNISTA JA KUULUU KAIKILLE!

OTAVA

Outline

Electrical impedance tomography is useful for medical chest imaging

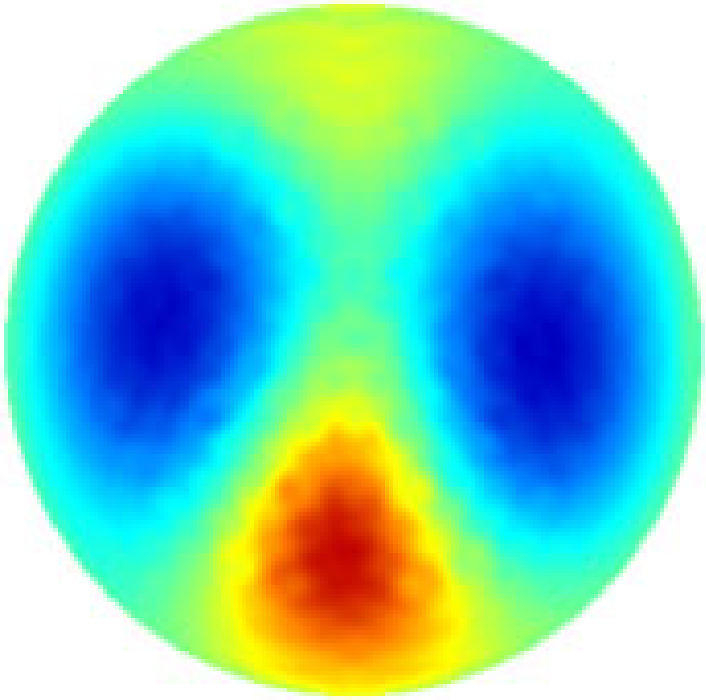

Lungs filled with air are resistive, shown as blue.

Blood in the heart appears red, as it is more conductive than air.

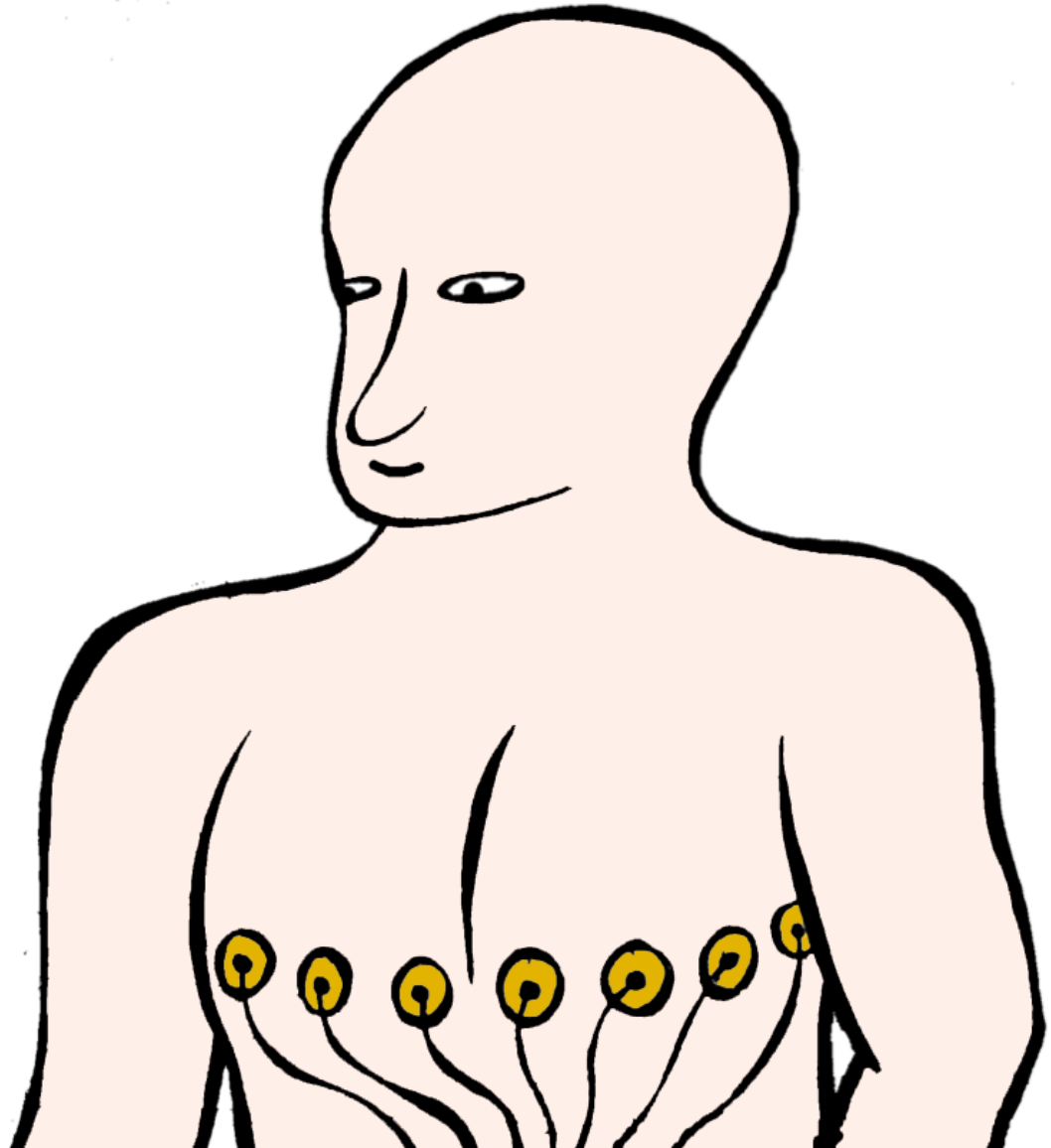

Note that EIT data collection involves applying several current patterns

Saline and agar phantom

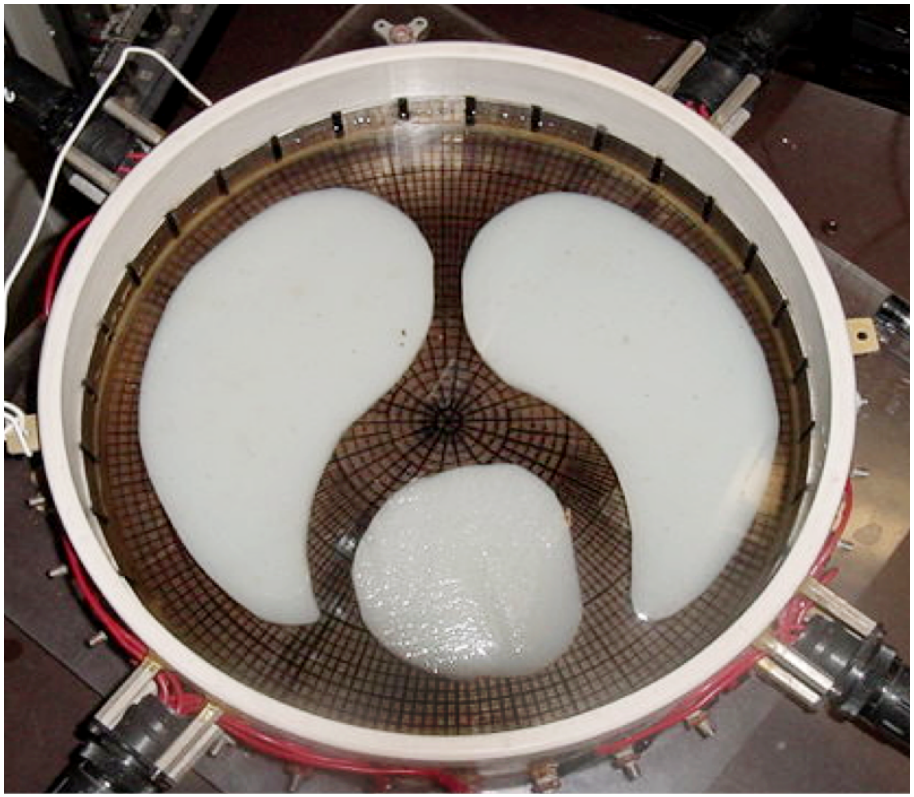

Phantom and data: Jon Newell, Rensselaer Polytechnic Institute

Apply current pattern $\cos\theta$

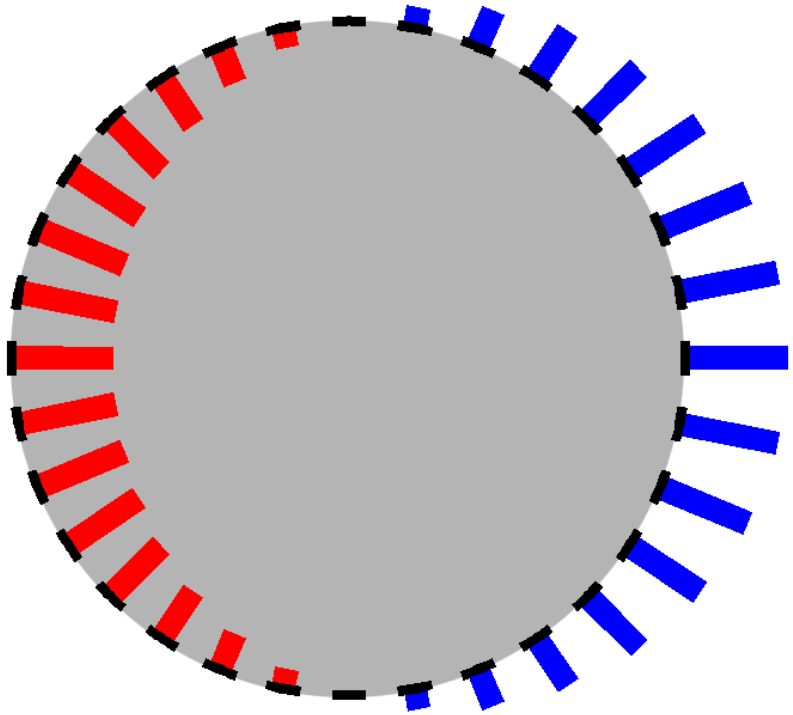

Measure the resulting voltages at all 32 electrodes

Note that EIT data collection involves applying several current patterns

Saline and agar phantom

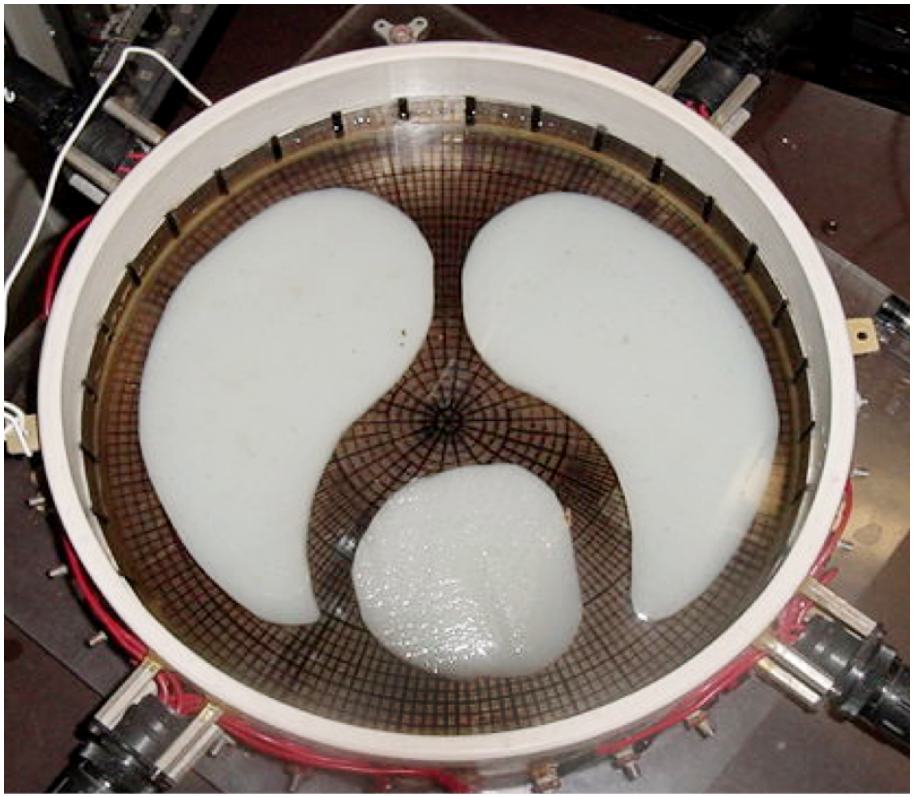

Phantom and data: Jon Newell, Rensselaer Polytechnic Institute

Apply current pattern $\cos 2\theta$

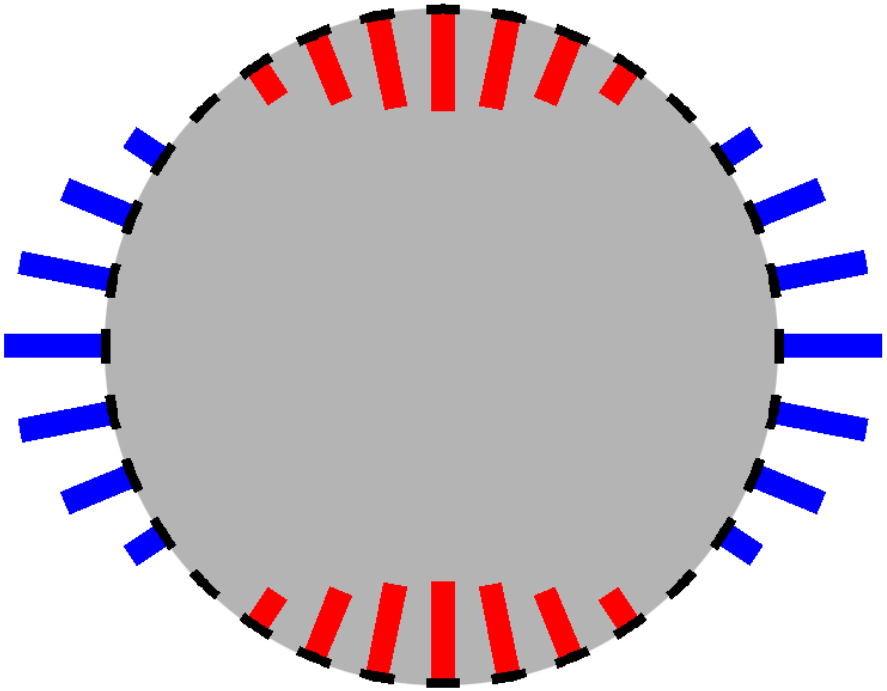

Measure the resulting voltages at all 32 electrodes

Note that EIT data collection involves applying several current patterns

Saline and agar phantom

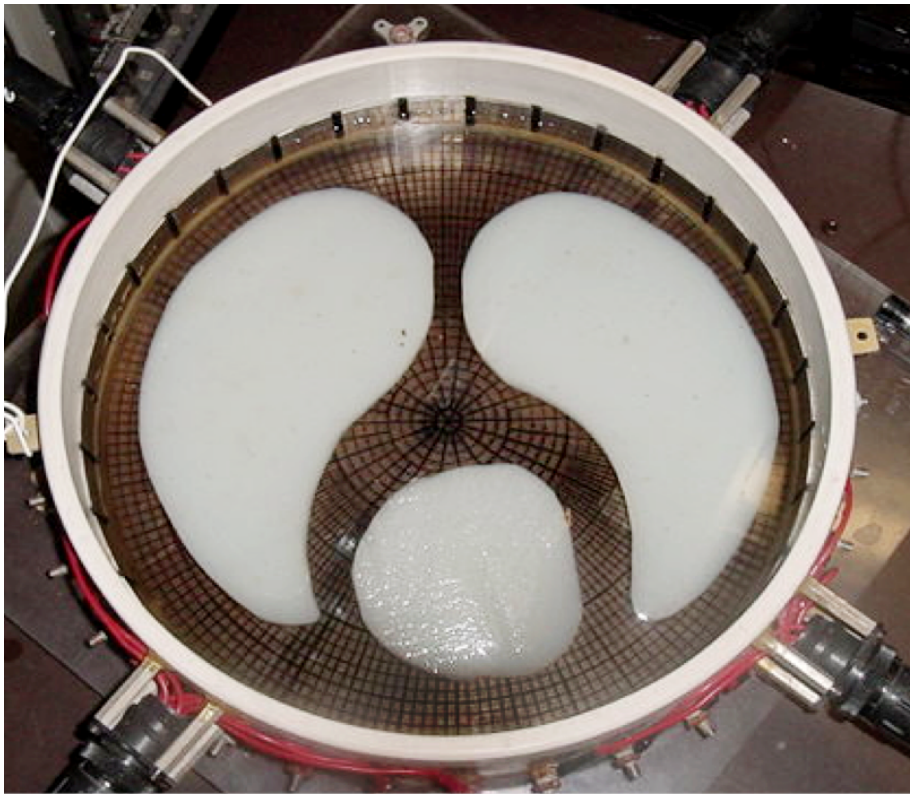

Phantom and data: Jon Newell, Rensselaer Polytechnic Institute

Apply current pattern $\cos 3\theta$

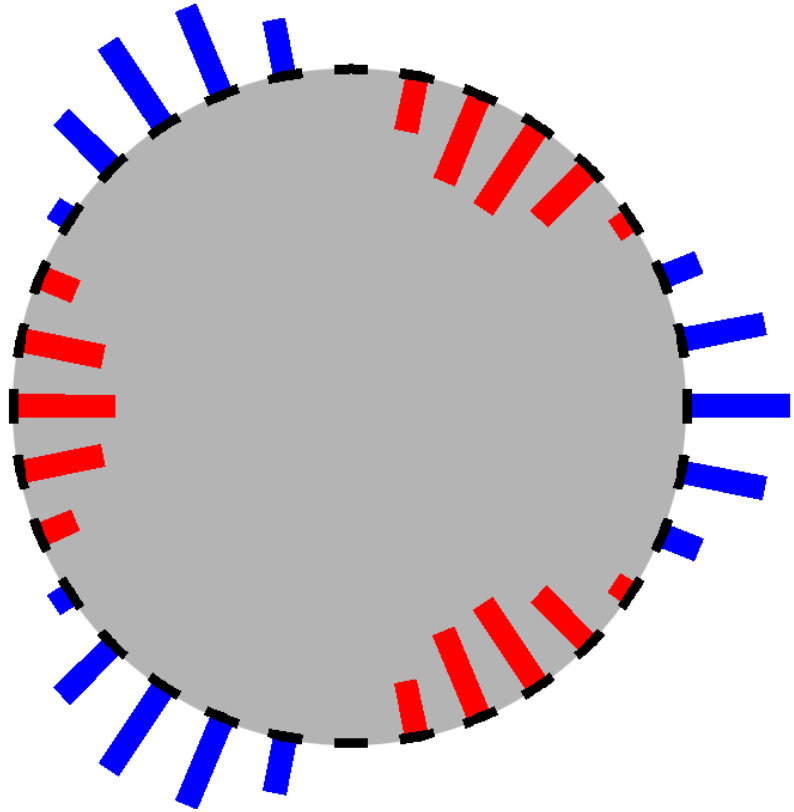

Measure the resulting voltages at all 32 electrodes

Note that EIT data collection involves applying several current patterns

Saline and agar phantom

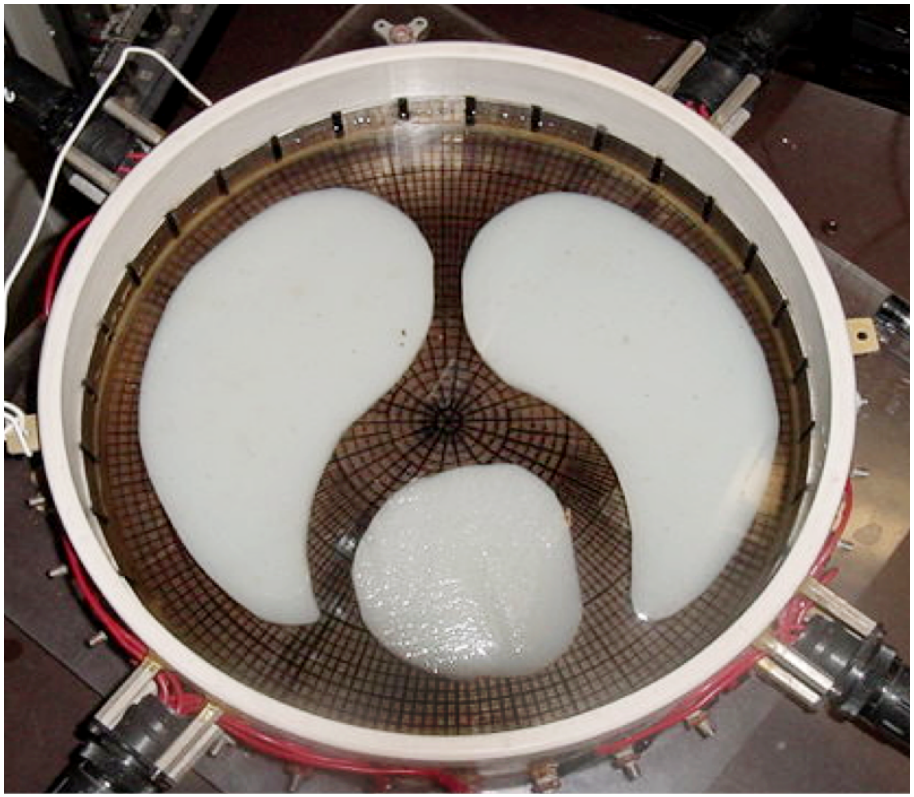

Phantom and data: Jon Newell, Rensselaer Polytechnic Institute

Apply current pattern $\cos 4\theta$

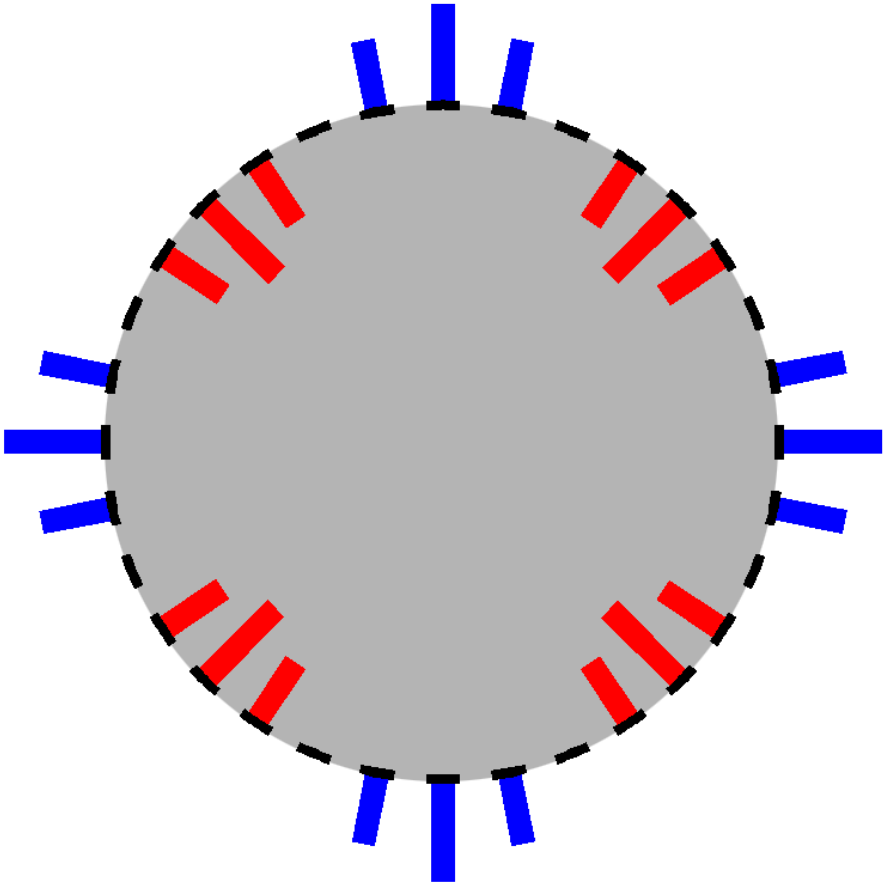

Measure the resulting voltages at all 32 electrodes

Note that EIT data collection involves applying several current patterns

Saline and agar phantom

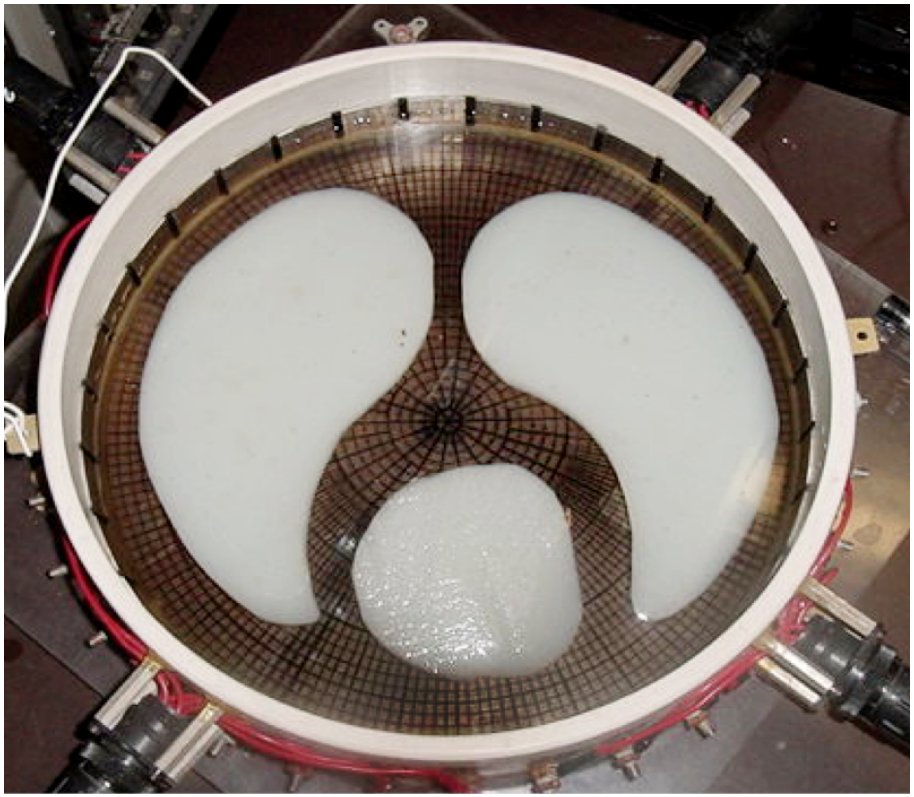

Phantom and data: Jon Newell, Rensselaer Polytechnic Institute

Apply current pattern $\cos 5\theta$

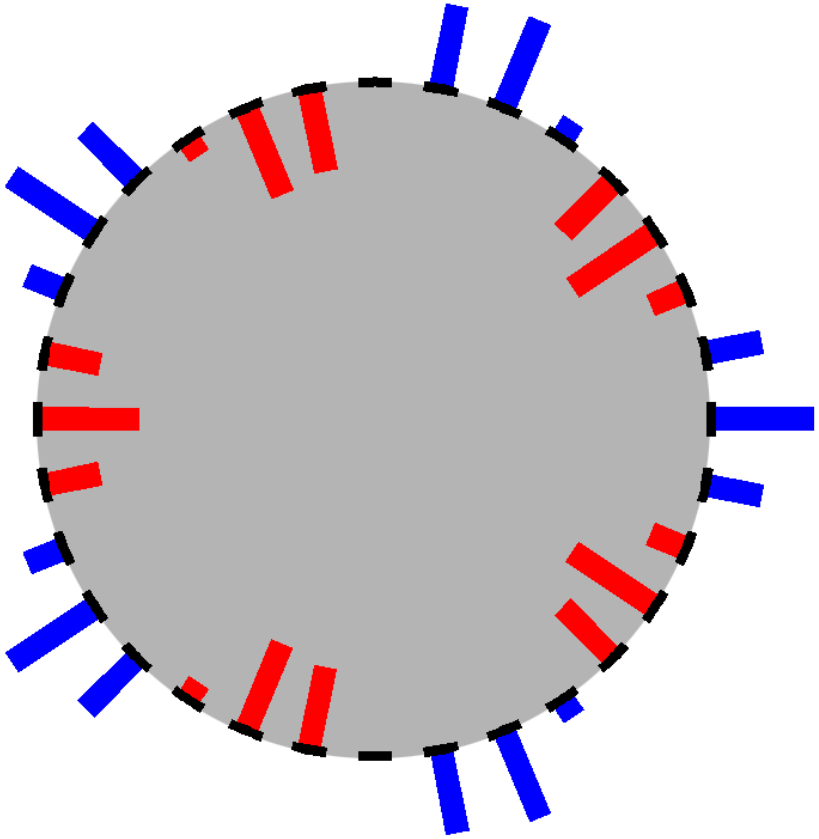

Measure the resulting voltages at all 32 electrodes

Note that EIT data collection involves applying several current patterns

Saline and agar phantom

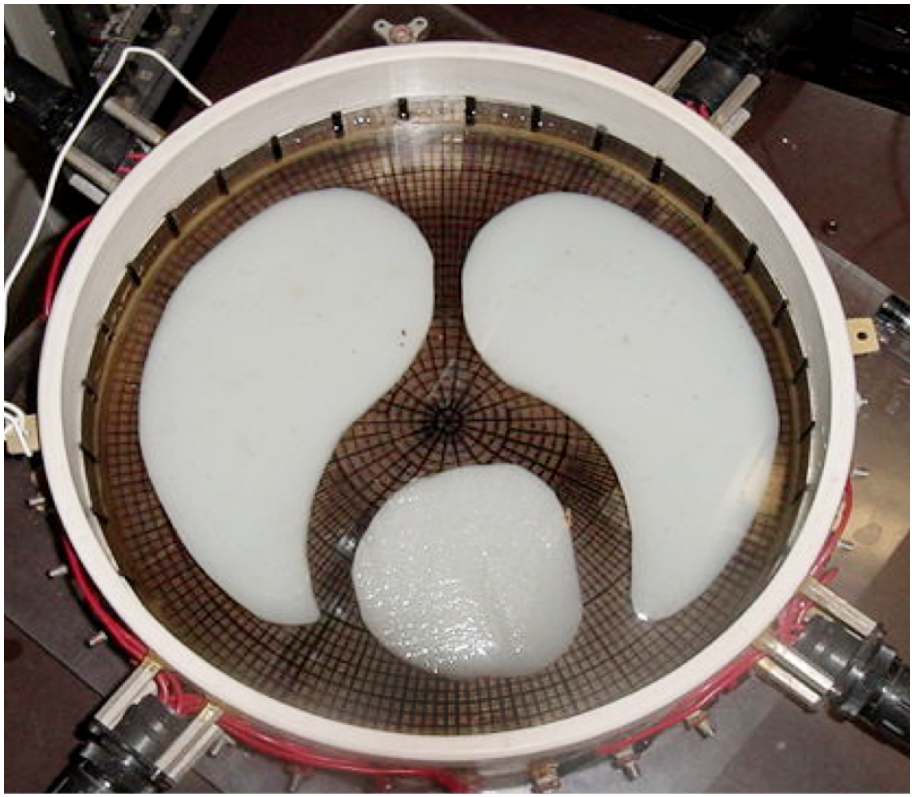

Phantom and data: Jon Newell, Rensselaer Polytechnic Institute

Apply current pattern $\cos 6\theta$

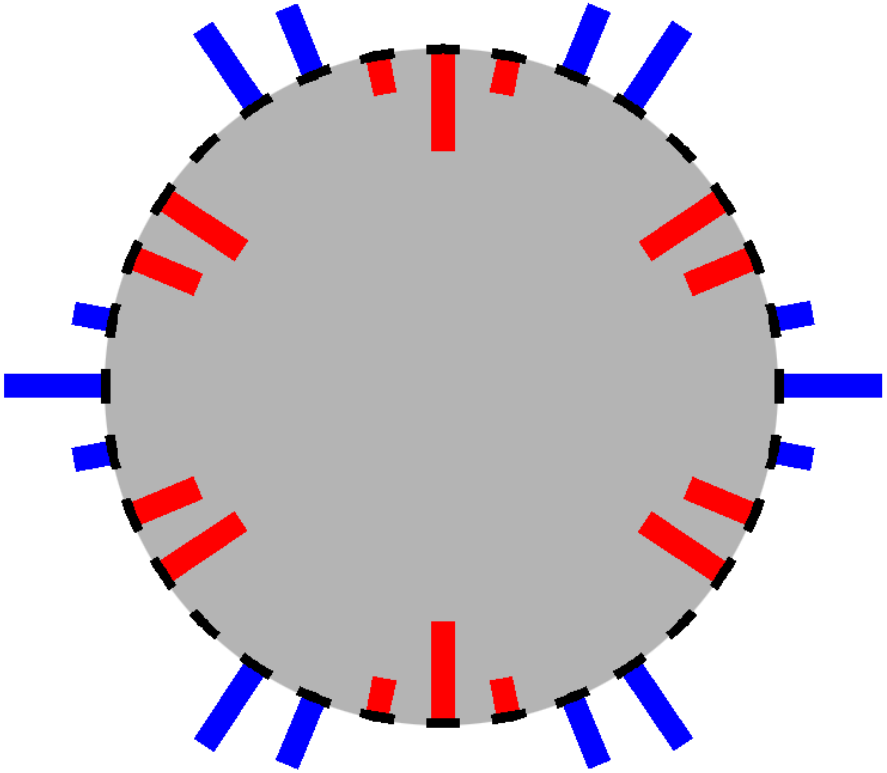

Measure the resulting voltages at all 32 electrodes

Note that EIT data collection involves applying several current patterns

Saline and agar phantom

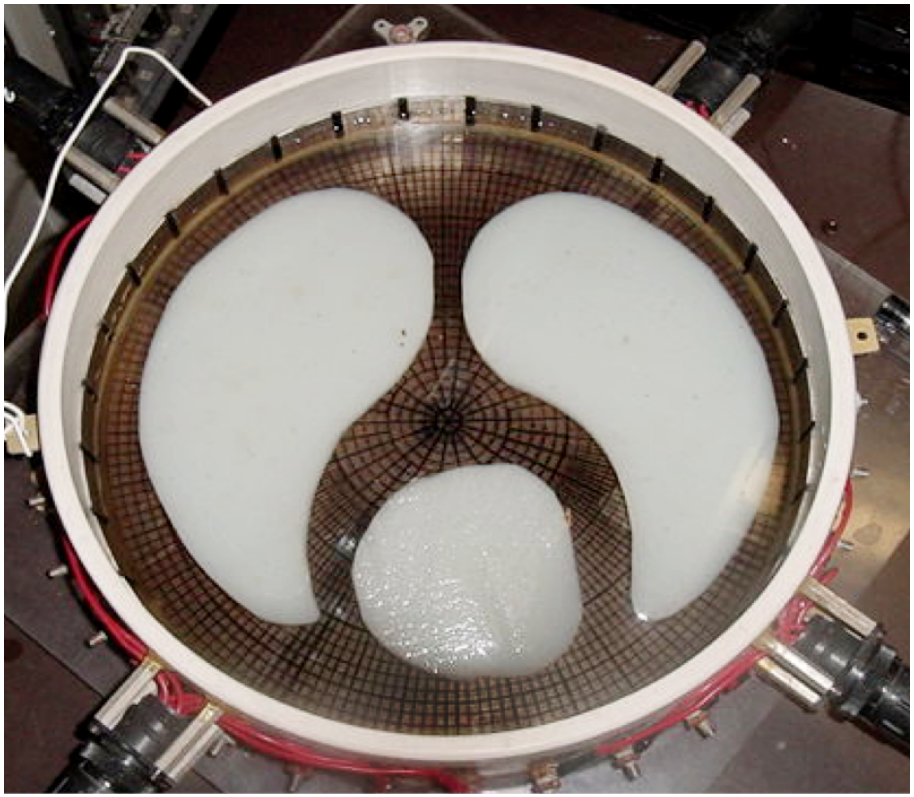

Phantom and data: Jon Newell, Rensselaer Polytechnic Institute

Apply current pattern $\cos 7\theta$

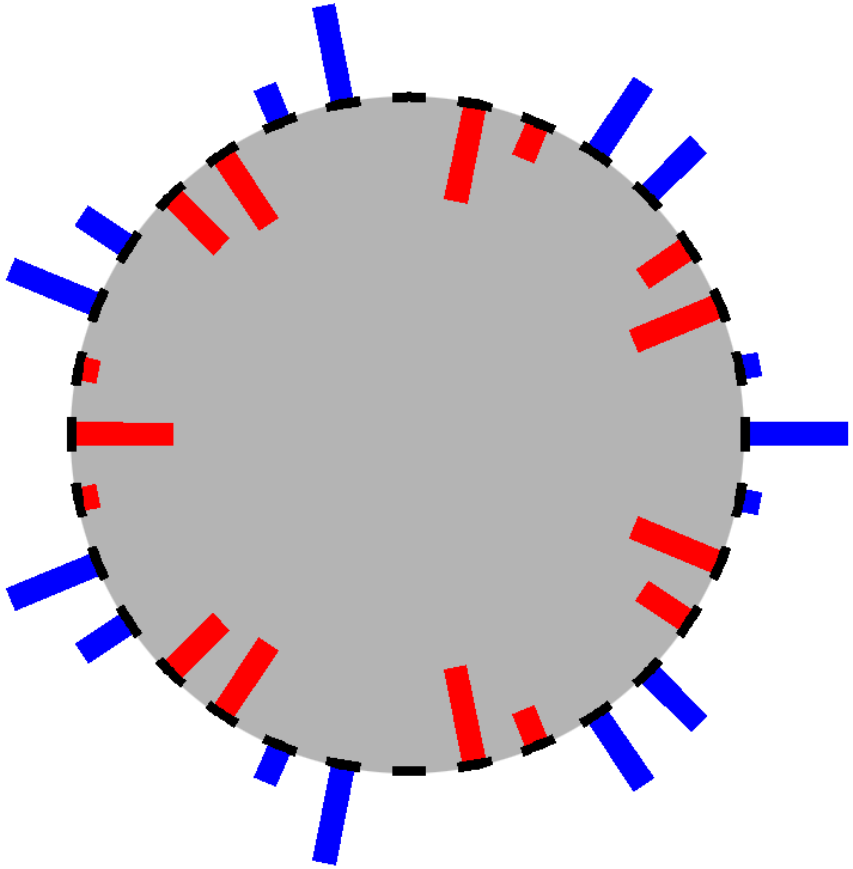

Measure the resulting voltages at all 32 electrodes

Note that EIT data collection involves applying several current patterns

Saline and agar phantom

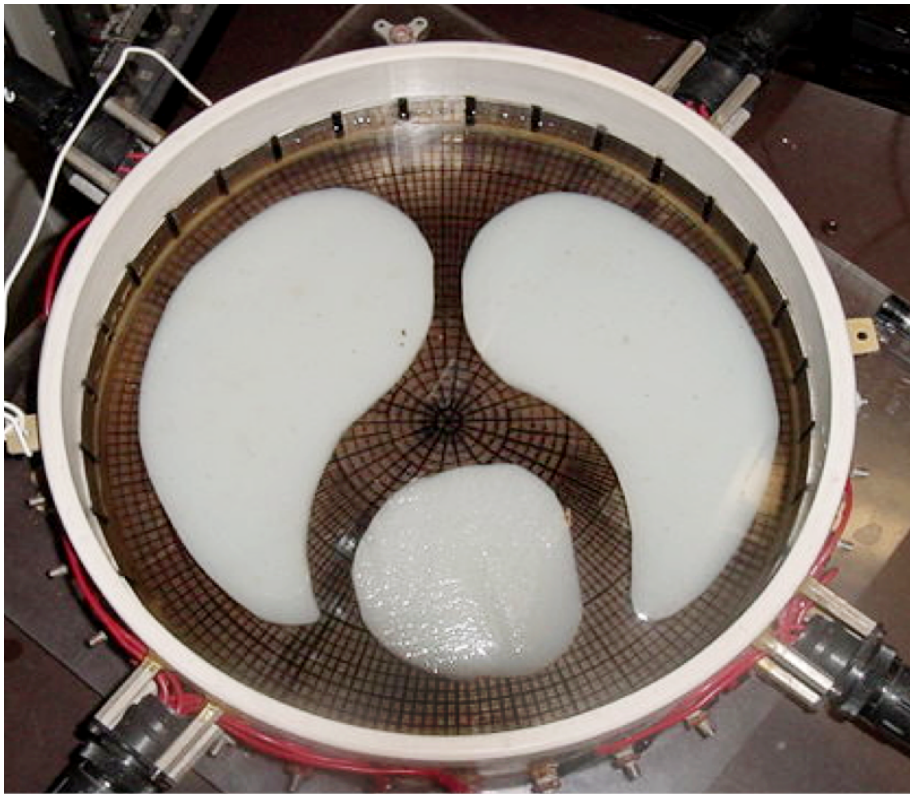

Phantom and data: Jon Newell, Rensselaer Polytechnic Institute

Apply current pattern $\cos 8\theta$

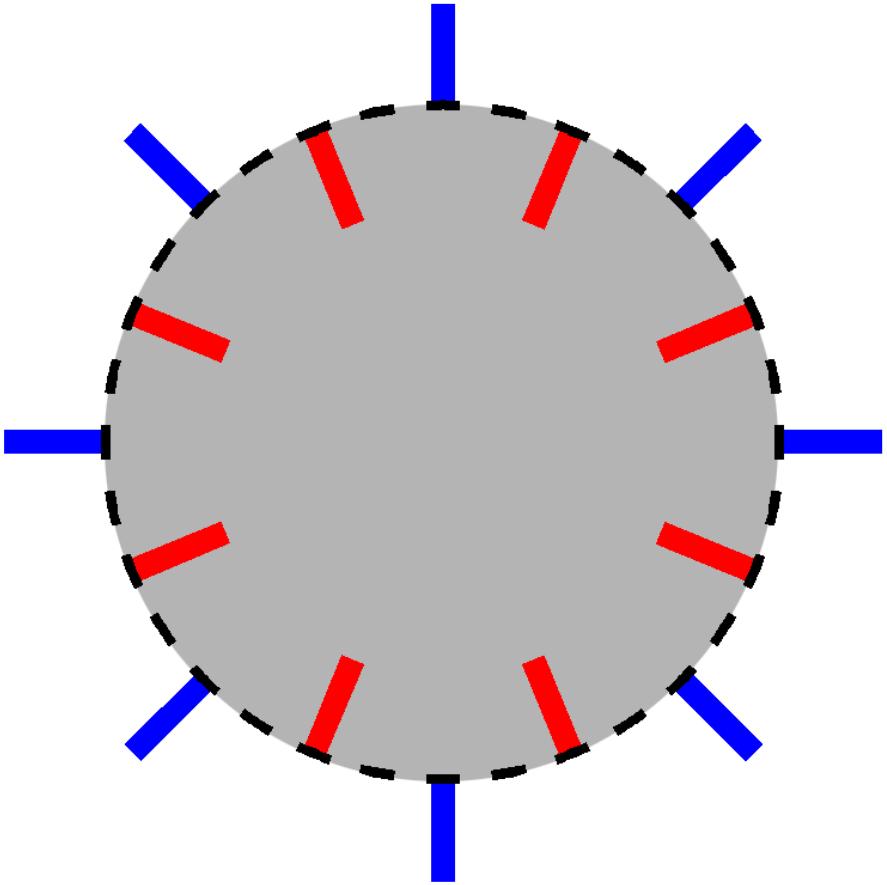

Measure the resulting voltages at all 32 electrodes

Note that EIT data collection involves applying several current patterns

Saline and agar phantom

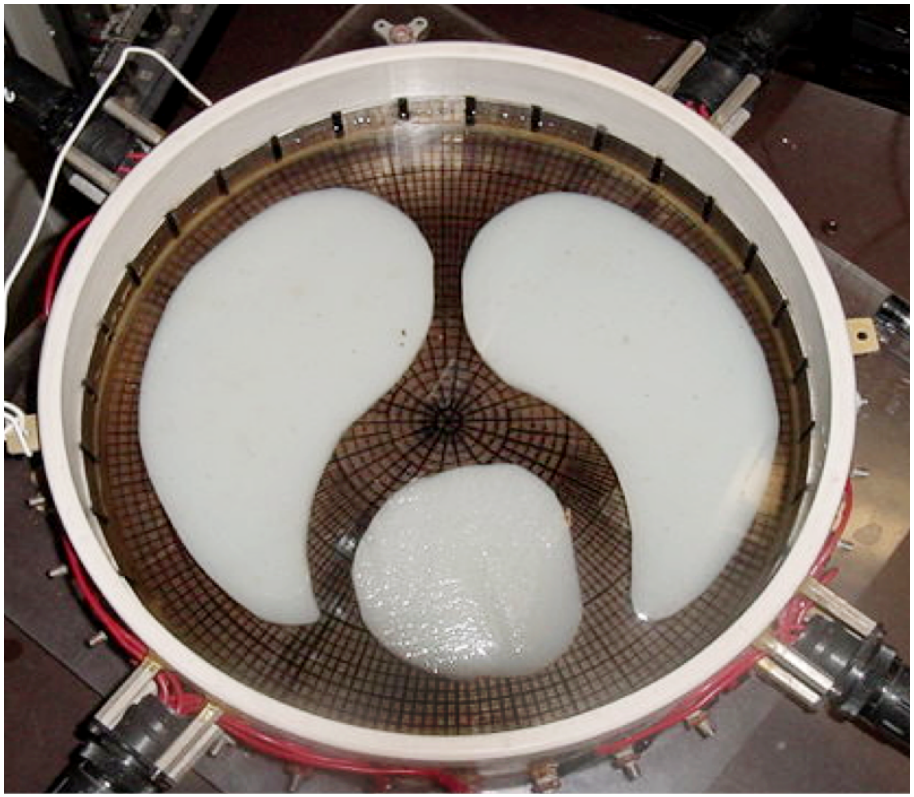

Phantom and data: Jon Newell, Rensselaer Polytechnic Institute

Apply current pattern $\cos 9\theta$

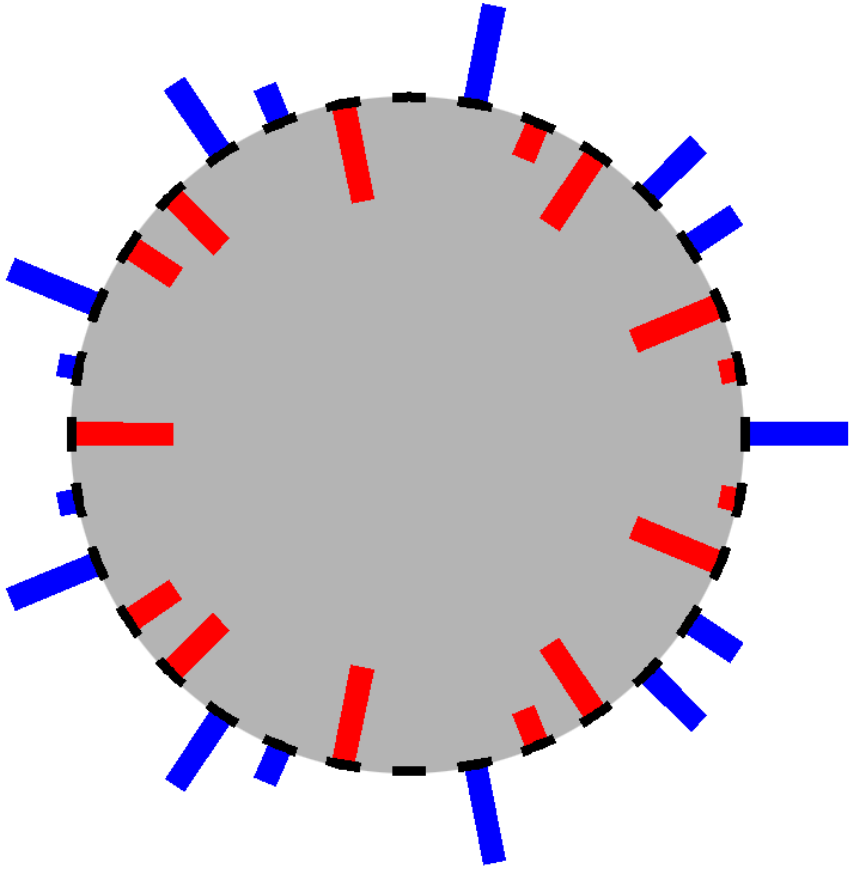

Measure the resulting voltages at all 32 electrodes

Note that EIT data collection involves applying several current patterns

Saline and agar phantom

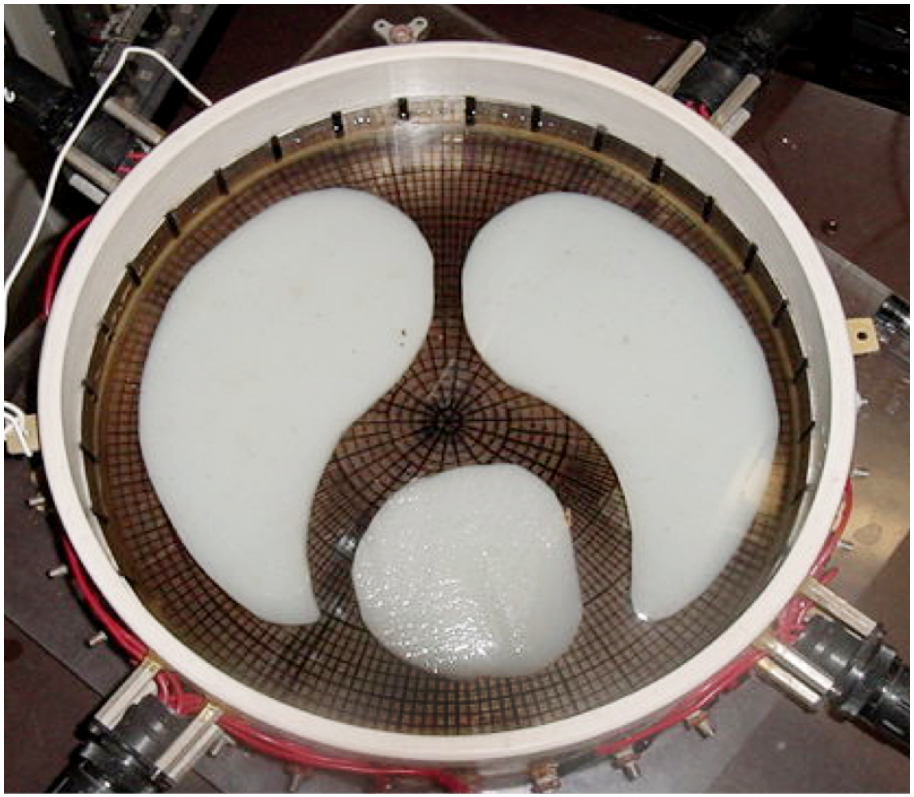

Phantom and data: Jon Newell, Rensselaer Polytechnic Institute

Apply current pattern $\cos 10\theta$

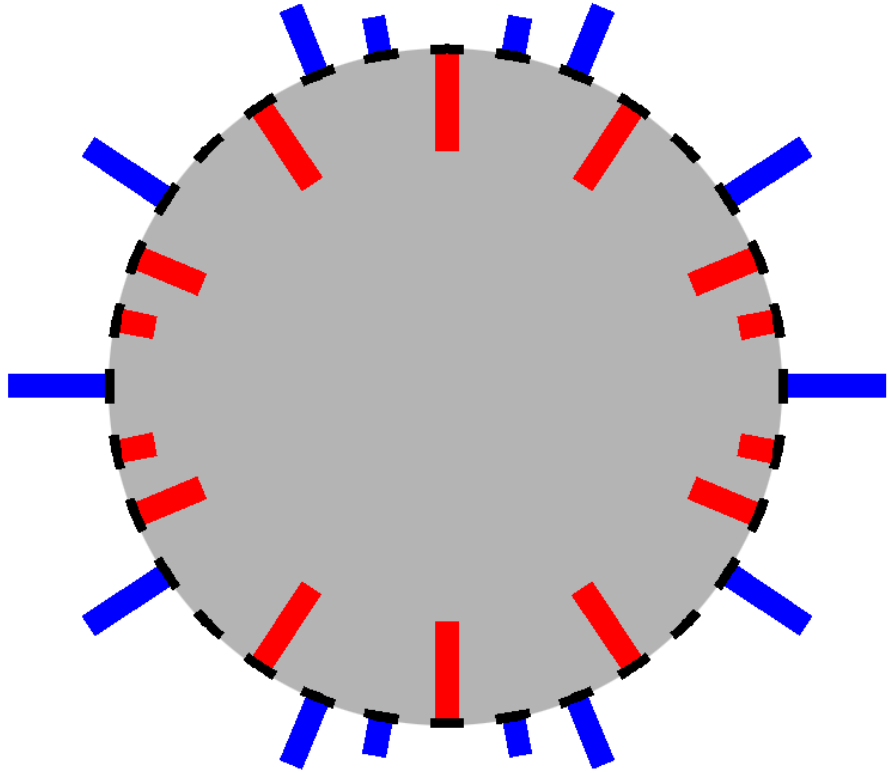

Measure the resulting voltages at all 32 electrodes

Note that EIT data collection involves applying several current patterns

Saline and agar phantom

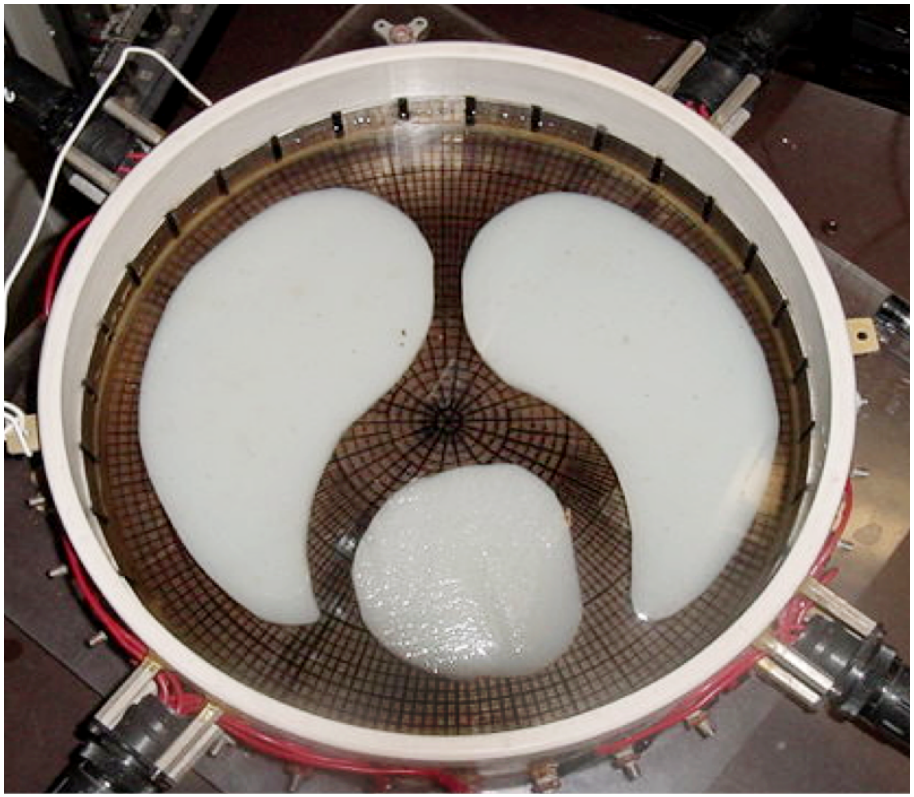

Phantom and data: Jon Newell, Rensselaer Polytechnic Institute

Apply current pattern $\cos 11\theta$

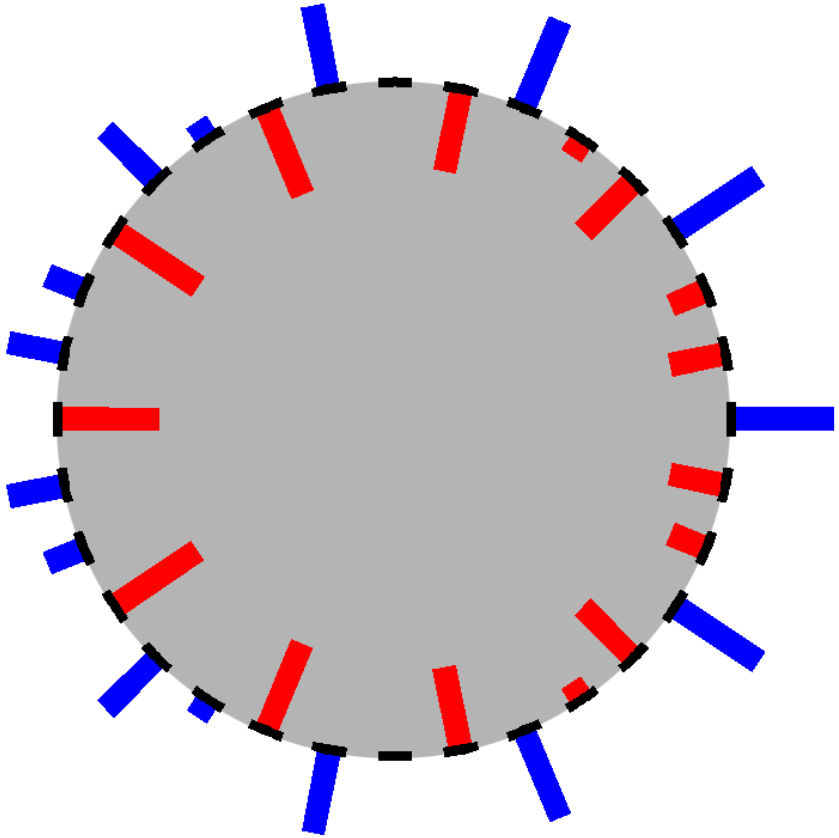

Measure the resulting voltages at all 32 electrodes

Note that EIT data collection involves applying several current patterns

Saline and agar phantom

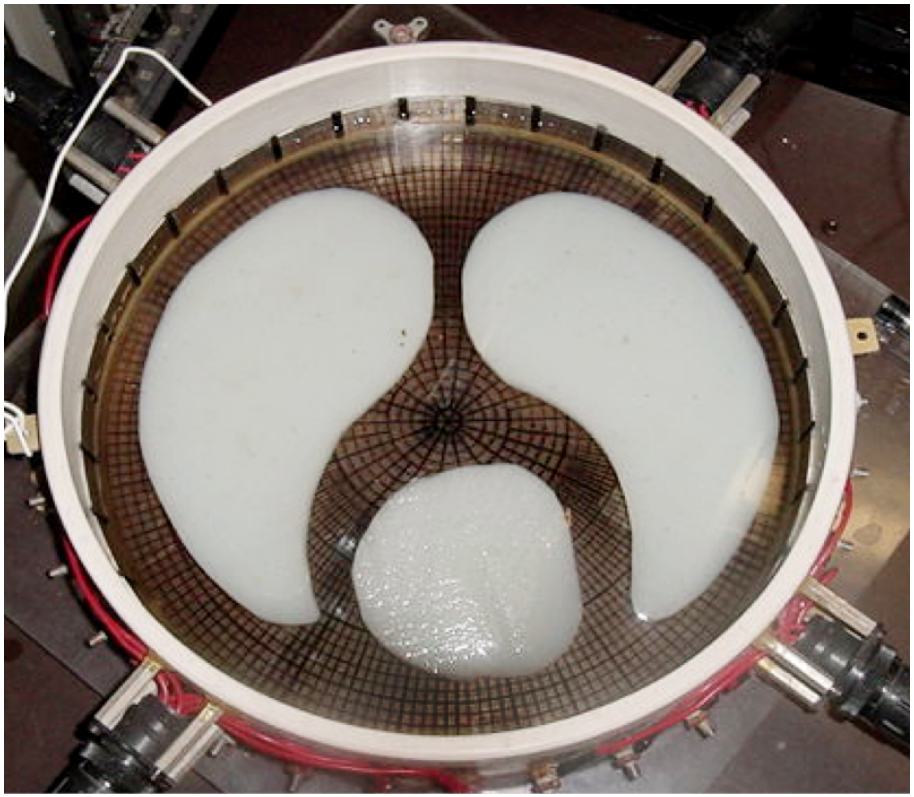

Phantom and data: Jon Newell, Rensselaer Polytechnic Institute

Apply current pattern $\cos 12\theta$

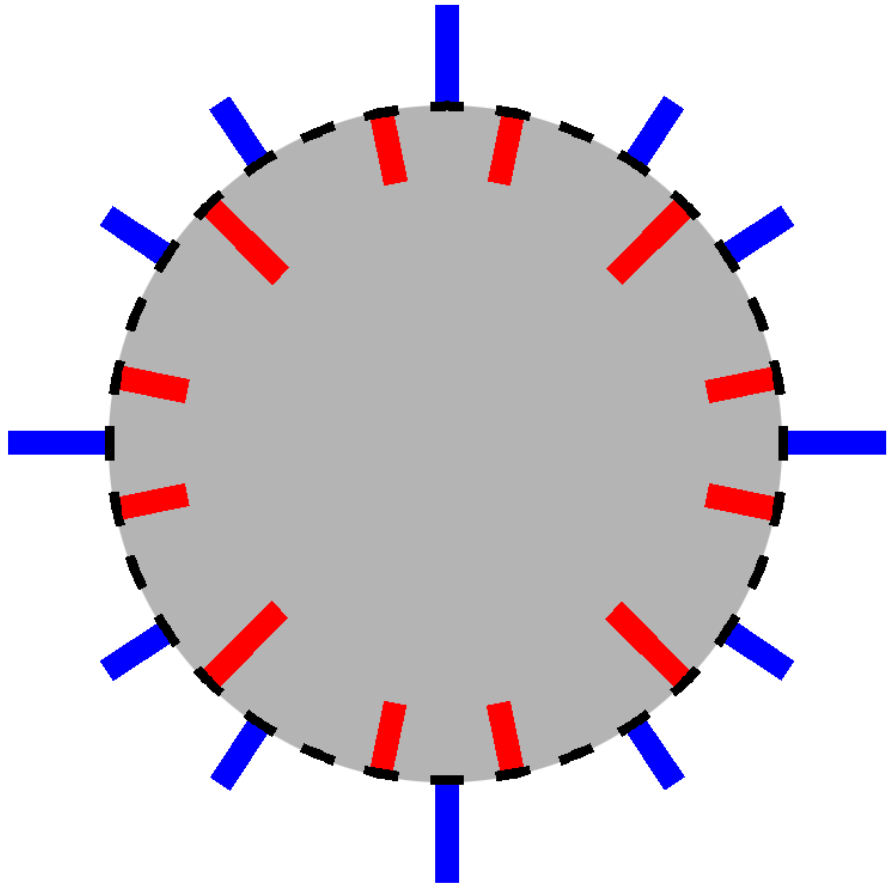

Measure the resulting voltages at all 32 electrodes

Note that EIT data collection involves applying several current patterns

Saline and agar phantom

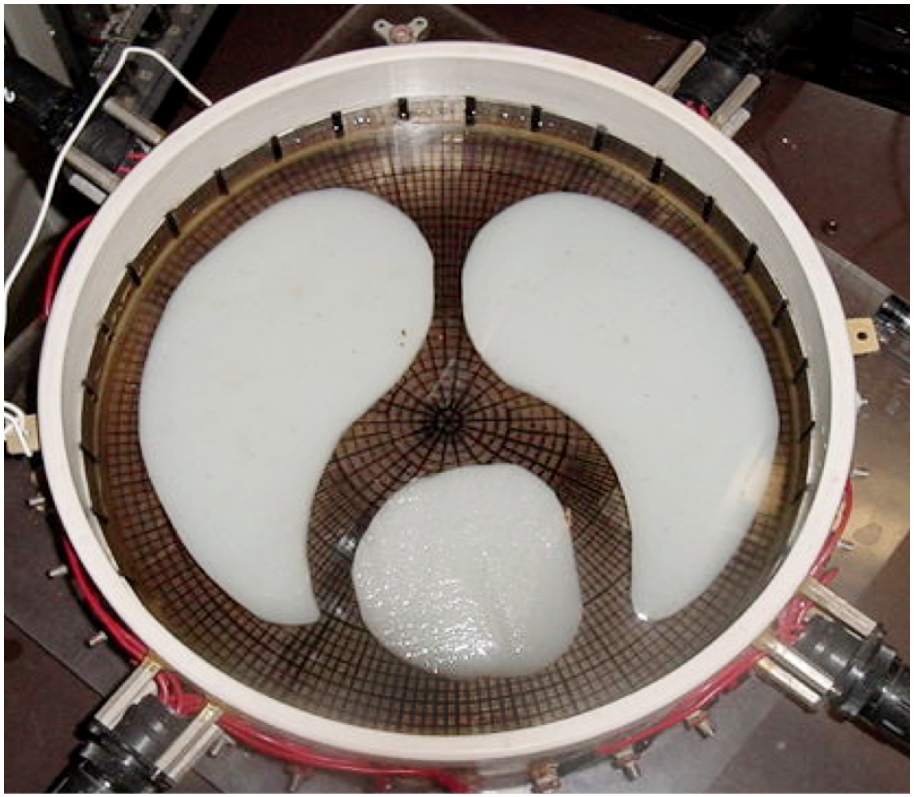

Phantom and data: Jon Newell, Rensselaer Polytechnic Institute

Apply current pattern $\cos 13\theta$

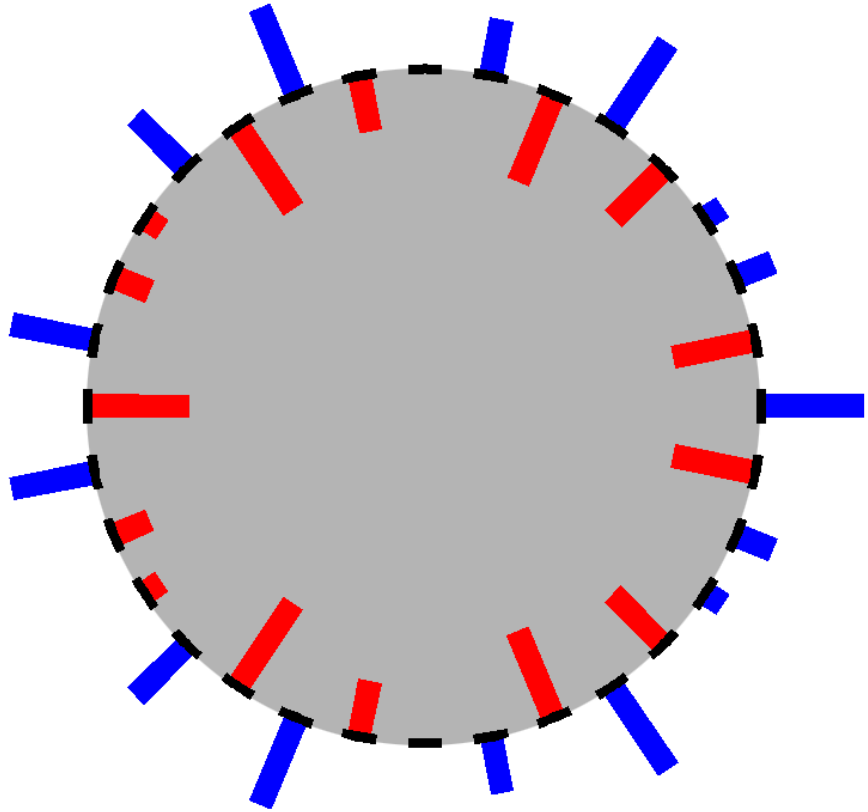

Measure the resulting voltages at all 32 electrodes

Note that EIT data collection involves applying several current patterns

Saline and agar phantom

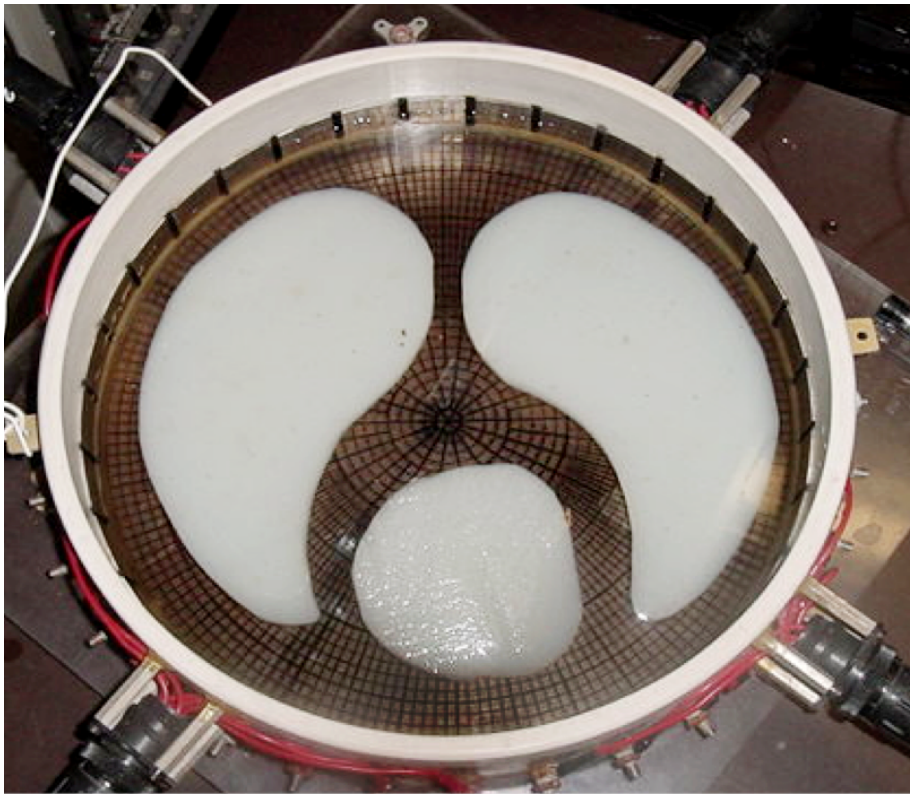

Phantom and data: Jon Newell, Rensselaer Polytechnic Institute

Apply current pattern $\cos 14\theta$

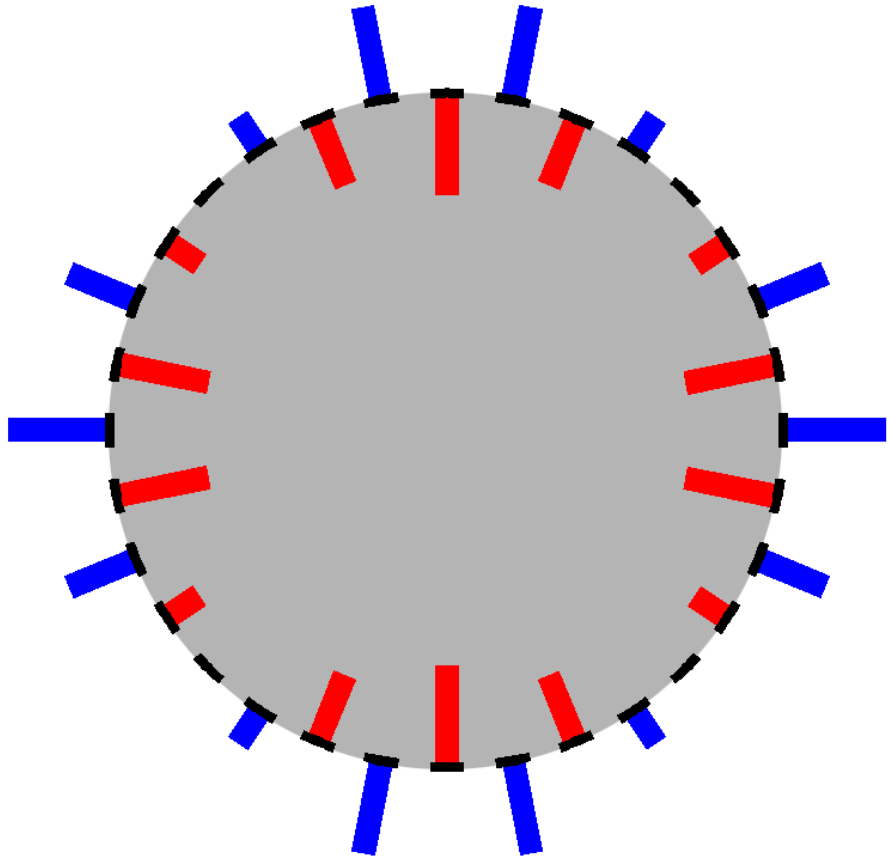

Measure the resulting voltages at all 32 electrodes

Note that EIT data collection involves applying several current patterns

Saline and agar phantom

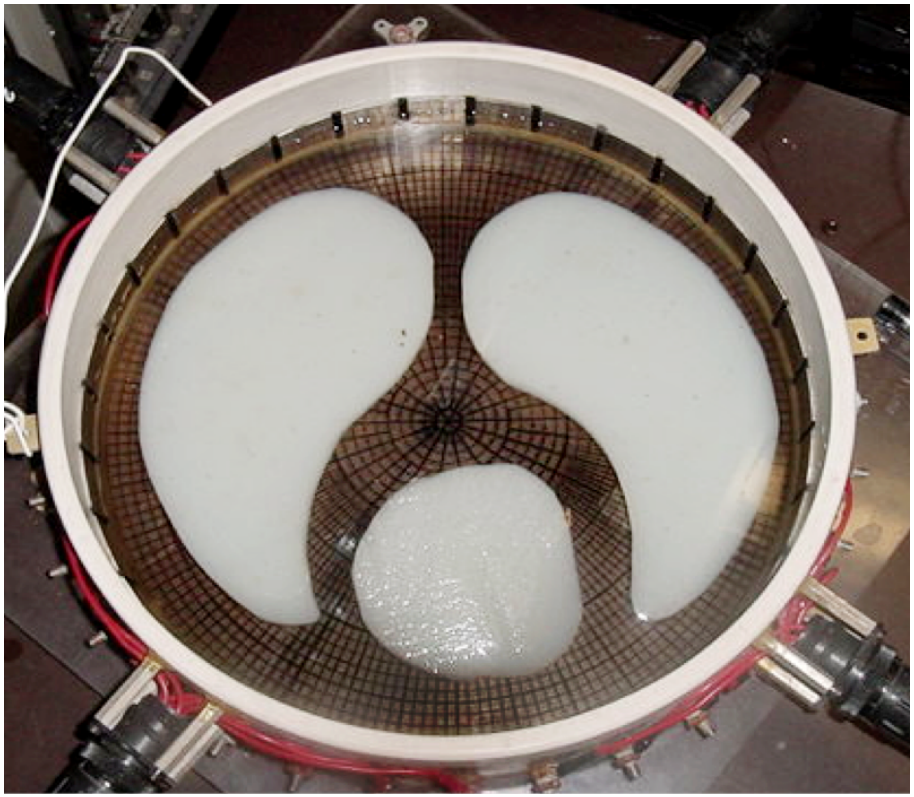

Phantom and data: Jon Newell, Rensselaer Polytechnic Institute

Apply current pattern $\cos 15\theta$

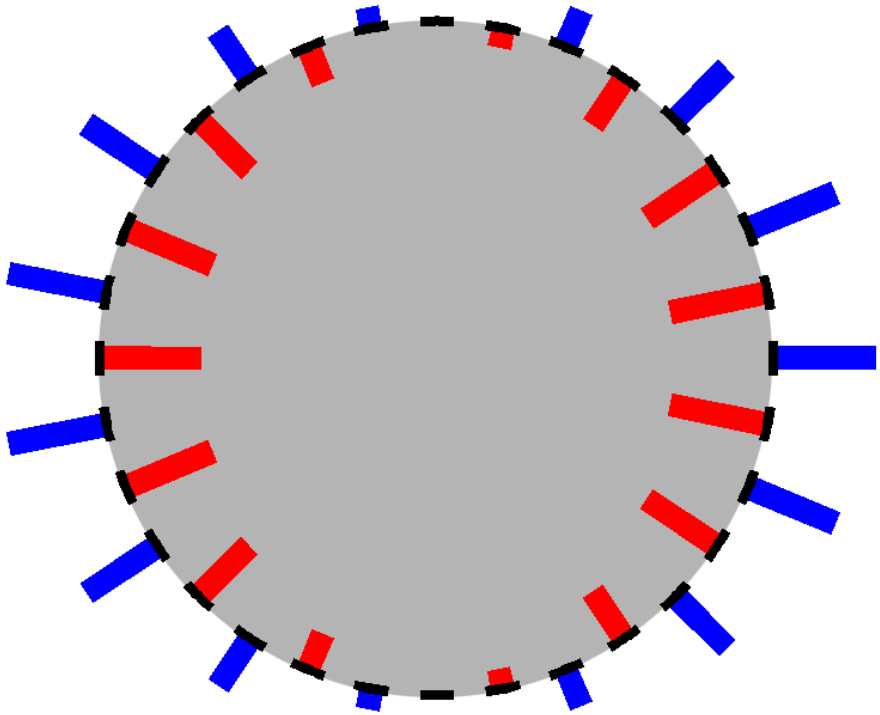

Measure the resulting voltages at all 32 electrodes

Note that EIT data collection involves applying several current patterns

Saline and agar phantom

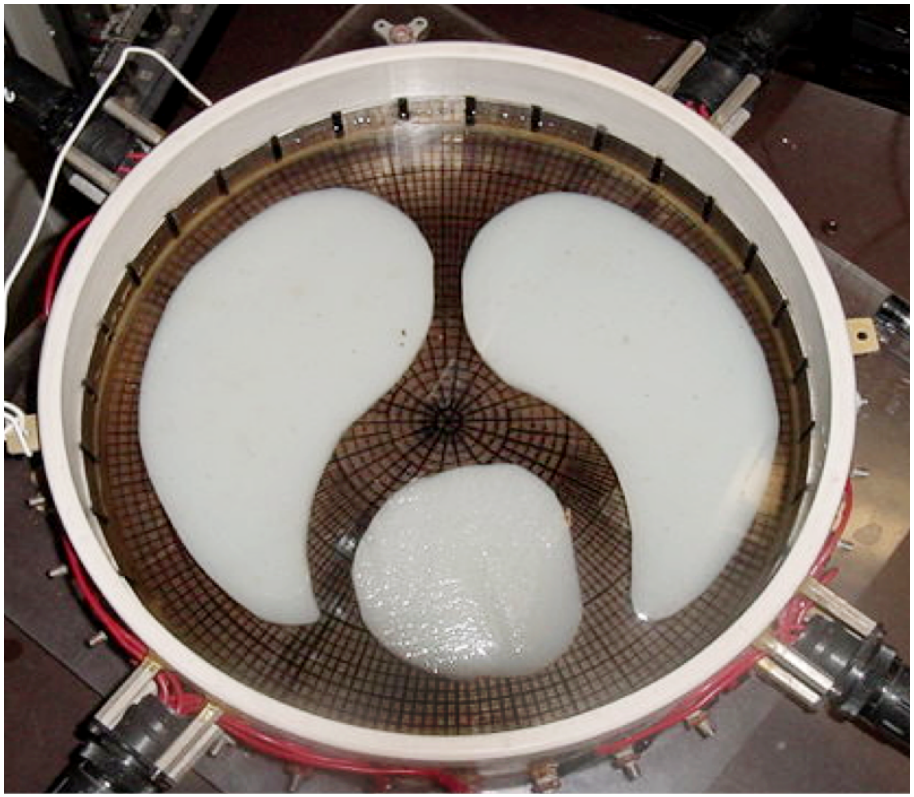

Phantom and data: Jon Newell, Rensselaer Polytechnic Institute

Apply current pattern $\cos 16\theta$

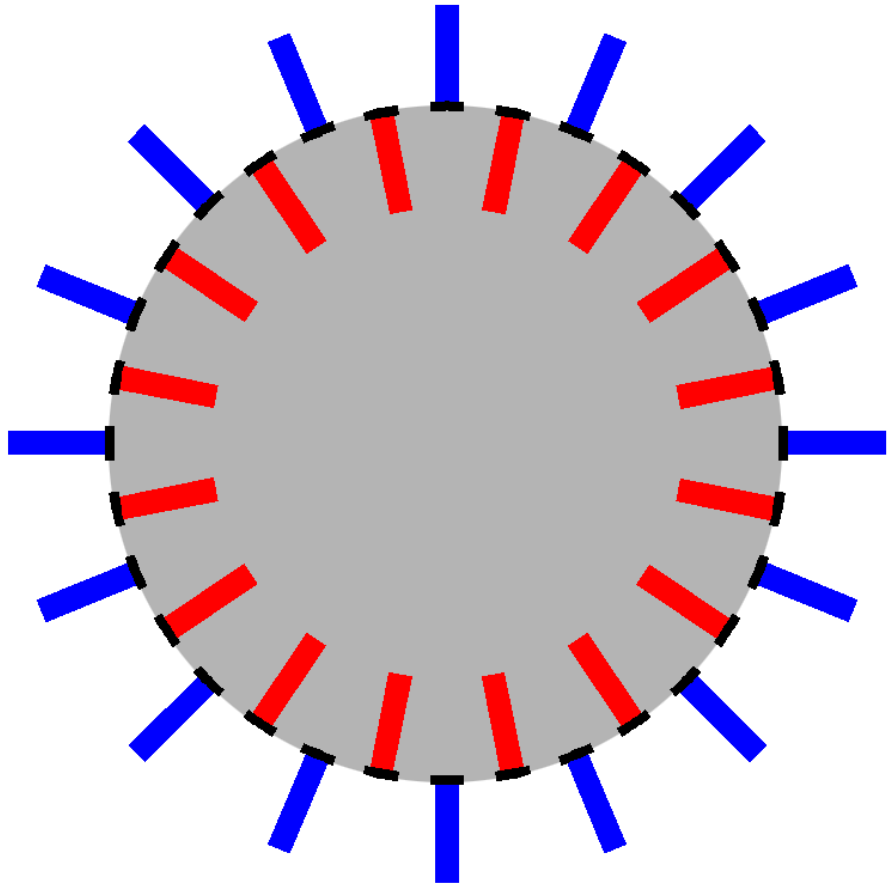

Measure the resulting voltages at all 32 electrodes

Here is a reconstruction of the conductivity, computed using a nonlinear Fourier transform

Saline and agar phantom

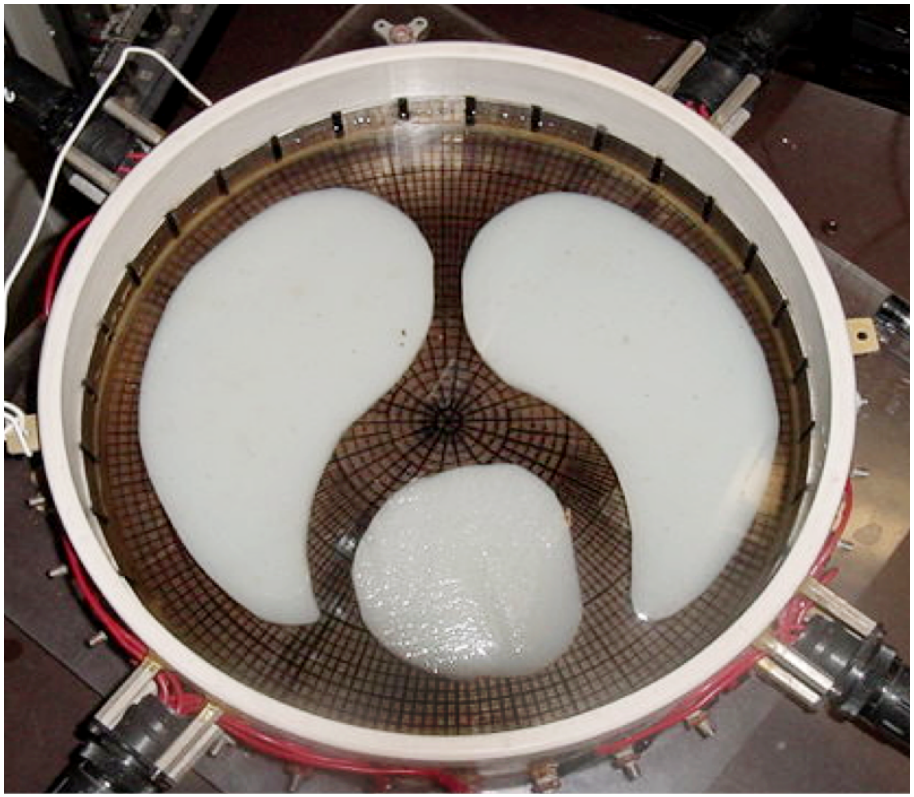

[Isaacson, Mueller, Newell & S 2004]
[Montoya 2012]

D-bar reconstruction

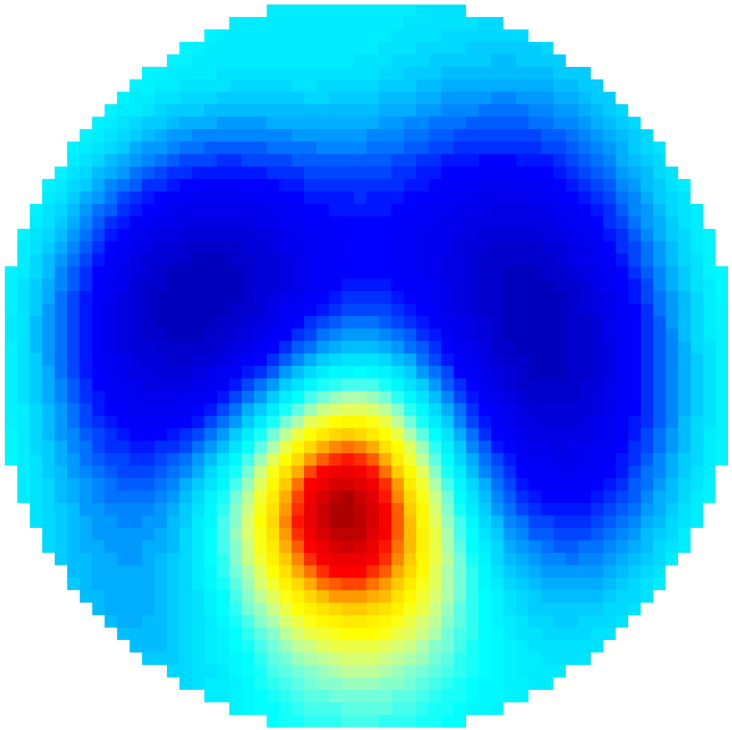

Cut-off frequency $R = 4$

The inverse conductivity problem introduced by Alberto Calderón is a mathematical model for EIT

Let $\Omega \subset \mathbb{R}^2$ be the unit disc and let conductivity $\sigma : \Omega \to \mathbb{R}$ satisfy

$$0 < M^{-1} \leq \sigma(z) \leq M.$$

Applying voltage f at the boundary $\partial\Omega$ leads to the elliptic PDE

$$\begin{cases} \nabla \cdot \sigma \nabla u &= 0 \text{ in } \Omega, \\ u|_{\partial\Omega} &= f. \end{cases}$$

The Dirichlet-to-Neumann map is a model for boundary measurements

$$\Lambda_\sigma : f \mapsto \sigma \frac{\partial u}{\partial \vec{n}}|_{\partial\Omega}.$$

Calderón's problem is to recover σ from the knowledge of Λ_σ.

This is a nonlinear task and an **ill-posed inverse problem.**

Ill-posed inverse problems are defined as opposites of well-posed direct problems

Hadamard (1903): a problem is well-posed if the following conditions hold.

1. A solution exists,
2. The solution is unique,
3. The solution depends continuously on the input.

Well-posed linear direct EIT problem:
Input σ, find infinite-precision data Λ_σ.

Ill-posed nonlinear inverse EIT problem:
Input noisy data Λ_σ^δ, reconstruct σ.

We illustrate the ill-posedness of EIT using a simulated example

σ_1

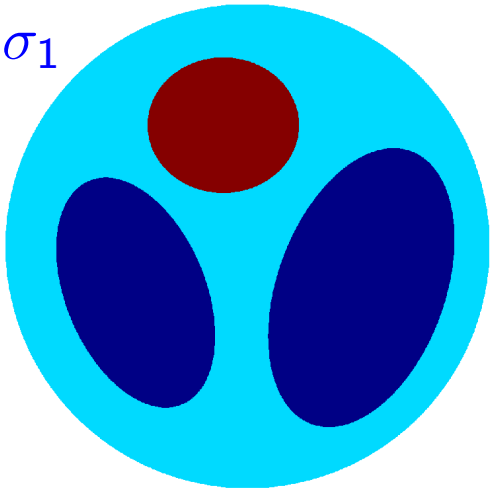

σ_2

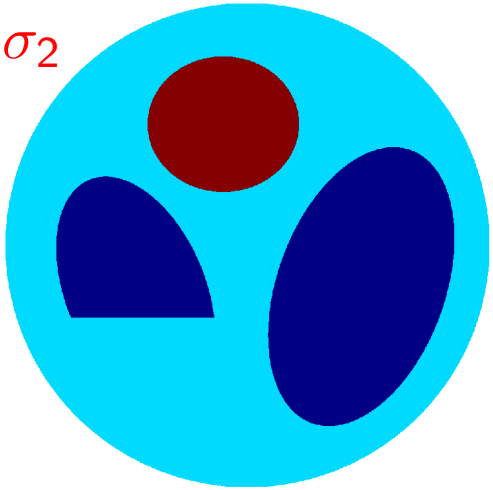

We apply the voltage distribution $f(\theta) = \cos\theta$ at the boundary of the two different phantoms

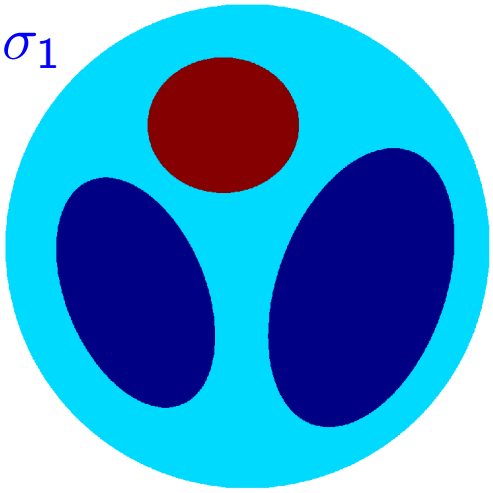

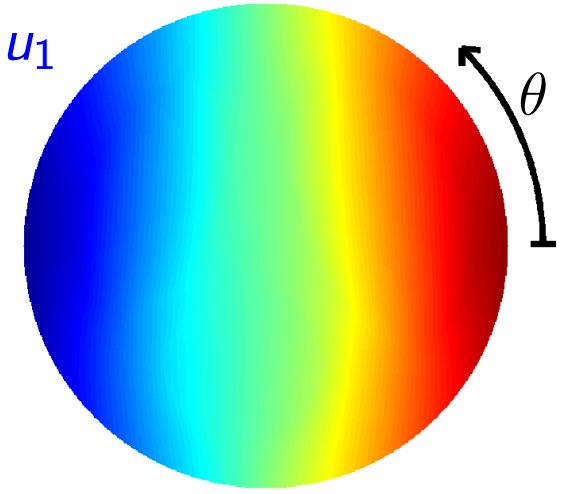

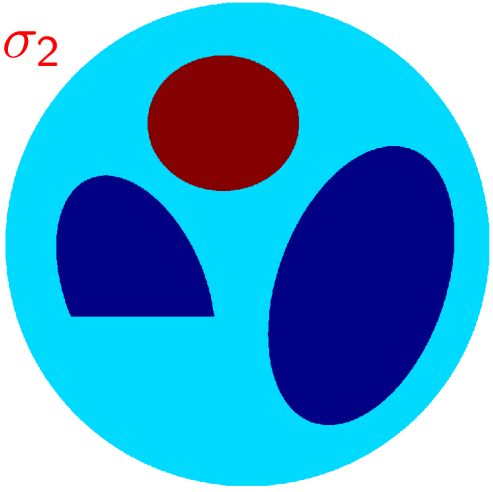

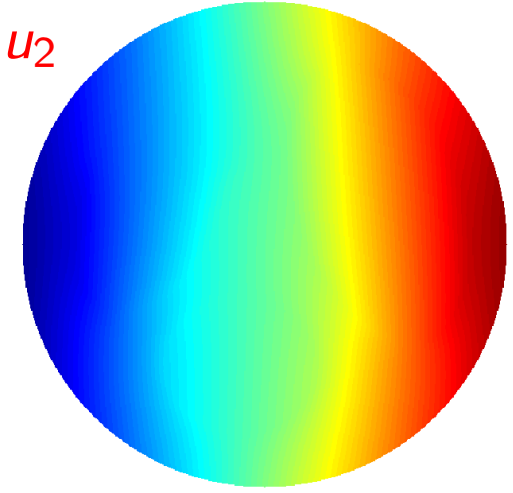

The measurement is the distribution of current through the boundary

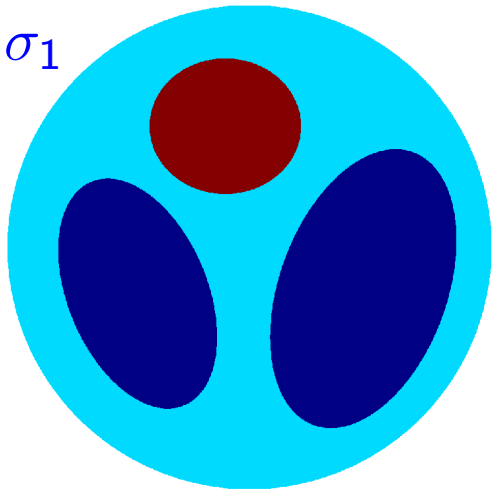

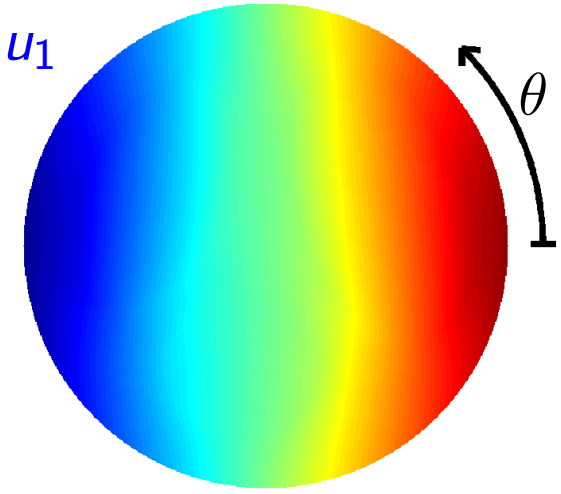

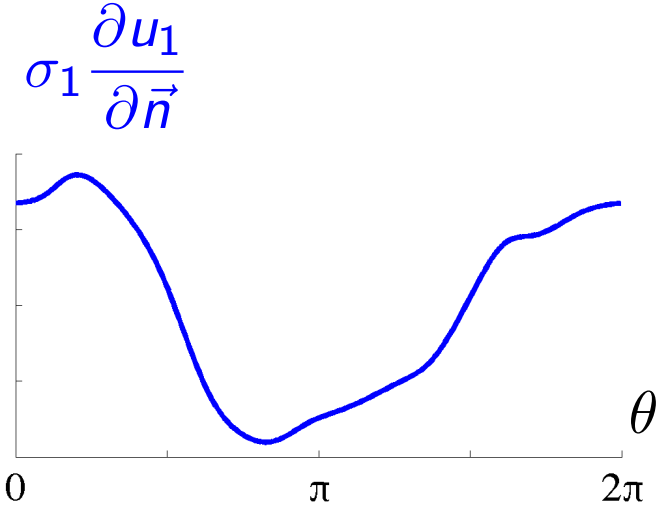

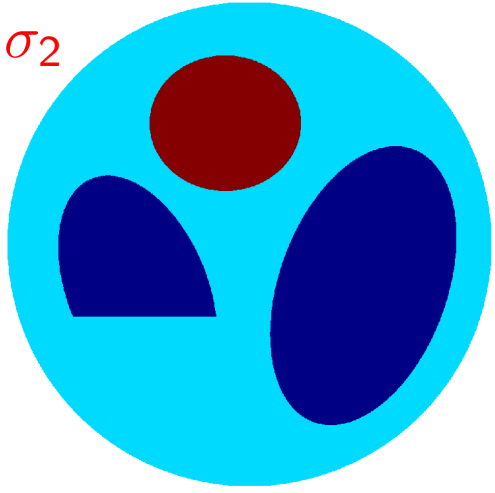

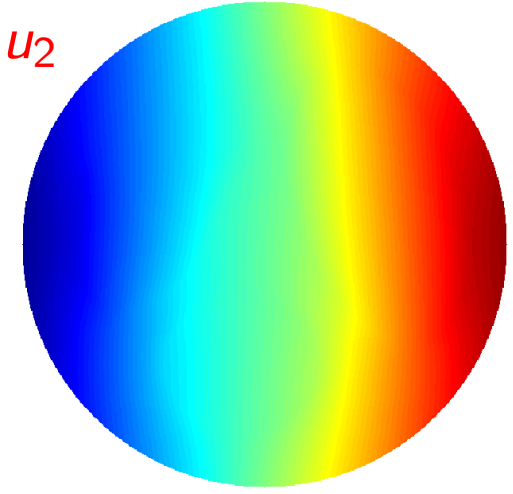

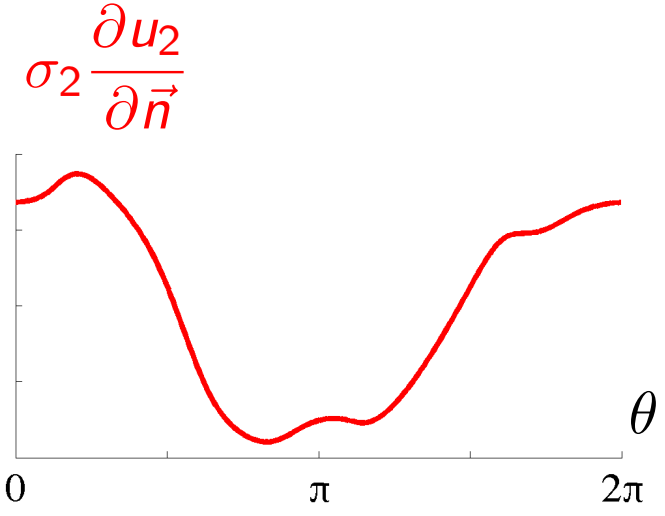

The current data are very similar, although the conductivities are quite different

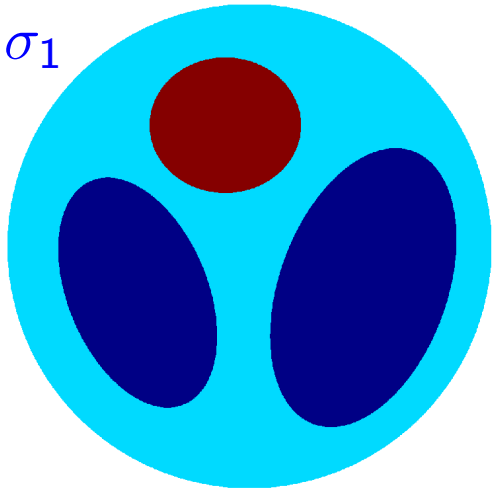

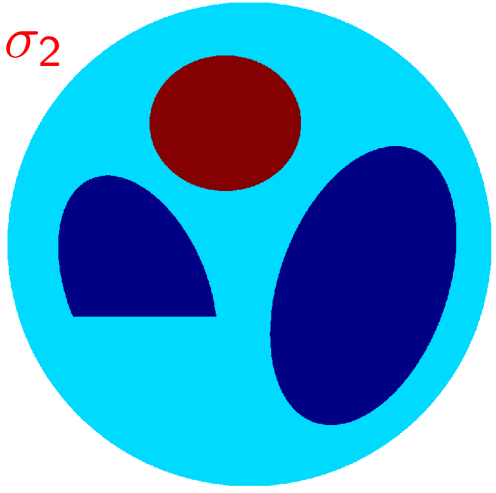

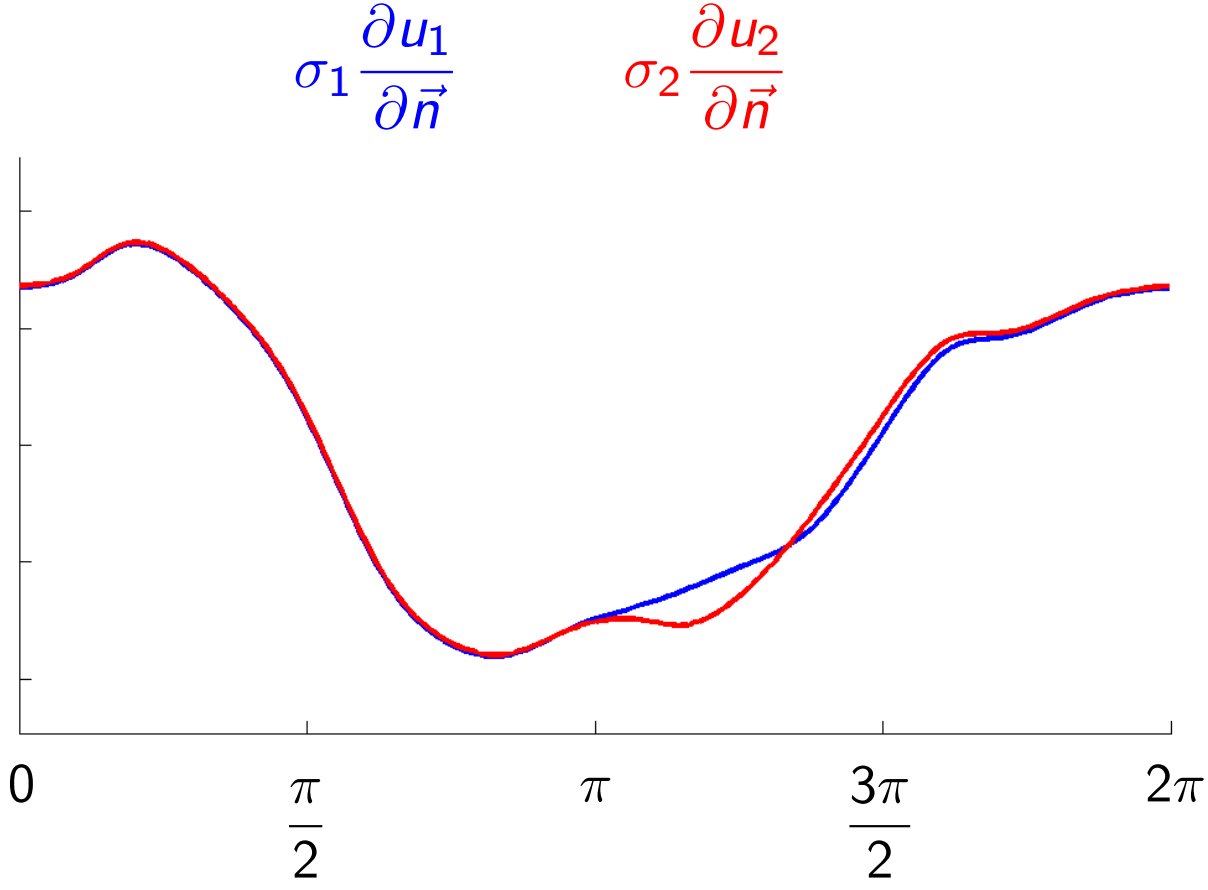

Let us apply the more oscillatory distribution $f(\theta) = \cos 2\theta$ of voltage at the boundary

σ_1

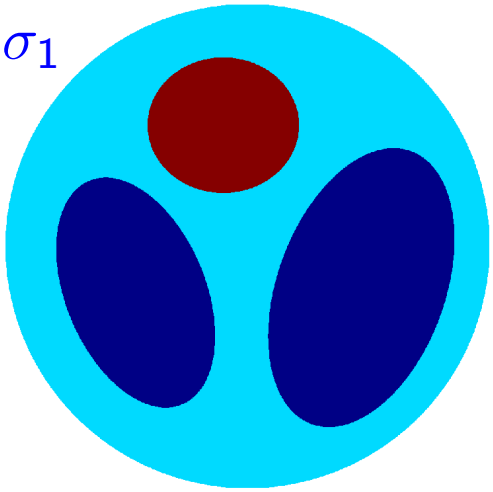

u_1

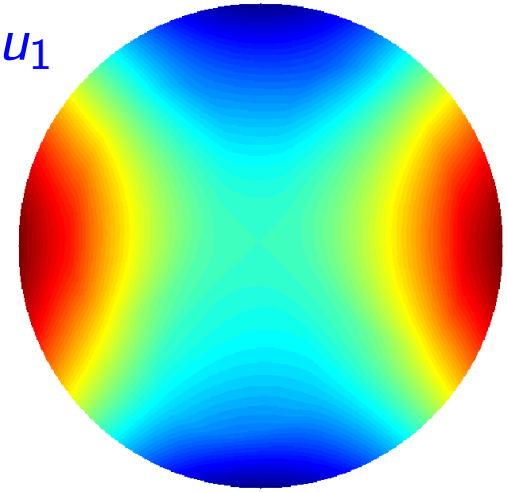

σ_2

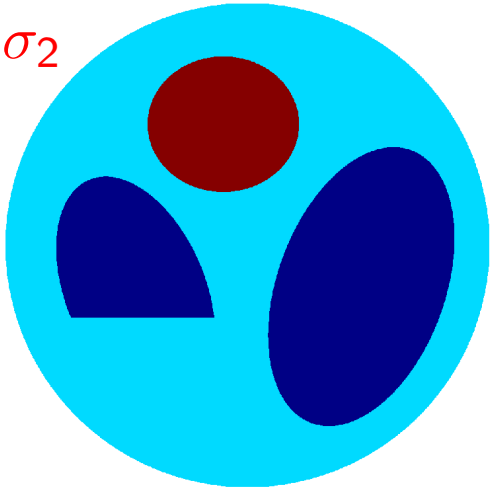

u_2

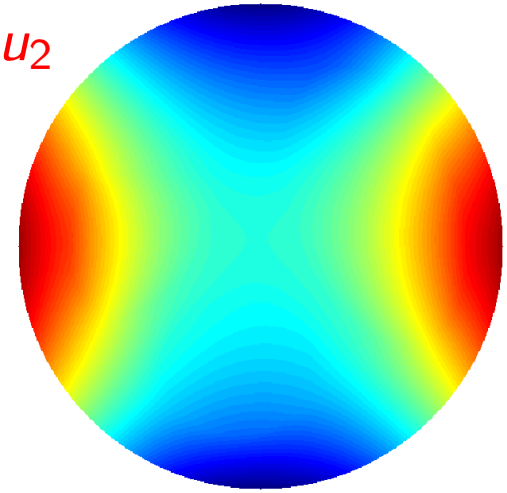

The measurement is again the distribution of current through the boundary

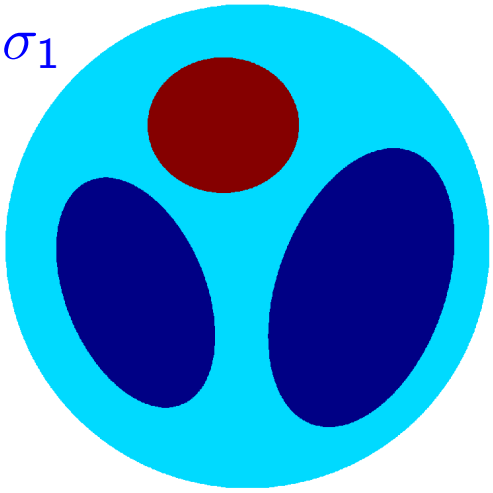

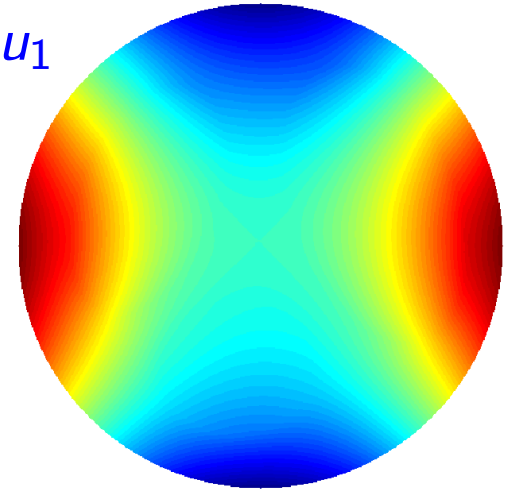

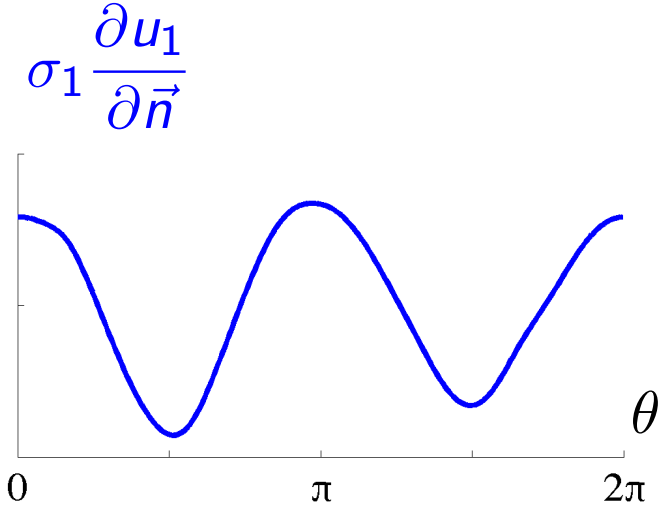

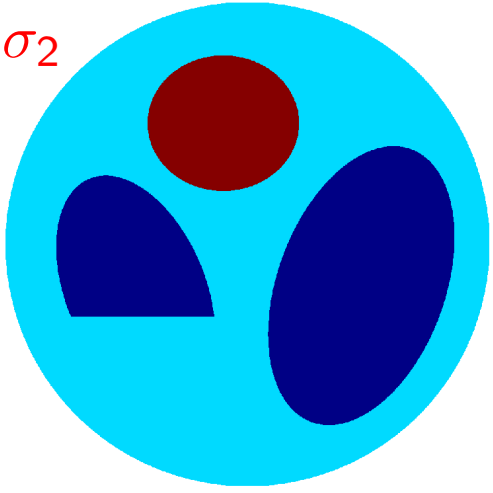

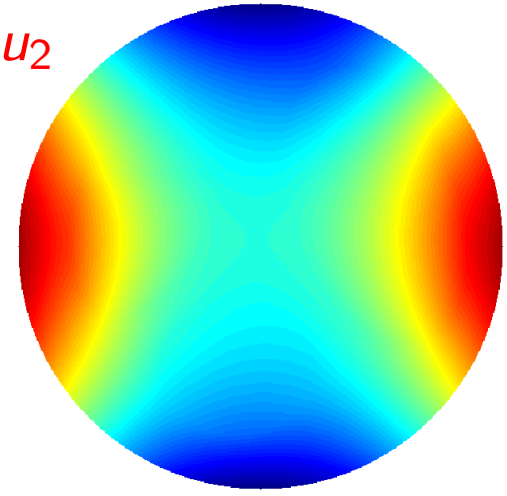

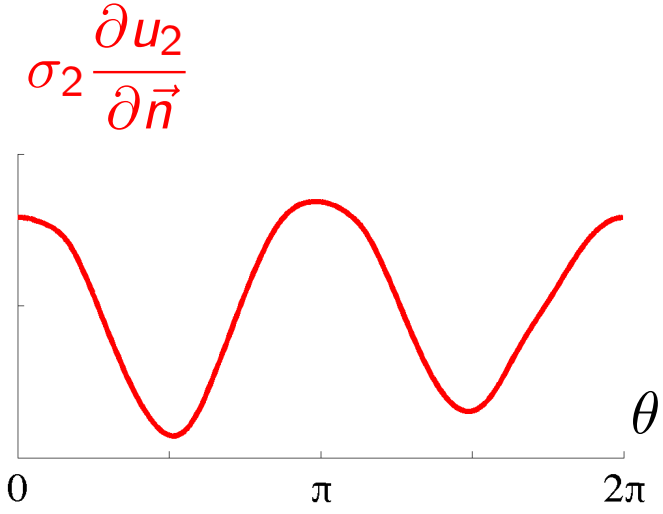

The current distribution measurements are almost the same

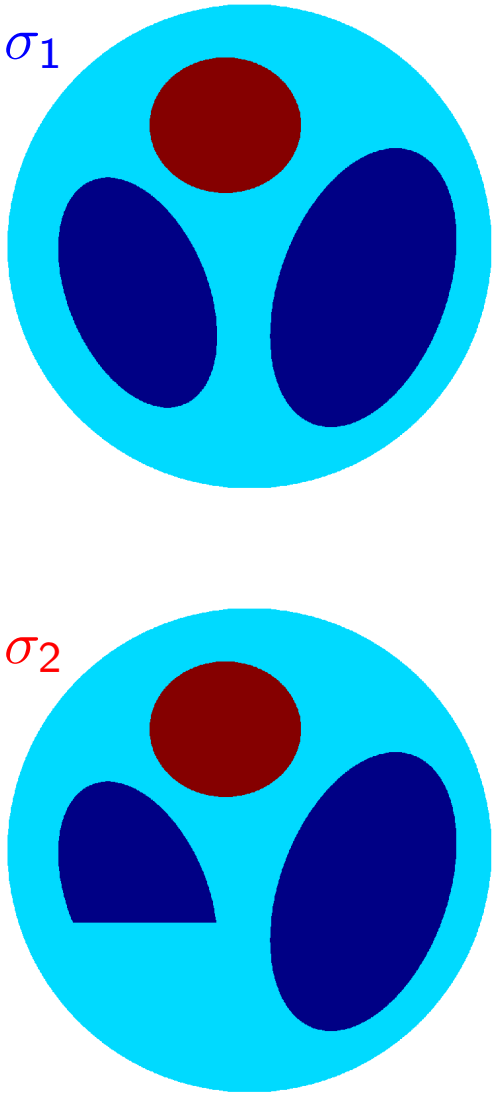

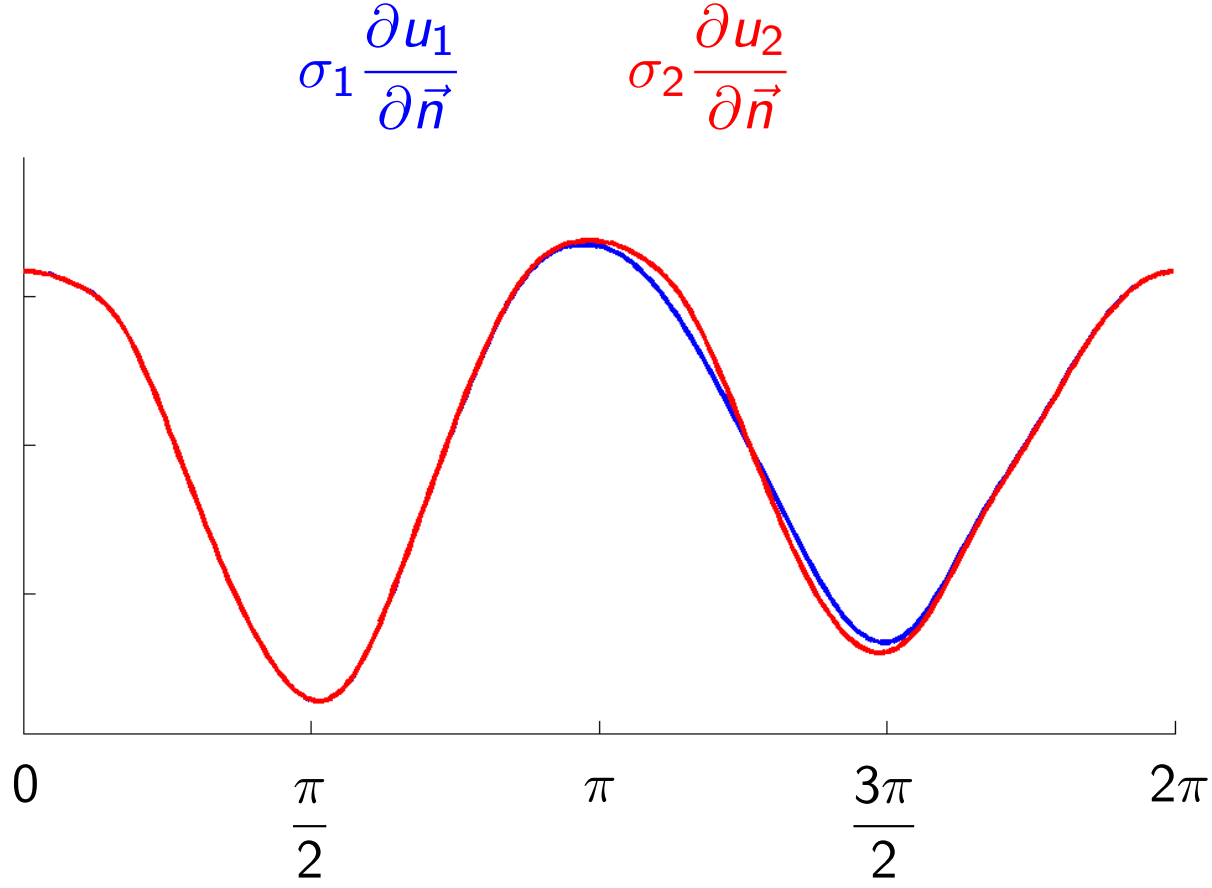

EIT is an ill-posed problem: big differences in conductivity cause only small effect in data

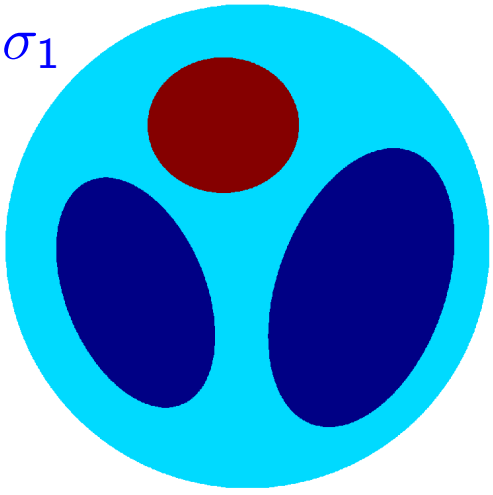

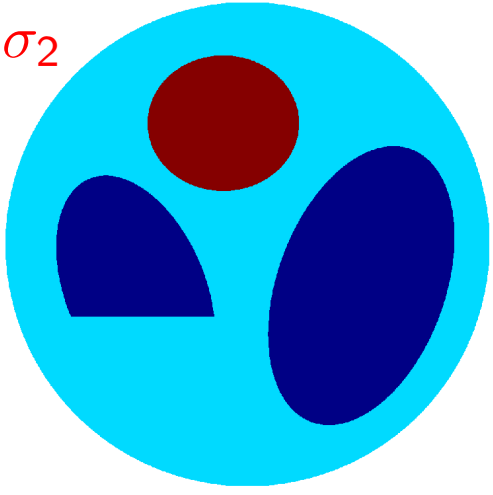

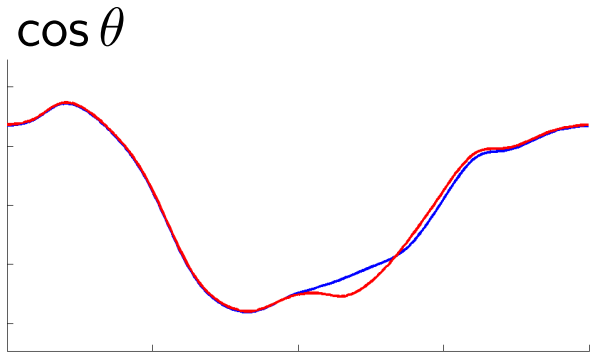

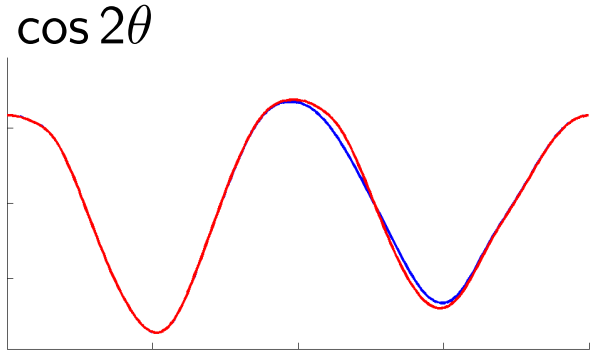

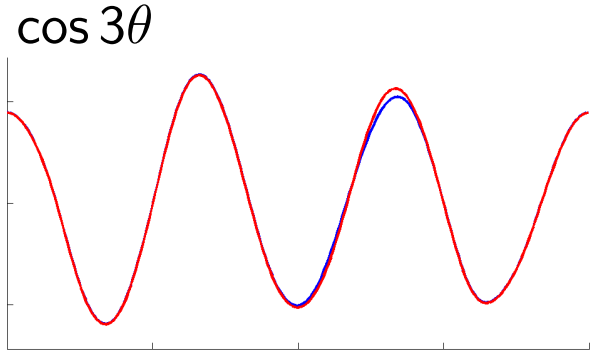

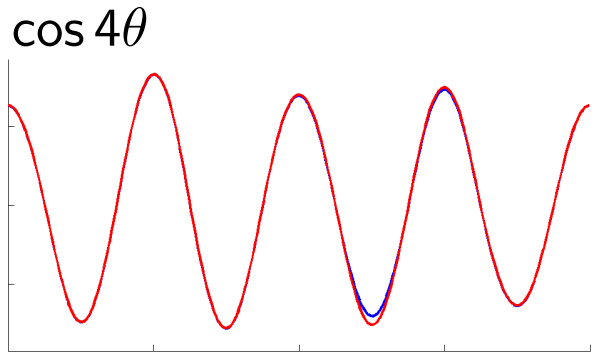

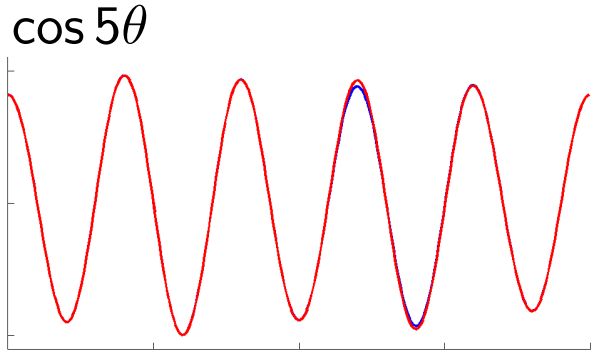

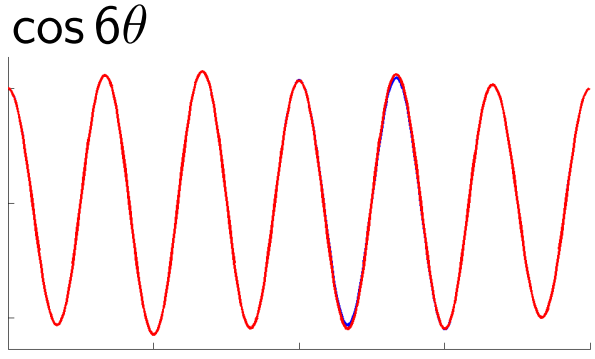

The forward map $F : X \supset \mathcal{D}(F) \to Y$ does not have a continuous inverse!

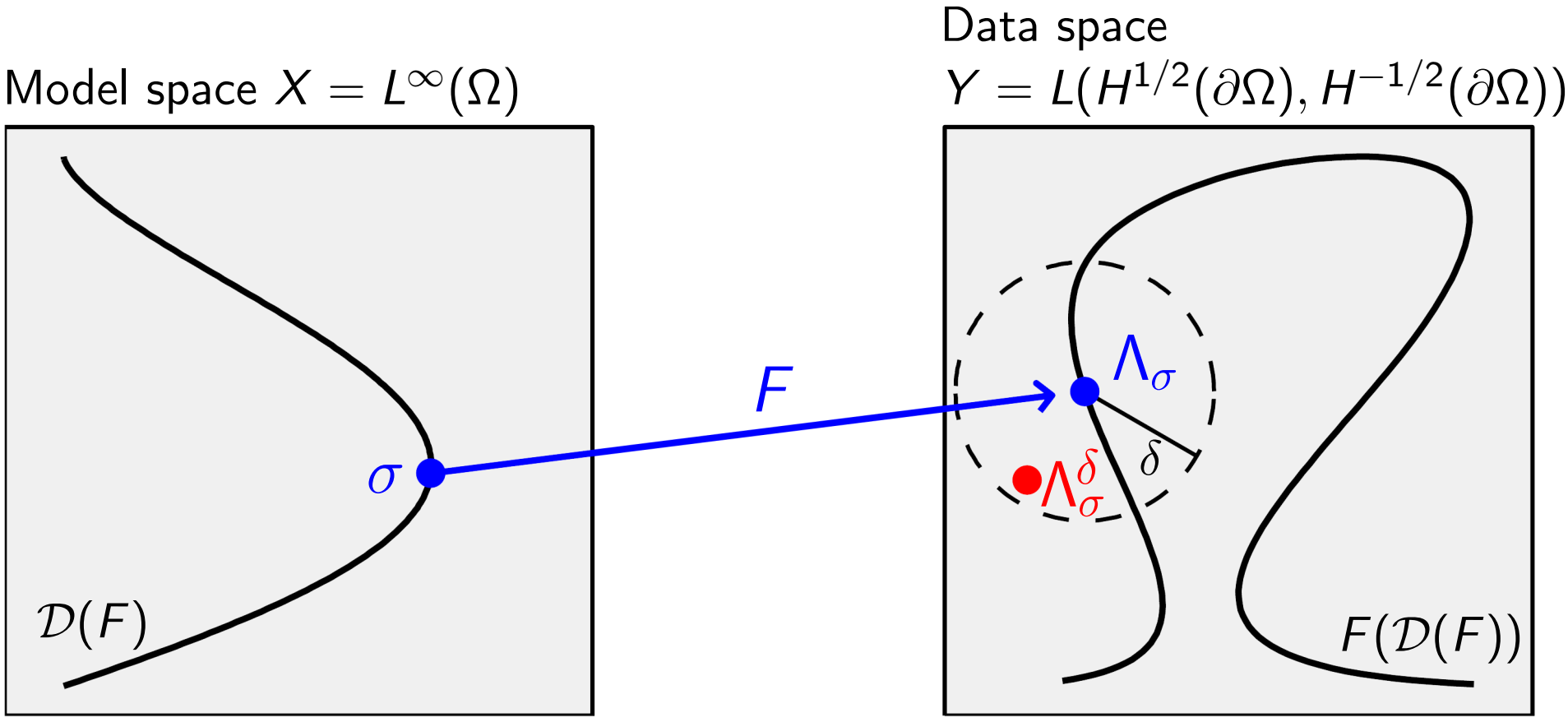

Furthermore, the noisy data Λ_σ^δ does not belong to the range $F(\mathcal{D}(F))$. So Hadamard's conditions 1 and 3 fail for EIT. How about uniqueness?

Ghosts, or invisible structures, when using point electrodes in electrical impedance tomography

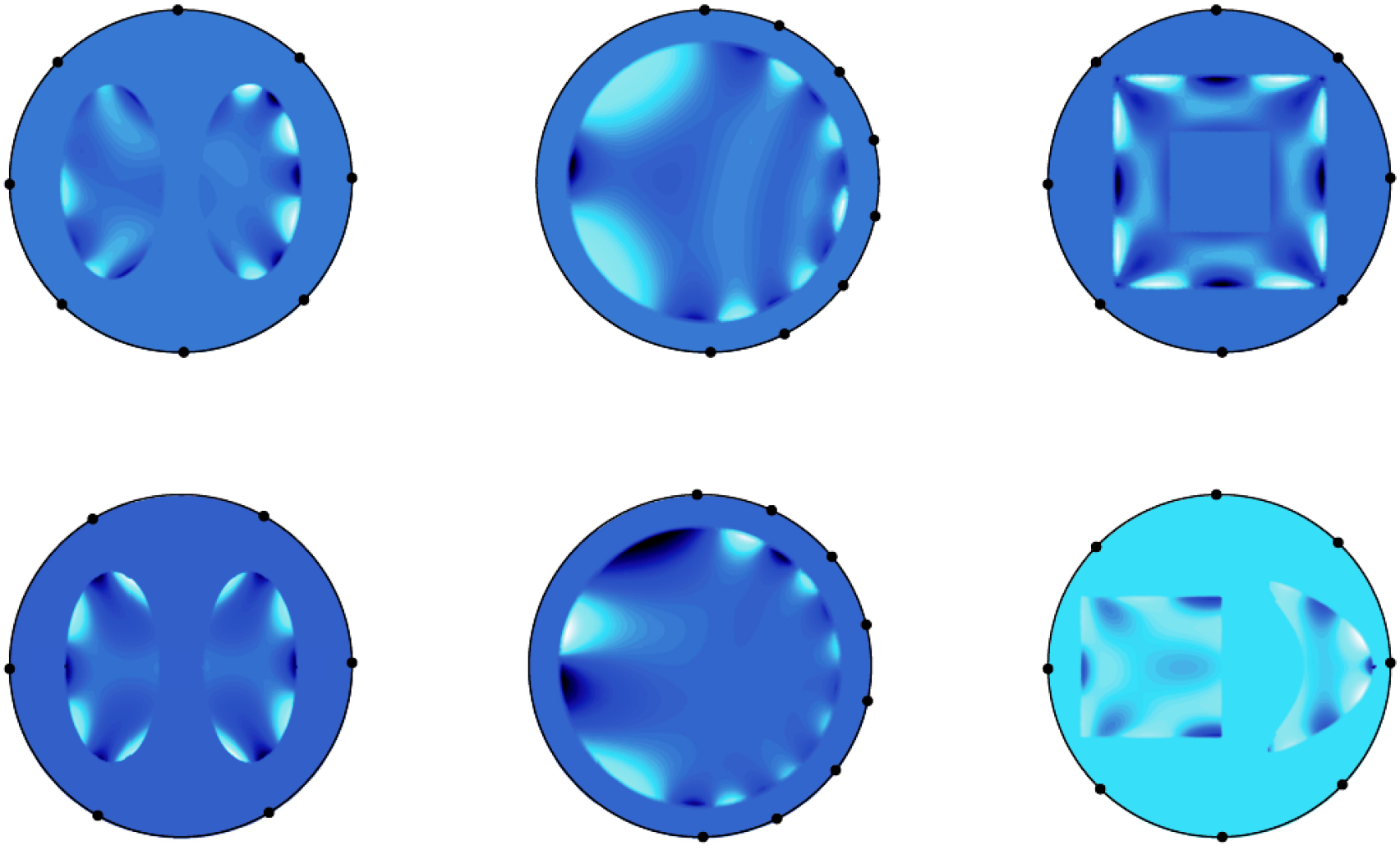

[Chesnel, Hyvönen & Staboulis 2014]

Regularization means constructing a continuous map $\Gamma_\alpha : Y \to X$ that inverts F approximately

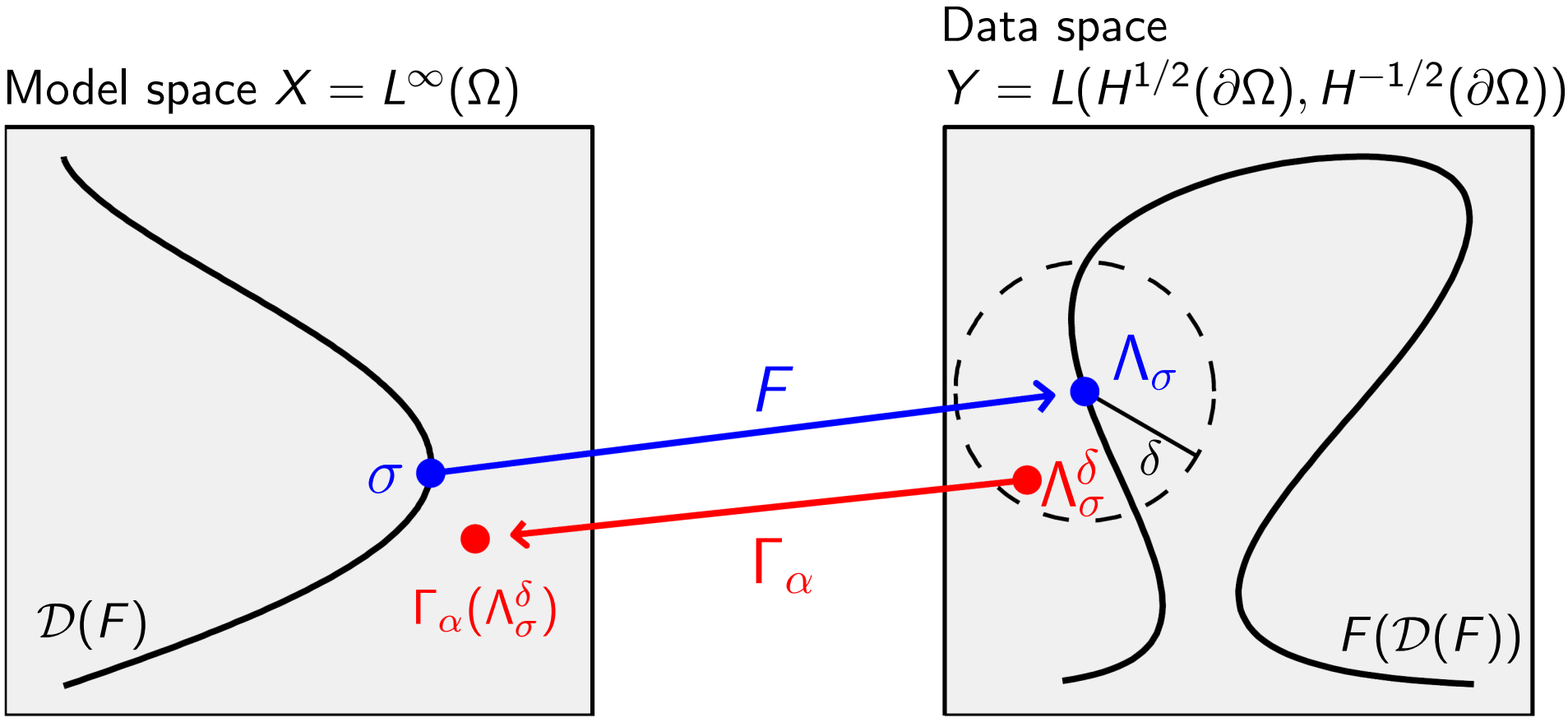

Regularization must be based on combining the incomplete measurement data with *a priori* information about the conductivity.

References about foundations of Electrical Impedance Tomography

Classical review article by the legendary EIT group of RPI:

Margaret Cheney, David Isaacson and Jon Newell (1999), *Electrical Impedance Tomography.* SIAM Review **41**.

Mathematical treatment of electrode measurements:

Erkki Somersalo, Margaret Cheney and David Isaacson (1992),

Nuutti Hyvönen (2009).

More recent review of EIT:

Jennifer Mueller and S (2012)

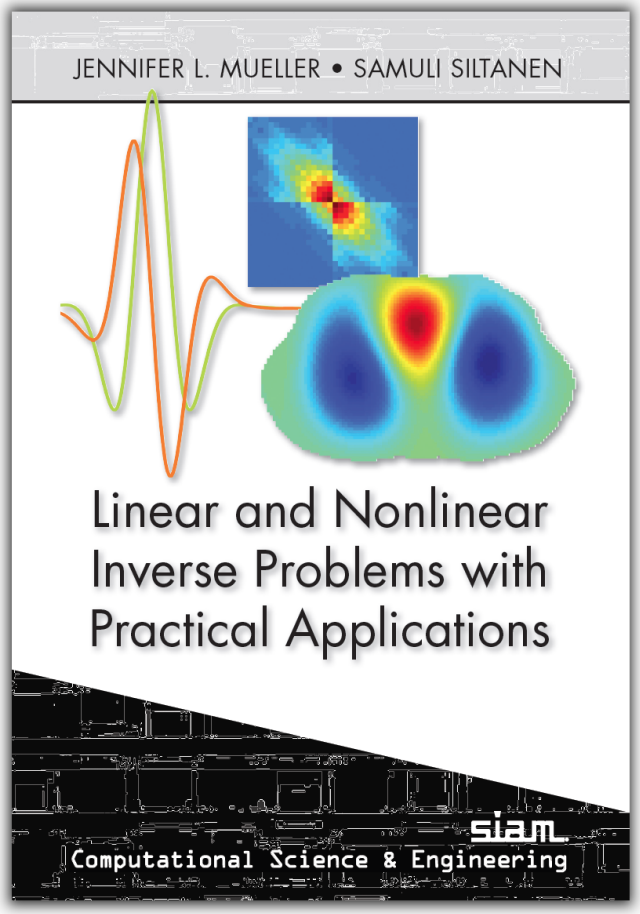

Outline

This part is a joint work with

David Isaacson, Rensselaer Polytechnic Institute, USA

Kim Knudsen, Technical University of Denmark

Matti Lassas, University of Helsinki, Finland

Jon Newell, Rensselaer Polytechnic Institute, USA

Jennifer Mueller, Colorado State University, USA

There exists a nonlinear Fourier transform adapted to electrical impedance tomography

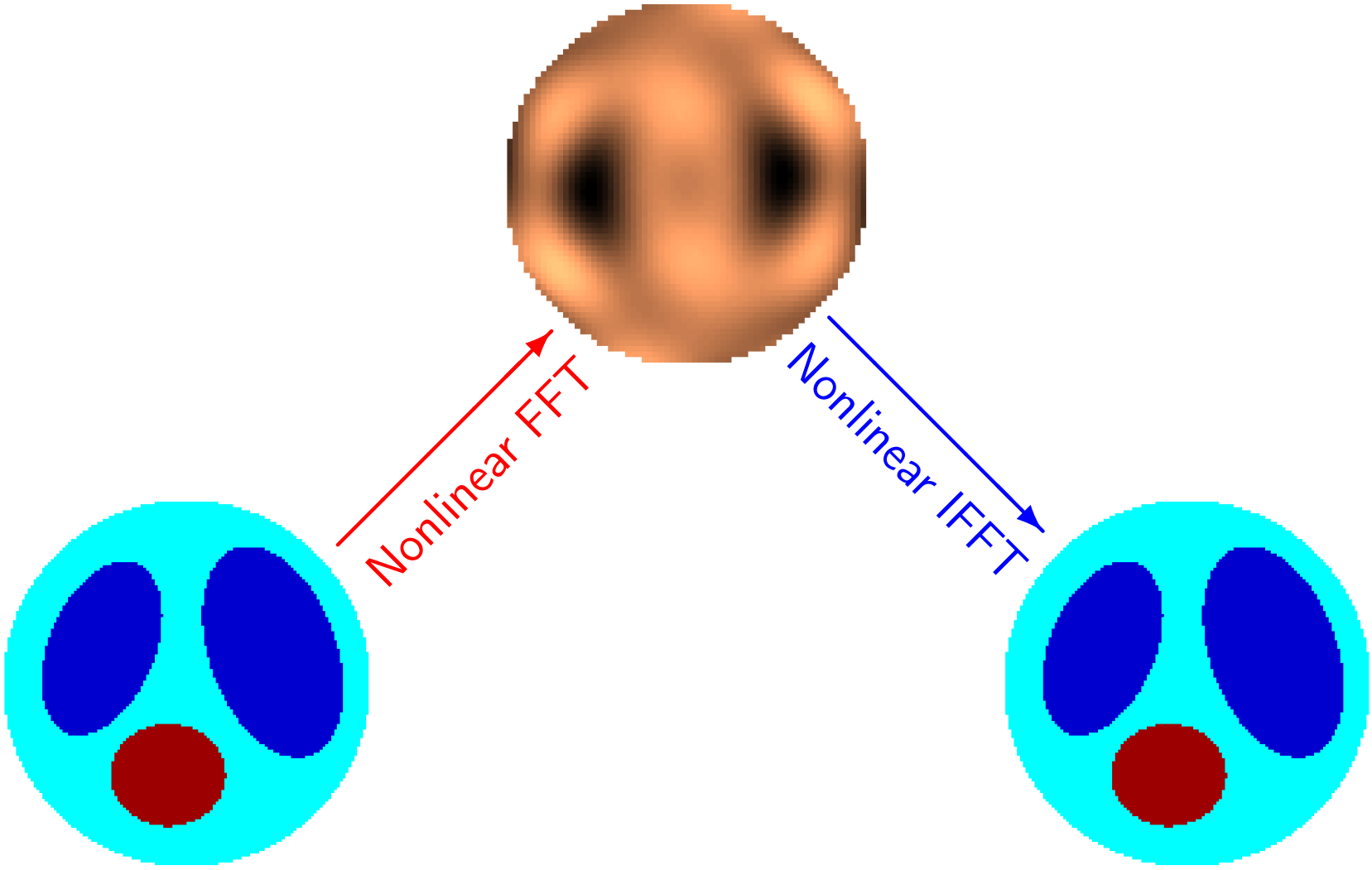

The nonlinear Fourier transform can be recovered from infinite-precision EIT measurements

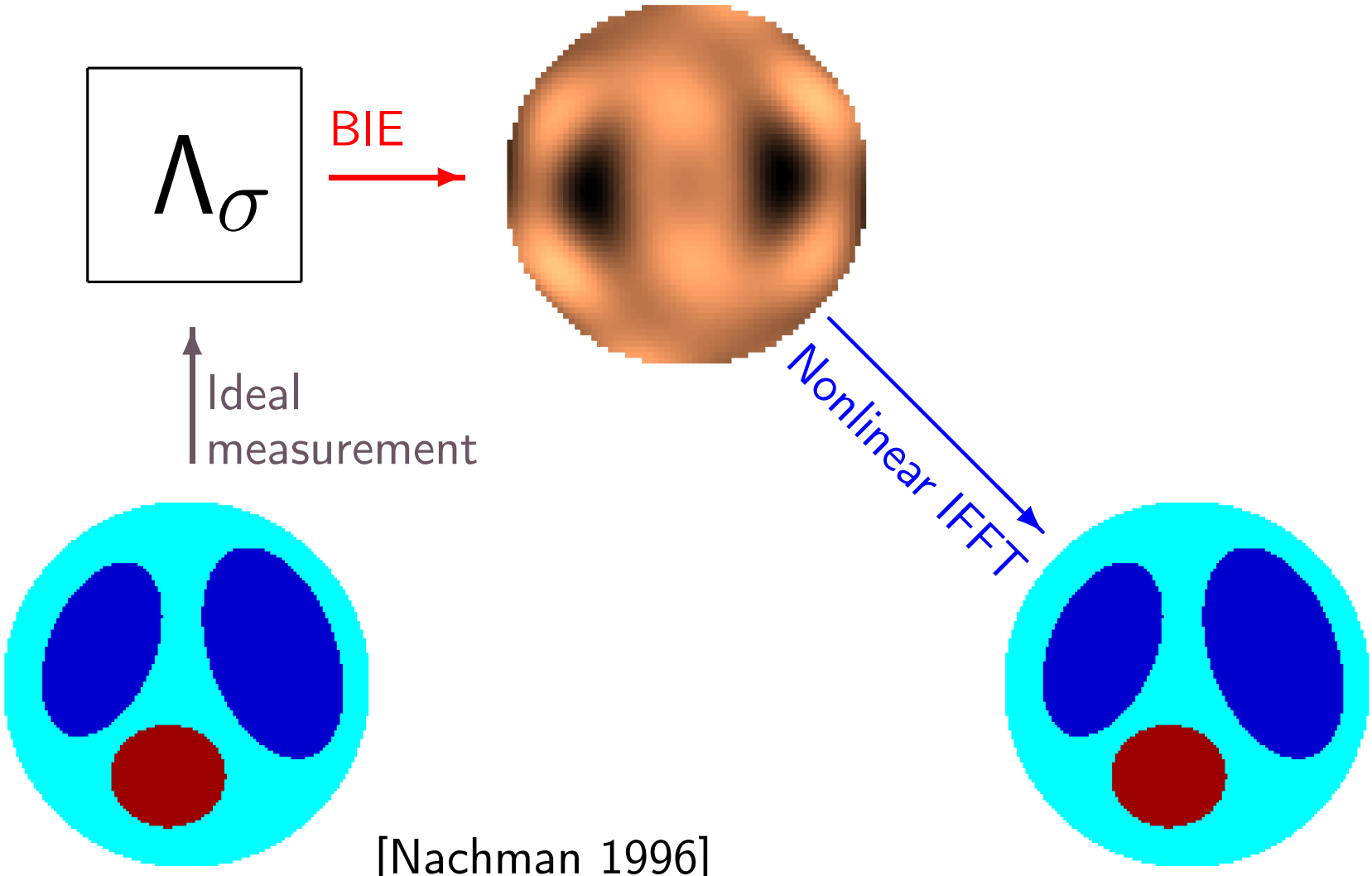

[Nachman 1996]

Measurement noise prevents the recovery of the nonlinear Fourier transform at high frequencies

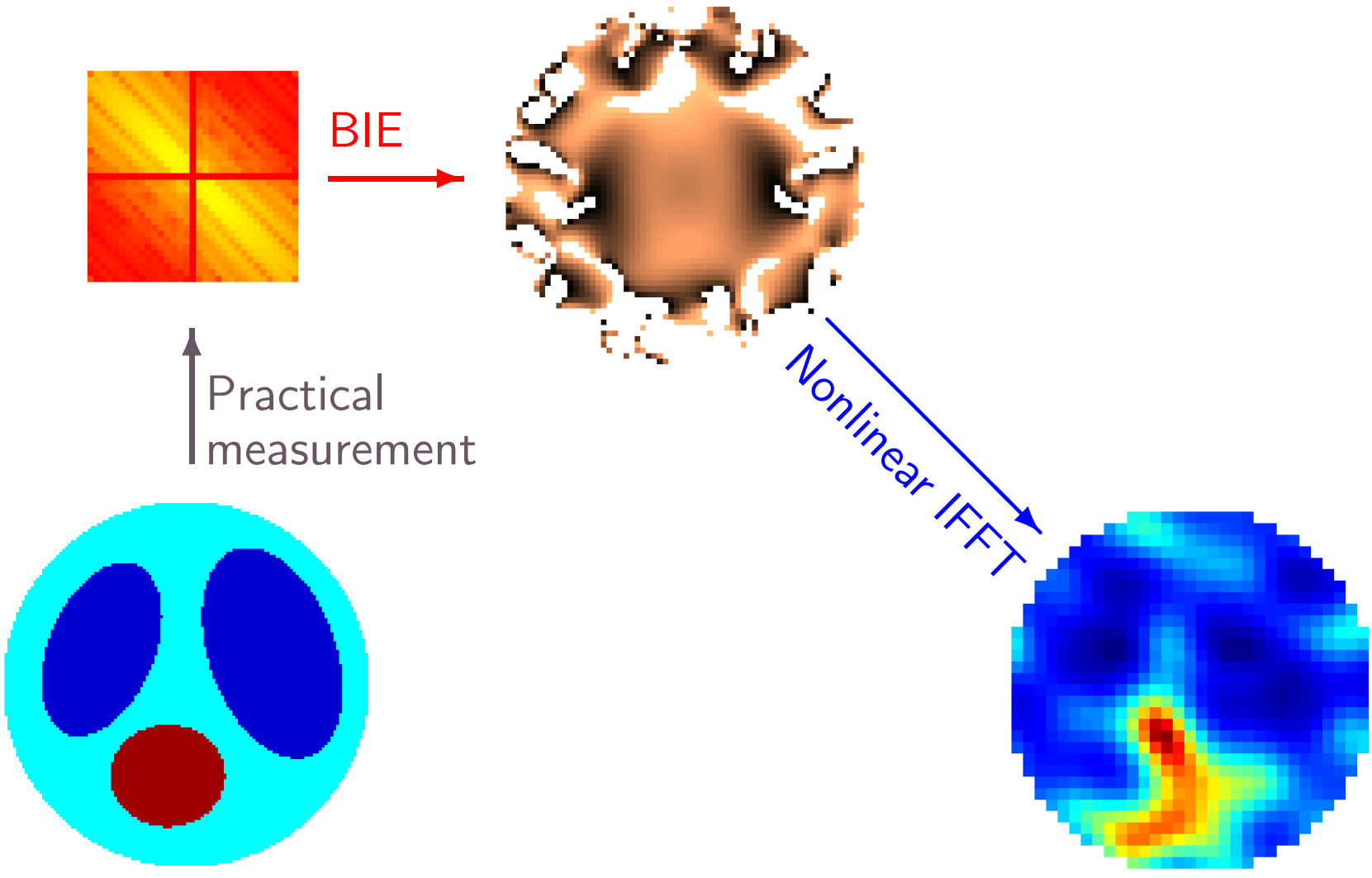

We truncate away the bad part in the transform; this is a nonlinear low-pass filter

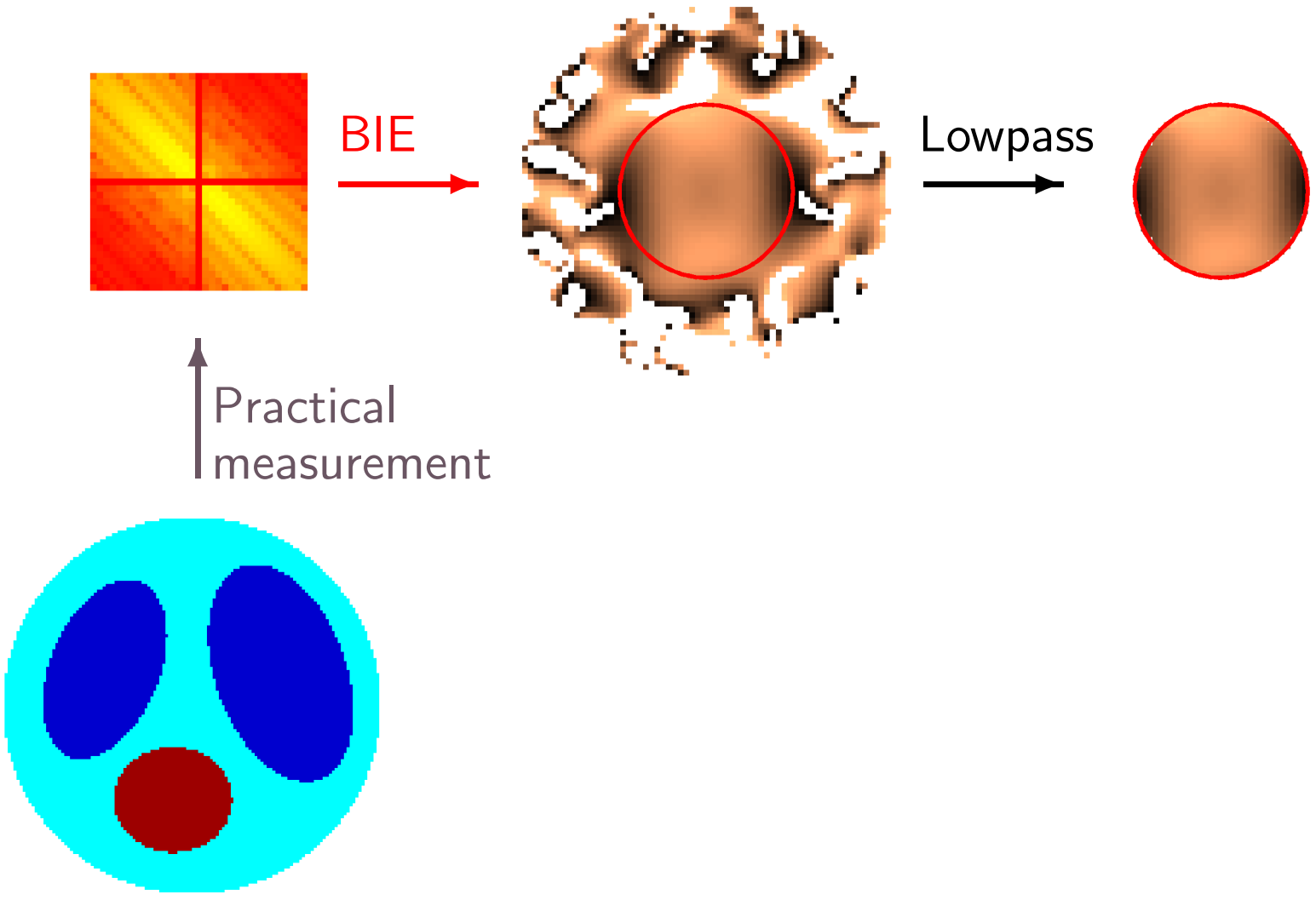

The D-bar method is a regularization strategy for reconstructing the full conductivity distribution

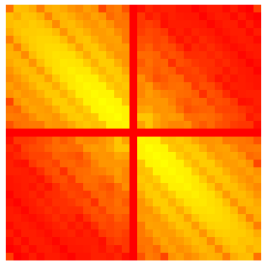

BIE

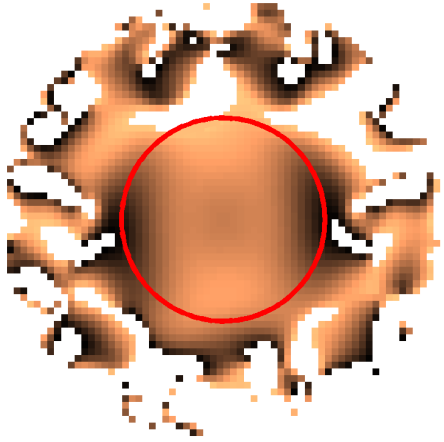

Lowpass

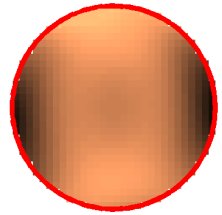

Nonlinear
IFFT

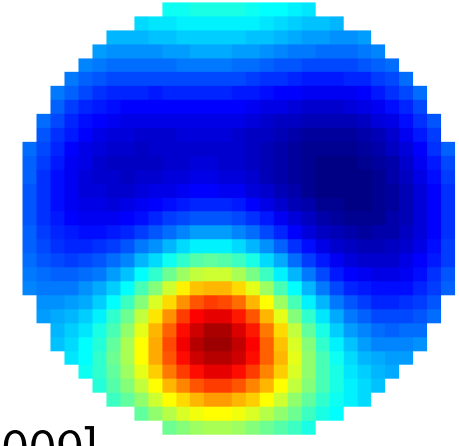

Practical
measurement

[S, Mueller & Isaacson 2000]
[Knudsen, Lassas, Mueller & S 2009]

This is a brief history of the two-dimensional regularized D-bar method for EIT

1966 Faddeev: Complex geometric optics (CGO) solutions

1987 Sylvester and Uhlmann: CGO solutions for inverse boundary-value problems; uniqueness for 3D EIT with smooth conductivities and infinite-precision data

1988 R. G. Novikov: Core ideas of the D-bar method

1988 Nachman: D-bar method for 3D EIT

1996 Nachman: Uniqueness and reconstruction for 2D EIT with C^2 conductivities and infinite-precision data

1999 S: First numerical evaluation of CGO solutions

2000 S, Mueller and Isaacson: Numerical implementation of Nachman's proof using a Born approximation

2006 Isaacson, Mueller, Newell and S: Application of the D-bar method to EIT data measured from a human subject

2009 Knudsen, Lassas, Mueller and S: Regularization proof

Nachman (1996) transforms to the Schrödinger equation and uses CGO solutions

Define a potential q by setting $q(z) \equiv 0$ for z outside Ω and

$$q(z) = \frac{\Delta\sqrt{\sigma(z)}}{\sqrt{\sigma(z)}} \quad \text{for } z \in \Omega.$$

Then $q \in C_0(\Omega)$. We look for solutions of the Schrödinger equation

$$(-\Delta + q)\psi(\,\cdot\,, k) = 0 \quad \text{in } \mathbb{R}^2$$

parametrized by $k \in \mathbb{C} \setminus 0$ and satisfying the asymptotic condition

$$e^{-ikz}\psi(z, k) - 1 \in W^{1,\tilde{p}}(\mathbb{R}^2),$$

where $\tilde{p} > 2$ and $ikz = i(k_1 + ik_2)(x + iy)$.

The CGO solutions are constructed using a generalized Lippmann-Schwinger equation

Define $\mu(z,k) = e^{-ikz}\psi(z,k)$. Then $(-\Delta + q)\psi = 0$ implies

$$(-\Delta - 4ik\overline{\partial}_z + q)\mu(\,\cdot\,,k) = 0, \tag{1}$$

where the D-bar operator is defined by $\overline{\partial}_z = \frac{1}{2}(\frac{\partial}{\partial x} + i\frac{\partial}{\partial y})$.

A solution of (1) satisfying $\mu(z,k) - 1 \in W^{1,\tilde{p}}(\mathbb{R}^2)$ can be constructed using the Lippmann-Schwinger type equation

$$\mu = 1 - g_k * (q\mu),$$

where g_k satisfies $(-\Delta - 4ik\overline{\partial}_z)g_k = \delta$ and is defined by

$$g_k(z) = \frac{1}{4\pi^2}\int_{\mathbb{R}^2} \frac{e^{iz\cdot\xi}}{|\xi|^2 + 2k(\xi_1 + i\xi_2)}\, d\xi_1 d\xi_2.$$

One of the breakthroughs in Nachman's 1996 article is showing uniqueness of μ

A solution of $(-\Delta - 4ik\overline{\partial}_z + q)\mu(\,\cdot\,, k) = 0$ satisfying $\mu(z,k) - 1 \in W^{1,\tilde{p}}(\mathbb{R}^2)$ can be constructed using the formula

$$\mu - 1 = [I + g_k * (q\cdot\,)]^{-1}(g_k * q),$$

provided that the inverse operator exists.

Now $q \in L^p(\mathbb{R}^2)$ with $1 < p < 2$ and $1/\tilde{p} = 1/p - 1/2$, and

$$\begin{aligned} q\cdot \quad &: \quad W^{1,\tilde{p}}(\mathbb{R}^2) \to L^p(\mathbb{R}^2) \quad \text{is bounded,} \\ g_k* \quad &: \quad L^p(\mathbb{R}^2) \to W^{1,\tilde{p}}(\mathbb{R}^2) \quad \text{is compact.} \end{aligned}$$

Thus $I + g_k * (q\cdot\,) : W^{1,\tilde{p}}(\mathbb{R}^2) \to W^{1,\tilde{p}}(\mathbb{R}^2)$ is Fredholm of index zero, and Nachman proved injectivity for all $k \neq 0$.

Progress on invertibility of $I + g_k * (q\cdot\,)$: Music, Perry & S (2013), Music (2014), Lakshtanov & Vainberg (2017)

The non-physical scattering transform $\mathbf{t}(k)$ is a nonlinear Fourier transform

We denote $z = x + iy \in \mathbb{C}$ and $z = (x, y) \in \mathbb{R}^2$. The scattering transform $\mathbf{t} : \mathbb{C} \to \mathbb{C}$ is defined by

$$\mathbf{t}(k) := \int_{\mathbb{R}^2} e^{i\bar{k}\bar{z}} q(z)\psi(z, k)\, dxdy.$$

Sometimes $\mathbf{t}(k)$ is called the nonlinear Fourier transform of q. This is because asymptotically $\psi(z, k) \sim e^{ikz}$ as $|z| \to \infty$, and substituting e^{ikz} in place of $\psi(z, k)$ above gives

$$\begin{aligned} \int_{\mathbb{R}^2} e^{i(kz+\bar{k}\bar{z})} q(z) dxdy &= \int_{\mathbb{R}^2} e^{-i(-2k_1, 2k_2)\cdot(x,y)} q(z) dxdy \\ &= \widehat{q}(-2k_1, 2k_2). \end{aligned}$$

Infinite-precision data:

Solve boundary integral equation

$$\psi(\,\cdot\,,k)|_{\partial\Omega} = e^{ikz} - \mathcal{S}_k(\Lambda_\sigma - \Lambda_1)\psi$$

for every complex number $k \in \mathbb{C} \setminus 0$.

Evaluate the scattering transform:

$$\mathbf{t}(k) = \int_{\partial\Omega} e^{i\bar{k}\bar{z}}(\Lambda_\sigma - \Lambda_1)\psi(\cdot,k)\,ds.$$

Fix $z \in \Omega$. Solve D-bar equation

$$\frac{\partial}{\partial\bar{k}}\mu(z,k) = \frac{\mathbf{t}(k)}{4\pi\bar{k}}e^{-i(kz+\bar{k}\bar{z})}\overline{\mu(z,k)}$$

with $\mu(z,\,\cdot\,) - 1 \in L^r \cap L^\infty(\mathbb{C})$.

Reconstruct: $\sigma(z) = (\mu(z,0))^2$.

Practical data:

Solve boundary integral equation

$$\psi^\delta(\,\cdot\,,k)|_{\partial\Omega} = e^{ikz} - \mathcal{S}_k(\Lambda^\delta_\sigma - \Lambda_1)\psi^\delta$$

for all $0 < |k| < R = -\frac{1}{10}\log\delta$.

For $|k| \geq R$ set $\mathbf{t}^\delta_R(k) = 0$. For $|k| < R$

$$\mathbf{t}^\delta_R(k) = \int_{\partial\Omega} e^{i\bar{k}\bar{z}}(\Lambda^\delta_\sigma - \Lambda_1)\psi^\delta(\cdot,k)\,ds.$$

Fix $z \in \Omega$. Solve D-bar equation

$$\frac{\partial}{\partial\bar{k}}\mu^\delta_R(z,k) = \frac{\mathbf{t}^\delta_R(k)}{4\pi\bar{k}}e^{-i(kz+\bar{k}\bar{z})}\overline{\mu^\delta_R(z,k)}$$

with $\mu^\delta_R(z,\,\cdot\,) - 1 \in L^r \cap L^\infty(\mathbb{C})$.

Set $\Gamma_{1/R(\delta)}(\Lambda^\delta_\sigma) := (\mu^\delta_R(z,0))^2$.

Nonlinear low-pass filtering yields a regularization strategy with convergence speed

Theorem (Knudsen, Lassas, Mueller & S 2009)

Fix a conductivity $\sigma \in \mathcal{D}(F)$. Assume given noisy data Λ_σ^δ satisfying

$$\|\Lambda_\sigma^\delta - \Lambda_\sigma\|_Y \leq \delta.$$

Then Γ_α with the choice

$$R(\delta) = -\frac{1}{10}\log\delta, \qquad \alpha(\delta) = \frac{1}{R(\delta)},$$

is well-defined, admissible and satisfies the estimate

$$\|\Gamma_{\alpha(\delta)}(\Lambda_\sigma^\delta) - \sigma\|_{L^\infty(\Omega)} \leq C(-\log\delta)^{-1/14}.$$

See also [Lytle, Perry & S 2019]

Regularized reconstructions from simulated data with noise amplitude $\|\delta\| = \|\Lambda_\sigma^\delta - \Lambda_\sigma\|_Y$

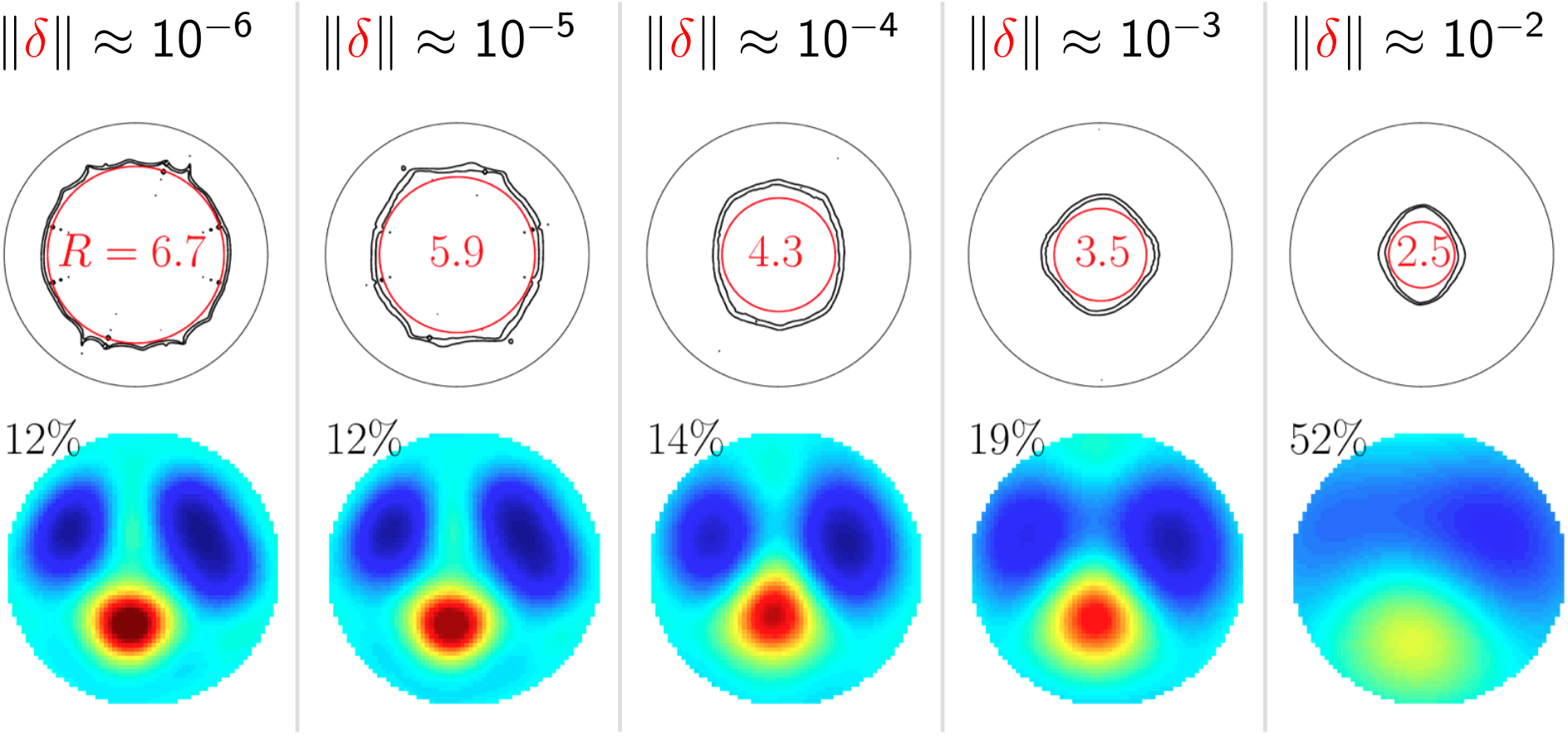

The percentages are the relative square norm errors in the reconstructions.

Here are the D-bar reconstructions from simulated EIT data using frequency cutoff $R = 4$

σ_1

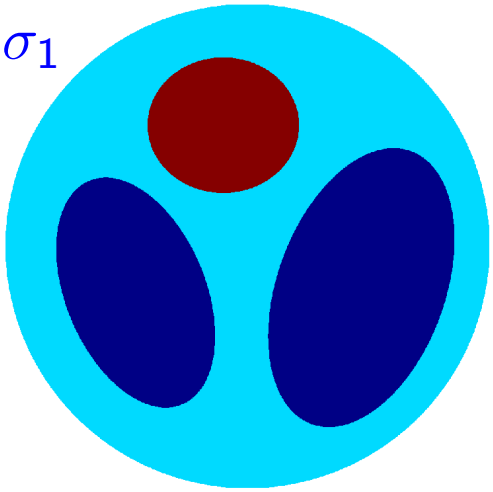

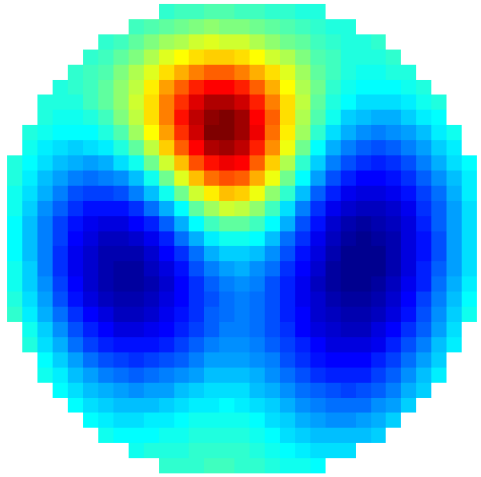

σ_2

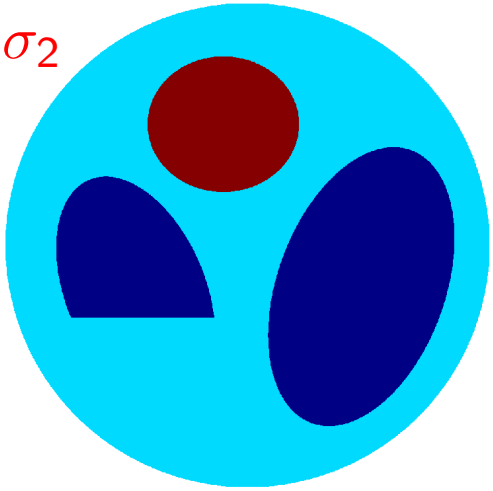

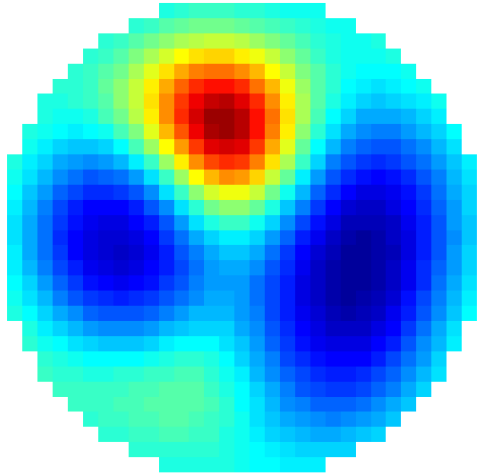

D-bar images can be sharpened by Deep Learning

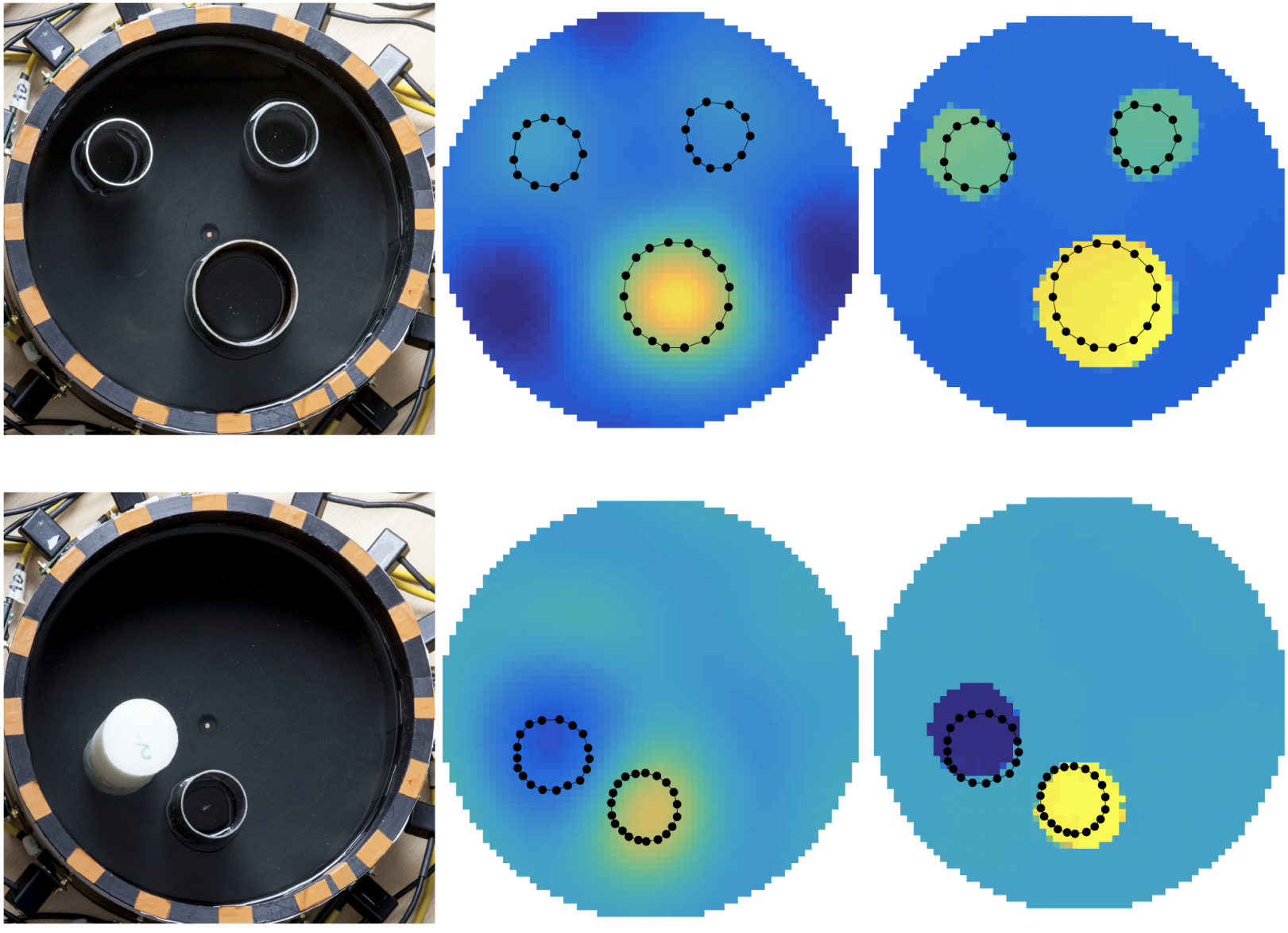

[Hamilton & Hauptmann 2017]

Medical application of EIT and the D-bar method: quantifying air-trapping in cystic fibrosis patients

All results on this slide are from Jennifer Mueller's group at Colorado State University.

Images: ventilation-perfusion index maps, computed from three subjects at Children's Hospital Colorado using EIT and the D-bar method.

Dark blue regions are well-perfused but poorly ventilated.

Radiologist's report for Subject B: extensive regions of air trapping, regional to the lung areas affected by plugging, approximately 50% of both lungs.

Healthy control
Average index 0.46

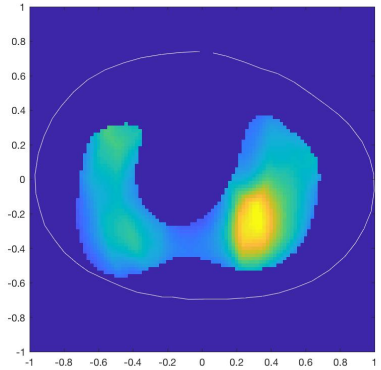

CF Subject A
Average index 0.34

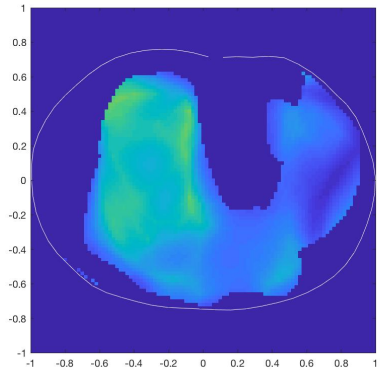

CF Subject B
Average index 0.10

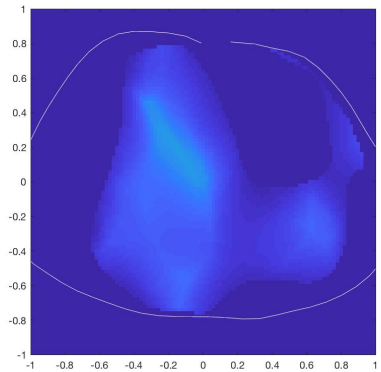

Outline

The results in this part are a joint work with

Juan Pablo Agnelli, Universidad Nacional de Córdoba, Argentina

Aynur Çöl, Sinop university, Turkey

Allan Greenleaf, University of Rochester, NY, USA

Matti Lassas, University of Helsinki, Finland

Rashmi Murthy, University of Helsinki, Finland

Matteo Santacesaria, University of Genoa, Italy

Gunther Uhlmann, University of Washington, USA

This is an X-ray tomography machine (not EIT)

Wikimedia commons

Simple example of tomographic imaging with a double-disc target

https://youtu.be/5DUGTXd26nA

We can back-project the measured data into the image, integrating over all directions

https://youtu.be/5DUGTXd26nA

Final FBP reconstruction involves filtering on top of the back-projection

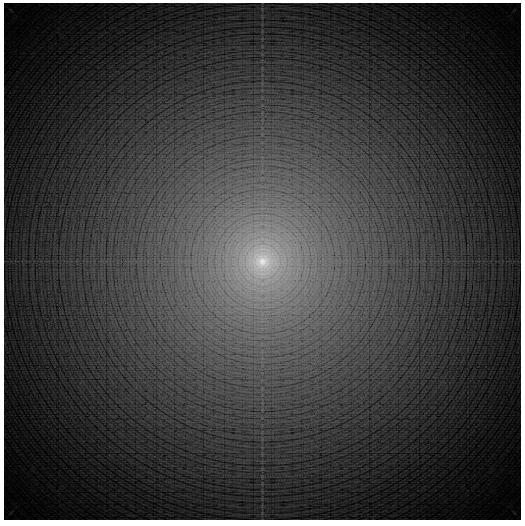

Multiplication by $|\xi|$

(Calderón's operator)

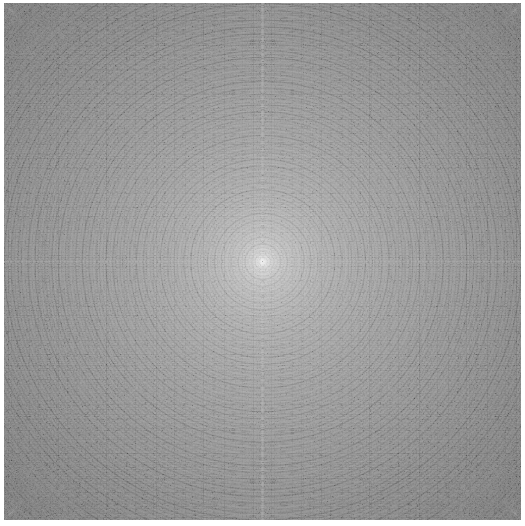

FFT

IFFT

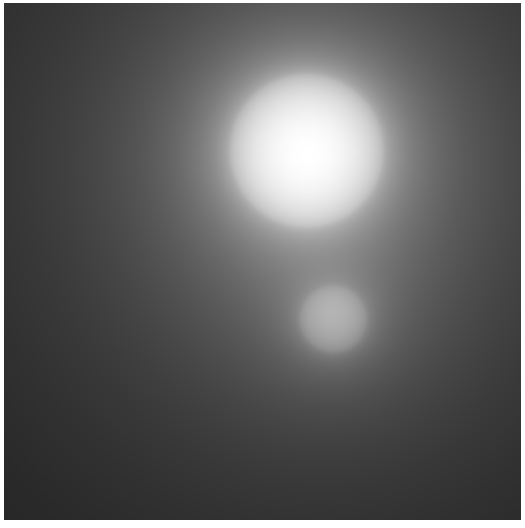

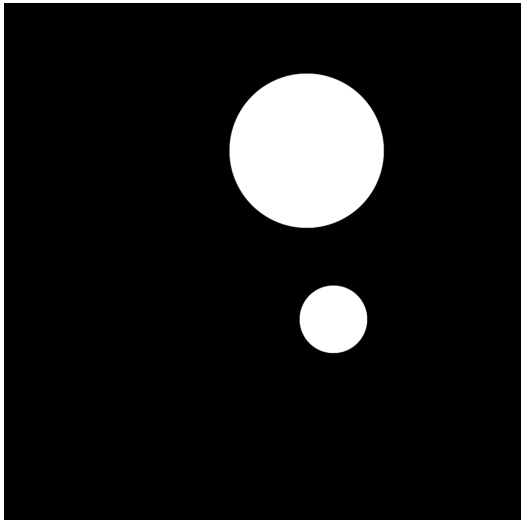

Medical application: classifying stroke

Ischemic stroke:
low conductivity.
CT image from
Jansen 2008

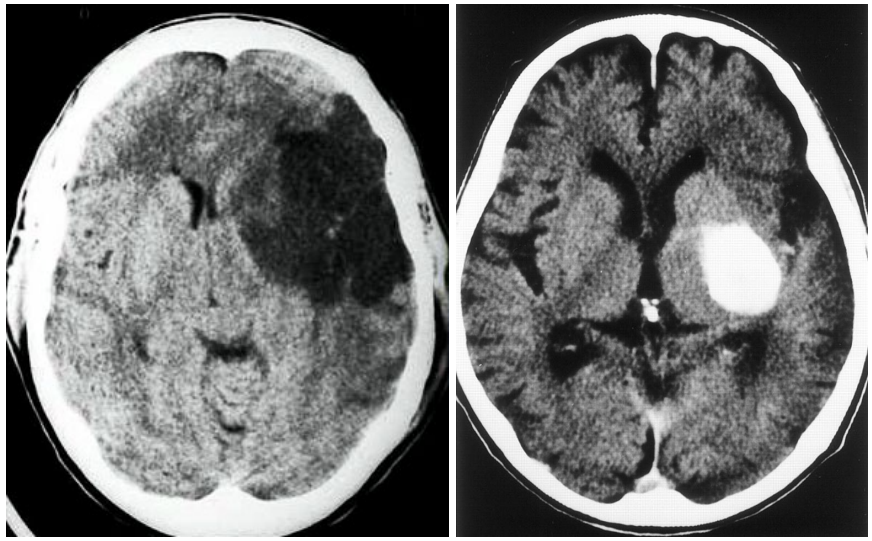

Hemorrhagic stroke:
high conductivity.
CT image from
Nakano *et al.* 2001

Same symptoms in both cases!

Back to EIT: analyse Complex Geometric Optics solutions using complex two-vectors

Consider complex two-vectors $\eta \in \mathbb{C}^2$ of the form

$$\eta = (\theta_1 + i\theta_2, -\theta_2 + i\theta_1),$$

where $\theta = \theta_1 + i\theta_2 \in \mathbb{C}$ is a unitary complex number: $|\theta| = 1$.

Denote a planar point by $x = (x_1, x_2) \in \mathbb{R}^2$. Because $\eta \cdot \eta = 0$ we see that $e^{i\tau\eta\cdot x} = 0$ is harmonic in x.

We next analyse solutions of the conductivity equation $\nabla \cdot \sigma \nabla u = 0$ of the form

$$u(x) = e^{i\tau\eta\cdot x} w(x, \tau).$$

(They are connected to the previously discussed CGO solutions via $k = \tau\theta$ and $z = x_1 + ix_2$, since then $e^{ikz} = e^{i\tau\theta z} = e^{i\tau\eta\cdot x}$.)

Since $u(x) = e^{i\tau\eta\cdot x} w(x,\tau)$ satisfies the conductivity equation,

$$
\begin{aligned}
0 &= \frac{1}{\sigma(x)} \nabla \cdot (\sigma(x) \nabla u(x)) \\
&= (\Delta + \frac{1}{\sigma}(\nabla\sigma)\cdot\nabla)(e^{i\tau\eta\cdot x} w(x,\tau)) \\
&= \left(\Delta w(x,\tau) + 2i\tau\eta\cdot\nabla w(x,\tau) + (\frac{1}{\sigma}\nabla\sigma)\cdot(\nabla + i\tau\eta) w(x,\tau) \right) e^{i\tau\eta\cdot x}.
\end{aligned}
$$

Hence, we have

$$
\Delta w(x,\tau) + 2i\tau\eta\cdot\nabla w(x,\tau) + (\frac{1}{\sigma}\nabla\sigma)\cdot(\nabla + i\tau\eta) w(x,\tau) = 0.
$$

New trick: apply one-dimensional Fourier transform to the complex spectral parameter

Let $\widehat{w}(x,t)$ be the Fourier transform of $w(x,\tau)$ in the τ variable:

$$\widehat{w}(x,t) = \mathcal{F}w(x,t) = \int_{-\infty}^{\infty} e^{-it\tau} w(x,\tau)\, d\tau.$$

We call t the *pseudo-time* corresponding to complex frequency τ. Then equation

$$\Delta w(x,\tau) + 2i\tau\eta \cdot \nabla w(x,\tau) + (\frac{1}{\sigma}\nabla\sigma)\cdot(\nabla + i\tau\eta)w(x,\tau) = 0$$

yields

$$\Delta \widehat{w}(x,t) + 2\eta\frac{\partial}{\partial t}\cdot\nabla\widehat{w}(x,t) + (\frac{1}{\sigma}\nabla\sigma)\cdot(\nabla + \eta\frac{\partial}{\partial t})\widehat{w}(x,t) = 0.$$

Complex principal type operator leads to singularities propagating along leaves

Denote $\eta = \eta_R + i\eta_I$. The principal part of the equation

$$\Delta \widehat{w}(x,t) + 2\eta \frac{\partial}{\partial t} \cdot \nabla \widehat{w}(x,t) + \frac{1}{\sigma}(\nabla\sigma) \cdot (\nabla + \eta \frac{\partial}{\partial t}) \widehat{w}(x,t) = 0$$

is given by the complex principal type operator

$$\Delta + 2\eta \frac{\partial}{\partial t} \cdot \nabla = \left(\Delta + 2\eta_R \frac{\partial}{\partial t} \cdot \nabla \right) + i \left(2\eta_I \frac{\partial}{\partial t} \cdot \nabla \right),$$

in the sense of Duistermaat and Hörmander (1972).

For a real principal type operator the characteristic singularities propagate along one-dimensional rays. For instance, for the wave equation the light-like singularities propagate along light rays.

For a complex principal type operator the characteristic singularities propagate along two-dimensional surfaces called *leaves*.

We use propagation and reflection of singularities along leaves for detecting inclusions

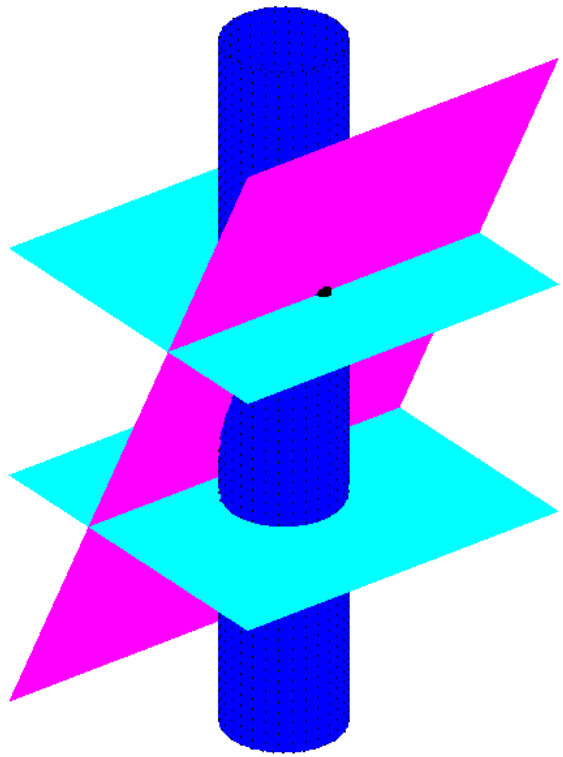

Here the magenta plane wave hits the blue surface, producing light blue reflected waves.

We use the Beltrami-type complex geometric optics (CGO) solutions

Set $\mu := (1-\sigma)/(1+\sigma)$. Write $f = u + iv$ and note that

$$\overline{\partial}_z f_\mu = \mu \overline{\partial_z f_\mu} \quad \Leftrightarrow \quad \nabla \cdot \sigma \nabla u = 0 \ \text{ and } \ \nabla \cdot \sigma^{-1} \nabla v = 0.$$

The CGO solutions of [Astala-Päivärinta 2006] have the form

$$\begin{aligned} f_\mu(z,k) &= e^{ikz}(1+\omega^+(z,k)), \\ f_{-\mu}(z,k) &= e^{ikz}(1+\omega^-(z,k)), \end{aligned}$$

with the asymptotic condition

$$\omega^\pm(z,k) = \mathcal{O}(\frac{1}{z}) \text{ as } |z| \to \infty.$$

Here $ikz = i(k_1 + ik_2)(x+iy)$ and $\overline{\partial}_z = \frac{1}{2}(\partial_x + i\partial_y)$.

This is a brief history of computational solution methods for the Beltrami CGO solutions

1987 Sylvester and Uhlmann: Introduction of CGO solutions
2000 S, Mueller and Isaacson: Numerical CGOs
2006 Astala and Päivärinta: Original Beltrami-type construction

2010 Astala, Mueller, Päivärinta and S:
First numerical solution method

2011 Astala, Mueller, Päivärinta, Perämäki and S:
Novel EIT reconstruction method

2012 Huhtanen and Perämäki:
Preconditioned Krylov subspace method for real-linear systems

2014 Astala, Päivärinta, Reyes and S:
Computational high-frequency experiments

2018 Greenleaf, Lassas, Santacesaria, S and Uhlmann:
Virtual Hybrid Edge Detection based on 1D Fourier technique

Recovery by "filtered back-projection"

Theorem. (Greenleaf, Lassas, Santacesaria, S and Uhlmann 2018) Define averaged operators $T_j^{\pm}$ for $j = 1, 2, 3, \ldots$ by the complex contour integral:

$$T_j^{\pm}\mu(t, e^{i\varphi}) \quad = \quad \frac{1}{2\pi i}\int_{\partial\Omega} \widehat{\omega}_j^{\pm}(z, t, e^{i\varphi})dz,$$

Then we have a filtered back-projection formula

$$(-\Delta)^{-1/2}(T_1^{\pm})^* T_1^{\pm}\mu = \mu.$$

Compare to X-ray tomography FBP formula $(-\Delta)^{1/2}R^*Rf = f$.

New result: inverse scattering methods can transform EIT into "X-ray tomography"

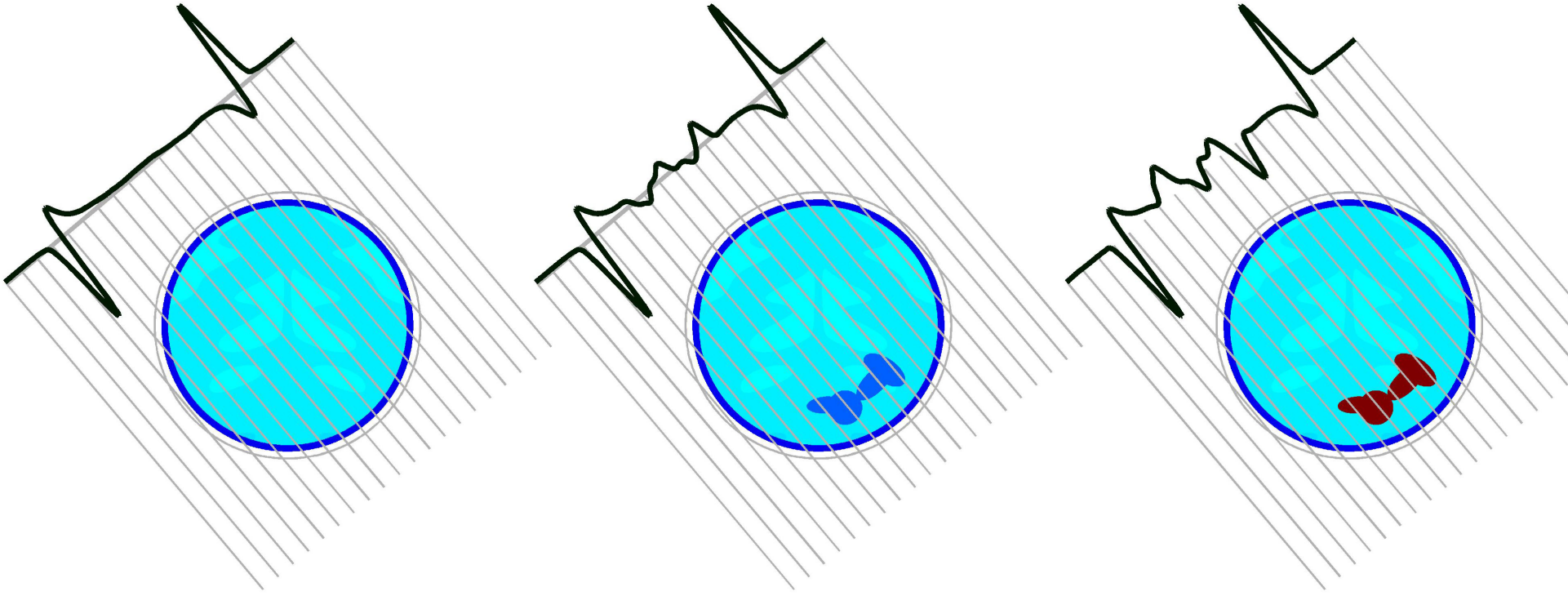

https://www.youtube.com/watch?v=37yOCfBfRJk

[Greenleaf, Lassas, Santacesaria, S and Uhlmann 2018]

Conductivity

Filtered back-projection

“Λ-tomography”

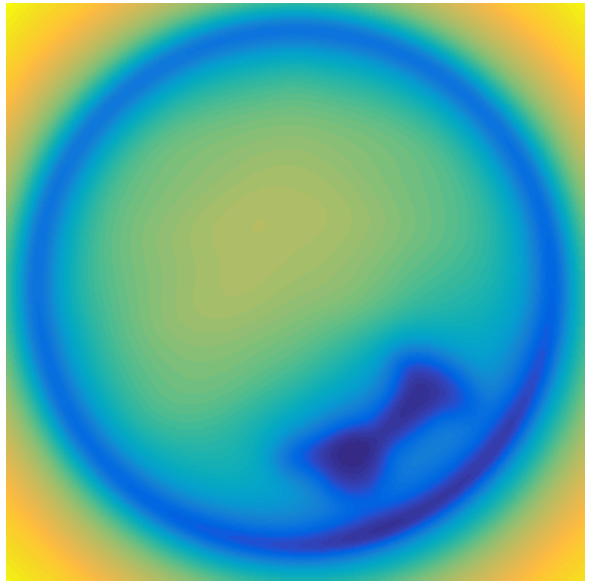

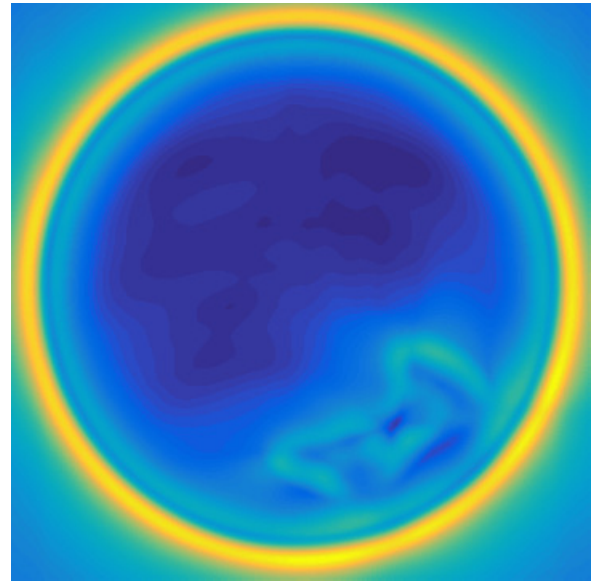

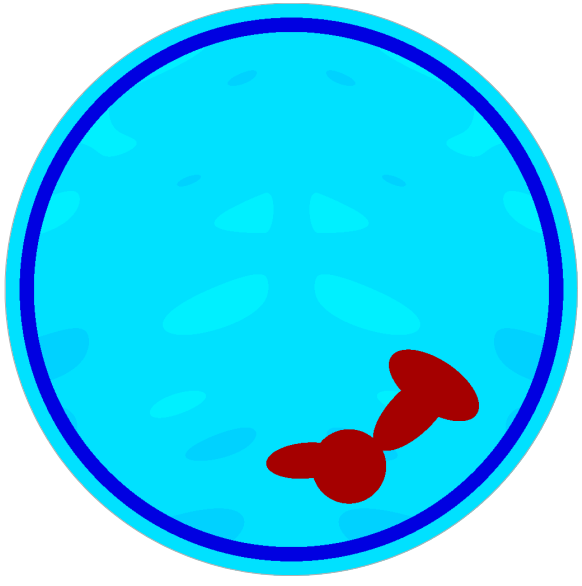

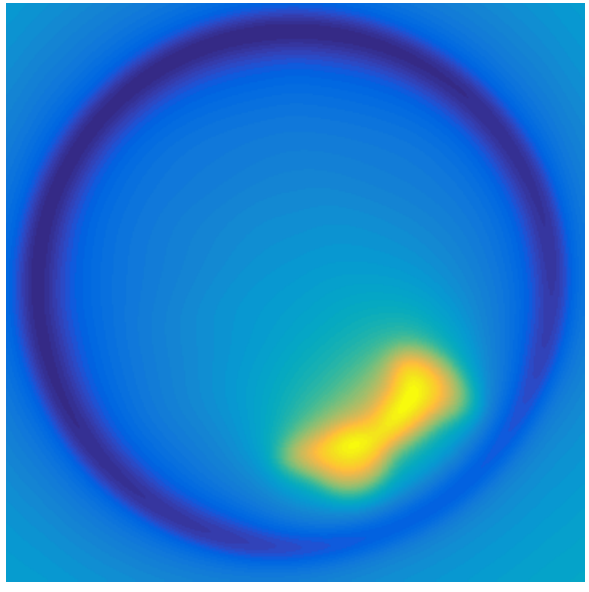

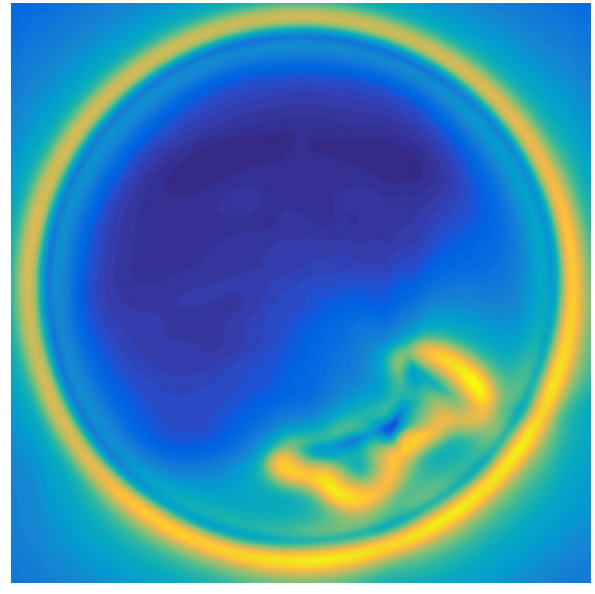

The idea would be to equip every ambulance with an EIT device for classifying strokes

In David Holder's lab at UCL

We have a collaboration network in place for the stroke-EIT project

Project funded for 2017–2020

- Jari Hyttinen & Antti Paldanius (U Tampere)
- Ville Kolehmainen, Asko Hänninen & Jussi Toivanen (U Eastern Finland)
- S, Matti Lassas & Rashmi Murthy (U Helsinki)

Finnish collaboration:

Stefan Björkman (U Helsinki)
Valentina Candiani (Aalto U)
Antti Hannukainen (Aalto U)
Nuutti Hyvönen (Aalto U)
Nina Forss
Daniel Strbian

International collaboration:

Juan Pablo Agnelli (U Córdoba)
Melody Alsaker (Gonzaga U)
Aynur Çöl (Sinop U)
Sarah Hamilton (Marquette U)
Andreas Hauptmann (UCL)
Jennifer Mueller (CSU),
Toshiaki Yachimura (Tohoku)

We can see the difference in conductivity reflected in the VHED projections (blue and red graphs)

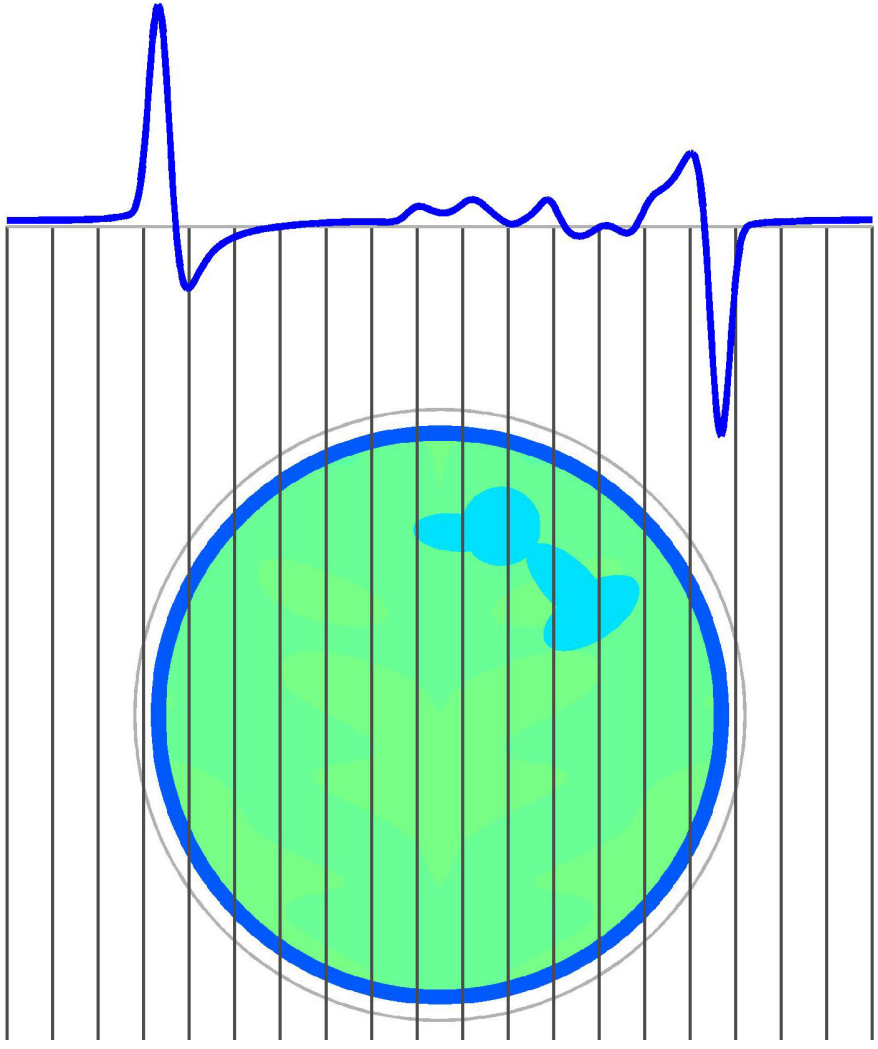

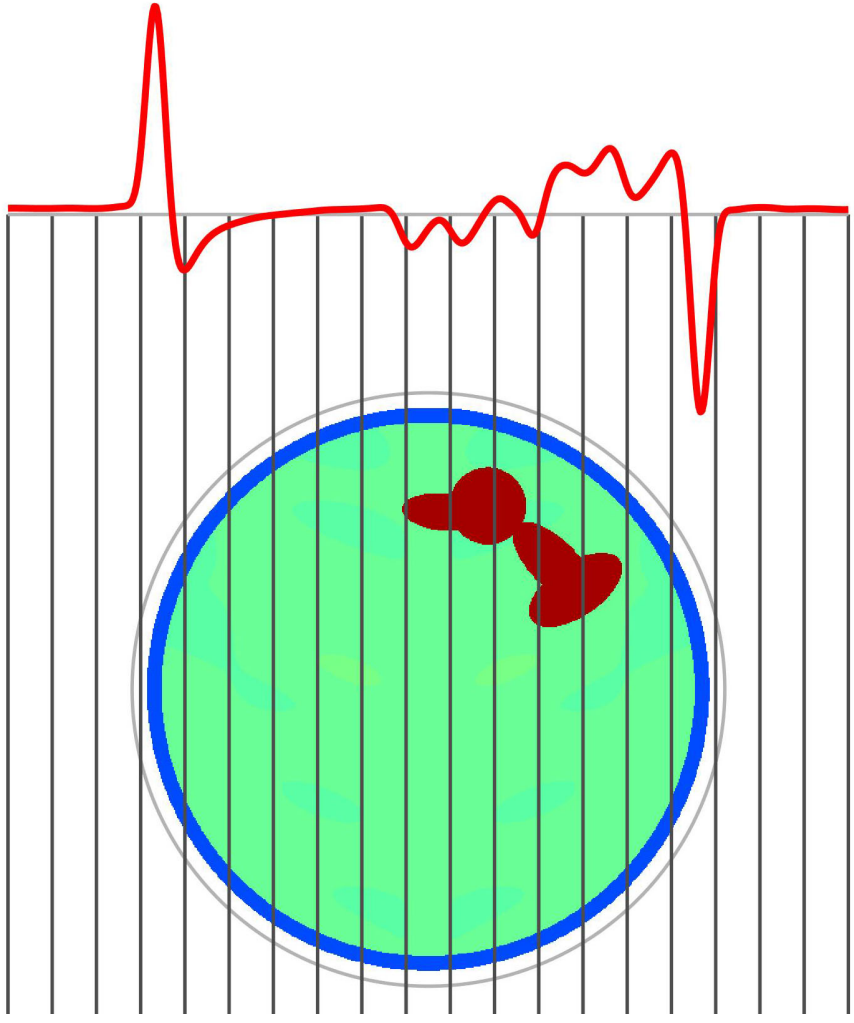

Given unrealistic-precision EIT measurements on full boundary we can classify the stroke easily

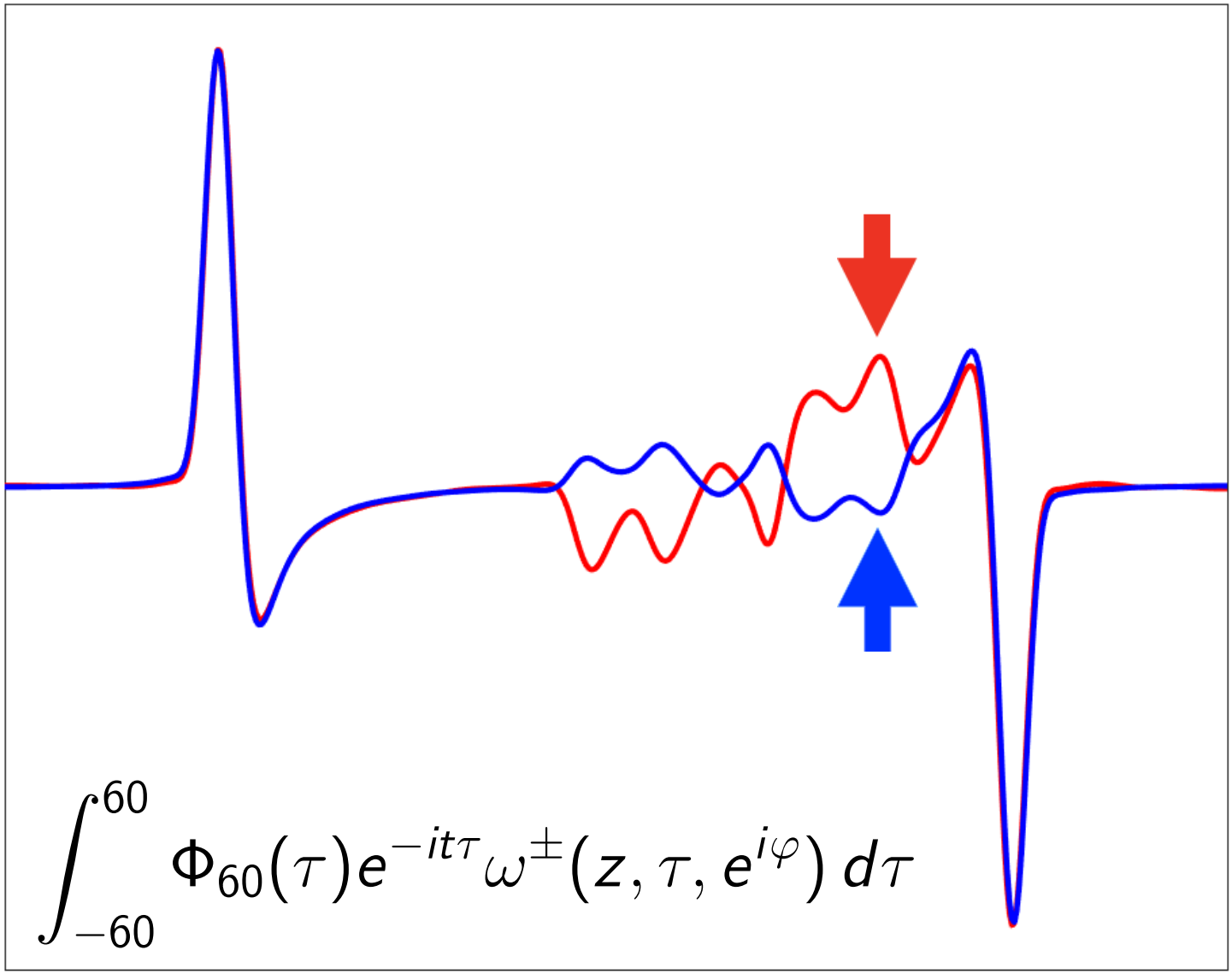

Remember the noise-induced stable and unstable parts of the nonlinear frequency domain

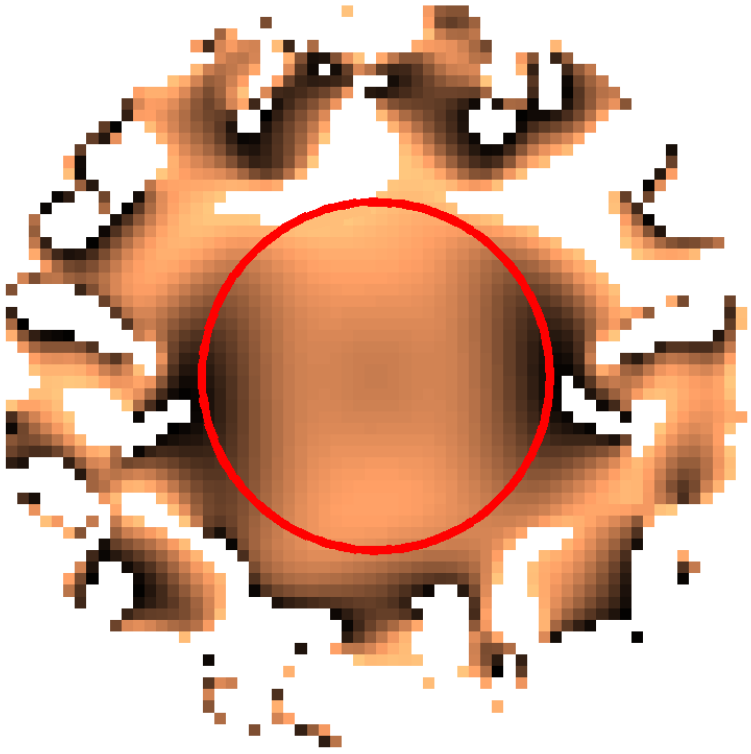

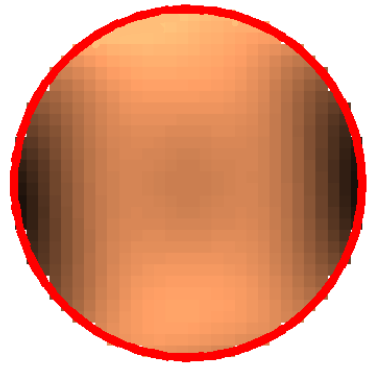

Practical EIT measurements blur the information due to heavily windowed Fourier transform

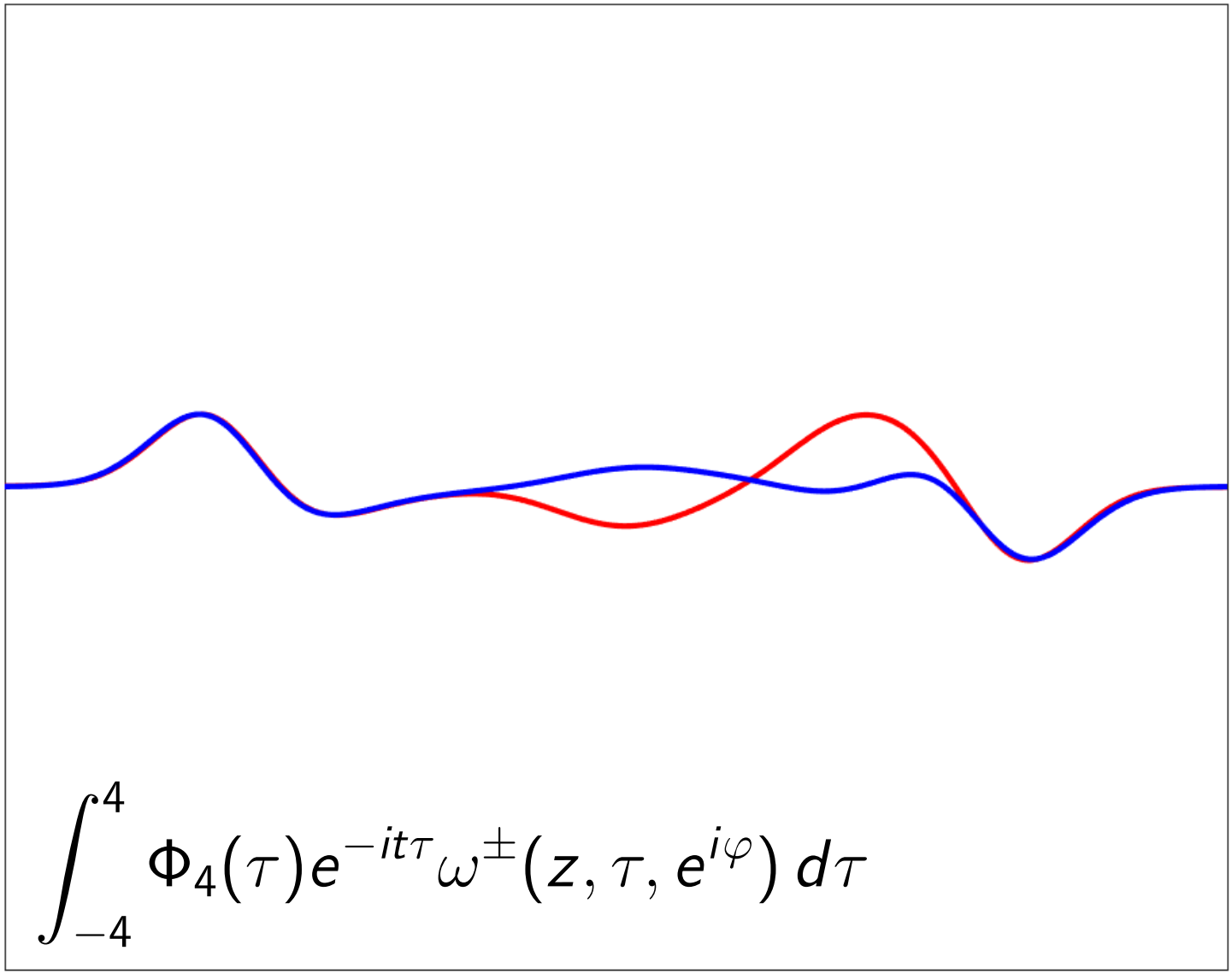

Perhaps machine learning will help us?

We simulate a set of 5000 conductivities with ischemic/hemorrhacig stroke on right hemisphere

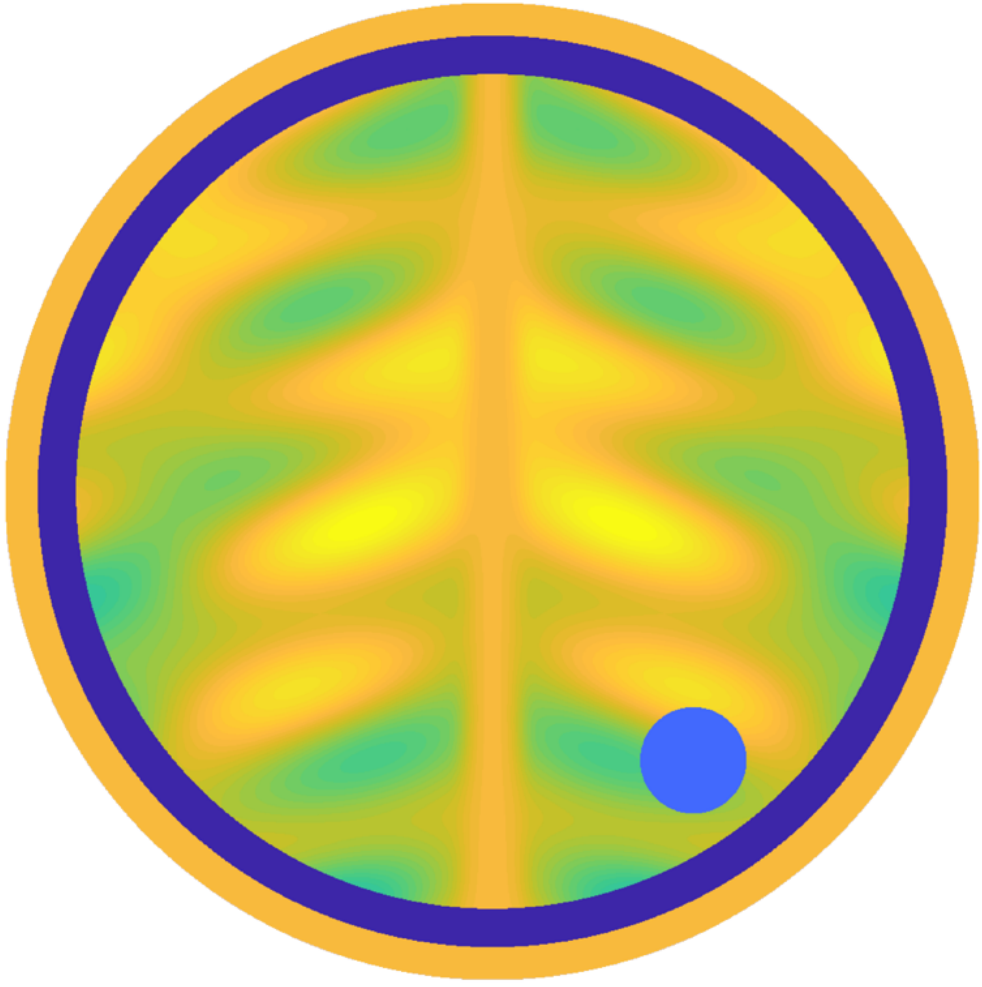

We simulate a set of 5000 conductivities with ischemic/hemorrhacig stroke on right hemisphere

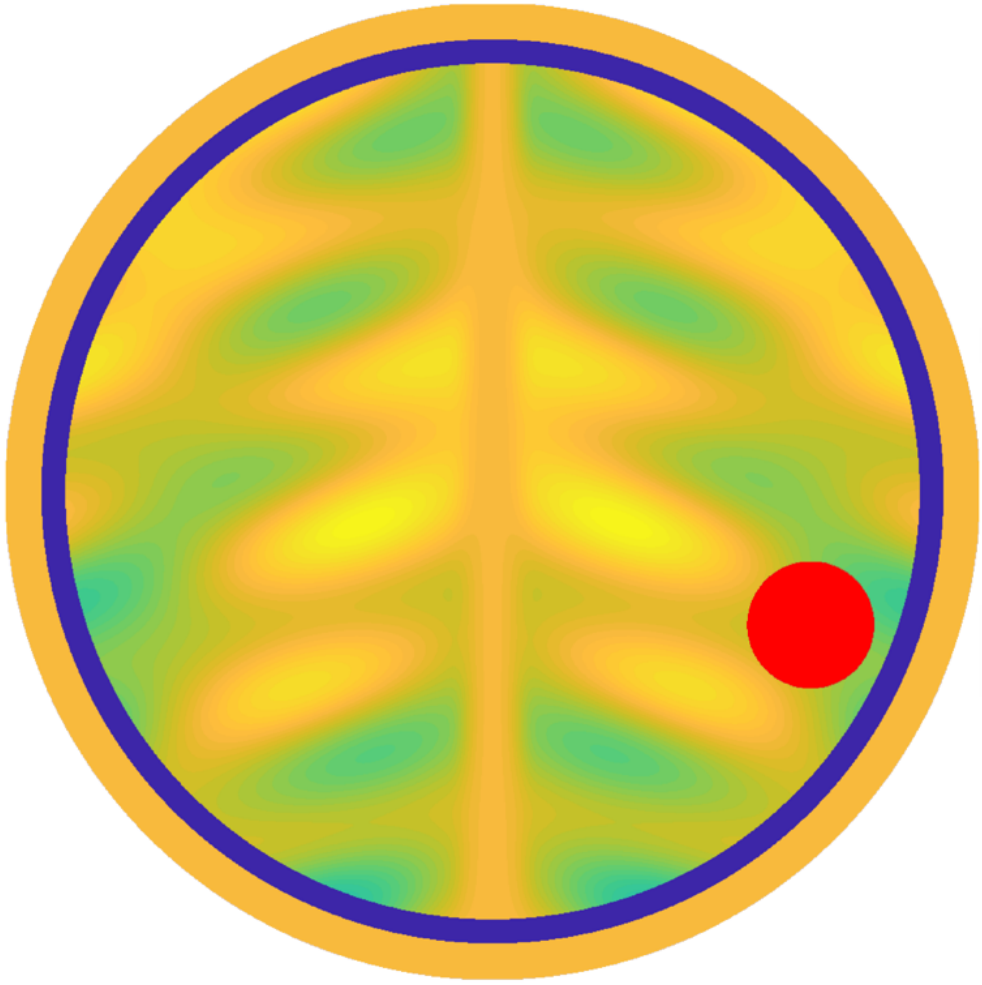

We simulate a set of 5000 conductivities with ischemic/hemorrhacig stroke on right hemisphere

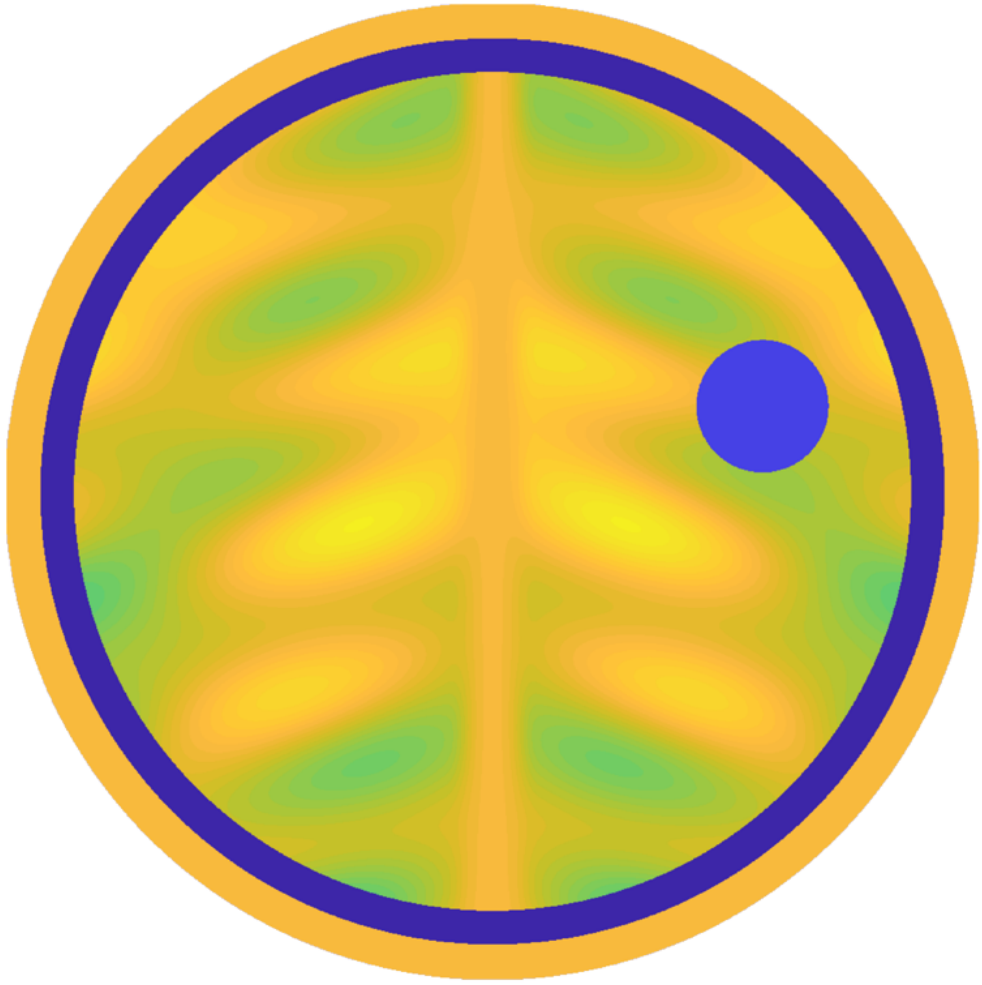

Preliminary results on using VHED as a nonlinear feature for machine learning

We trained each Fully Connected Neural Network (FCNN) using 5000 disc inclusions and then we tested each network using 3500 samples corresponding to disc inclusions not used for training.

We repeated this process 10 times and then we computed the average accuracy of each network in each data set.

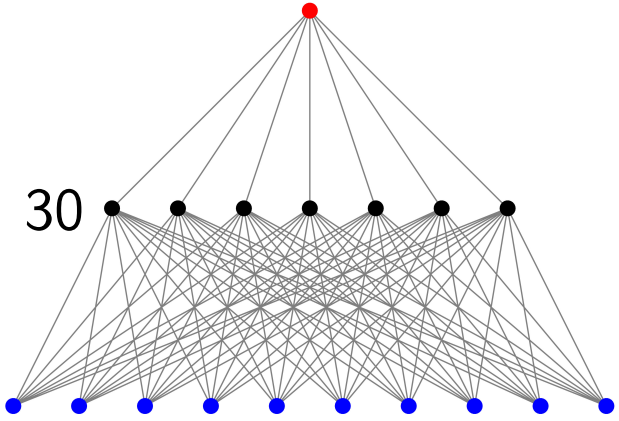

ND matrix	**0.979**
DN matrix	**0.970**
VHED	**0.997**

[Agnelli, Çöl, Murthy and Siltanen, unpublished results]

Outline

This part is a joint work with

Ryan Croke, University of Colorado—Boulder, USA

Matti Lassas, University of Helsinki, Finland

Jennifer Mueller, Colorado State University, USA

Michael Music, University of Michigan, USA

Peter Perry, University of Kentucky, USA

Andreas Stahel, BFH-TI Biel, Switzerland

Korteweg and de Vries formulated in 1895 an equation for waves in shallow water

$$u_\tau + u_{xxx} + 6uu_x = 0, \qquad x \in \mathbb{R}, \quad \tau \geq 0$$

Assumptions: wave height is small compared to the depth, which in turn is small compared to the length of the wave.

The KdV equation is a nonlinear, dispersive wave equation.

It allows solitary wave solutions observed by Russell (1845), and was studied by Boussinesq (1871) and lord Rayleigh (1876).

Gardner, Greene, Kruskal and Miura (1967) found a striking connection between the KdV equation and Schrödinger scattering

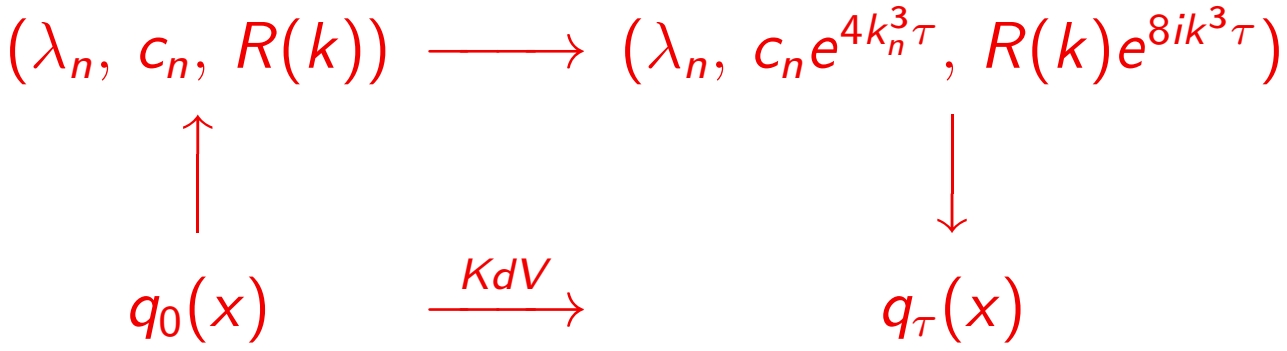

The inverse scattering step is due to

1946 Borg

1949 Levinson

1951 Gelfand-Levitan

1952 Marchenko

1953 Krein

Novikov-Veselov equation is the most natural 2D generalization of the KdV equation

Korteveg-de Vries equation, dimension (1+1):

$$\dot{q} + \frac{\partial^3 q}{\partial x^3} + 6q\frac{\partial q}{\partial x} = 0.$$

Kadomtsev-Petviashvili equation, dimension (2+1):

$$\frac{\partial}{\partial x}\left(\dot{q} + \frac{\partial^3 q}{\partial x^3} + 6q\frac{\partial q}{\partial x}\right) = \pm\frac{\partial^2 q}{\partial y^2}.$$

Novikov-Veselov equation, dimension (2+1):

$$\dot{q} + \partial_z^3 q + \overline{\partial}_z^3 q - 3\partial_z(qv) - 3\overline{\partial}_z(q\overline{v}) = 0, \qquad \overline{\partial}_z q = \partial_z v.$$

Here $z = x + iy$ and $\overline{\partial}_z = \frac{1}{2}(\frac{\partial}{\partial_x} + i\frac{\partial}{\partial_y})$.

The inverse scattering method is one way to solve the Novikov-Veselov equation

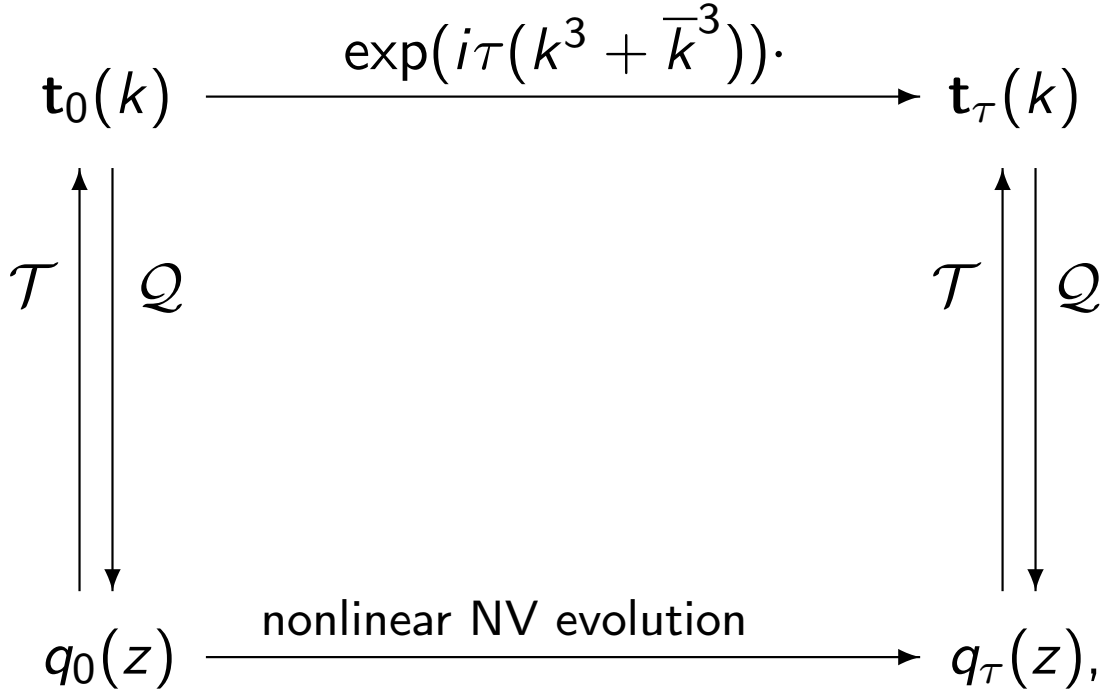

The direct and inverse nonlinear Fourier transforms $\mathcal{T}$ and $\mathcal{Q}$ are defined as follows:

The direct transform $q_\tau \mapsto \mathcal{T} q_\tau$ is given by

$$(\mathcal{T} q_\tau)(k) = \int_{\mathbb{R}^2} e^{i\overline{k}\overline{z}} q_\tau(z) \psi_\tau(z,k) dz,$$

where $(-\Delta + q_\tau)\psi_\tau(\,\cdot\,, k) = 0$ and $\psi_\tau(z,k) \sim e^{ikz}$ as $|z| \to \infty$.

The inverse transform $\mathbf{t}_\tau \mapsto \mathcal{Q}\mathbf{t}_\tau$ is given by

$$(\mathcal{Q}\mathbf{t}_\tau)(z) = \frac{i}{\pi^2} \overline{\partial}_z \int_{\mathbb{C}} \frac{\mathbf{t}_\tau(k)}{\overline{k}} e^{-ikz} \overline{\psi_\tau(z,k)} dk,$$

where $\psi_\tau(z,k) = e^{ikz}\mu_\tau(z,k)$ and μ_τ satisfies the D-bar equation

$$\frac{\partial}{\partial \overline{k}} \mu_\tau(z,k) = \frac{\mathbf{t}_\tau(k)}{4\pi\overline{k}} e^{-i(kz+\overline{k}\overline{z})} \overline{\mu_\tau(z,k)}, \qquad \mu_\tau(z,\,\cdot\,) \sim 1.$$

Zero-energy inverse scattering & NV equation

1984 **Novikov & Veselov**: Periodic case.

1987 **Boiti, Leon, Manna & Pempinelli**: Formal non-periodic analysis assuming no exceptional points.

1993 **Tsai**: Formal analysis assuming no exceptional points.

1996 **Nachman**: Conductivity-type q_0 have no exceptional points.

2007 **Lassas, Mueller & S**: Inverse scattering evolution q_τ^{IS} well-defined for conductivity-type initial data q_0.

2012 **Lassas, Mueller, S & Stahel**: Evolution q_τ^{IS} preserves conductivity-type, numerical evidence for $q_\tau^{\mathsf{IS}} = q_\tau^{\mathsf{NV}}$.

2012 **Perry**: $q_\tau^{\mathsf{IS}} = q_\tau^{\mathsf{NV}}$ holds for conductivity-type q_0.

2013 **Music, Perry & S**: Supercritical exceptional points exist.

2014 **Music**: Subcritical q_0 have no exceptional points.

2015 **Croke, Mueller, Music, Perry, S & Stahel**: Review of NV eq.

2015 **Music & Perry**: Global existence for critical and subcritical q_0.

2016 **Angelopoulos**: Local well-posedness of NV equation.

Let's look at an example. Here is a smooth and rotationally symmetric conductivity function $\sigma(z)$

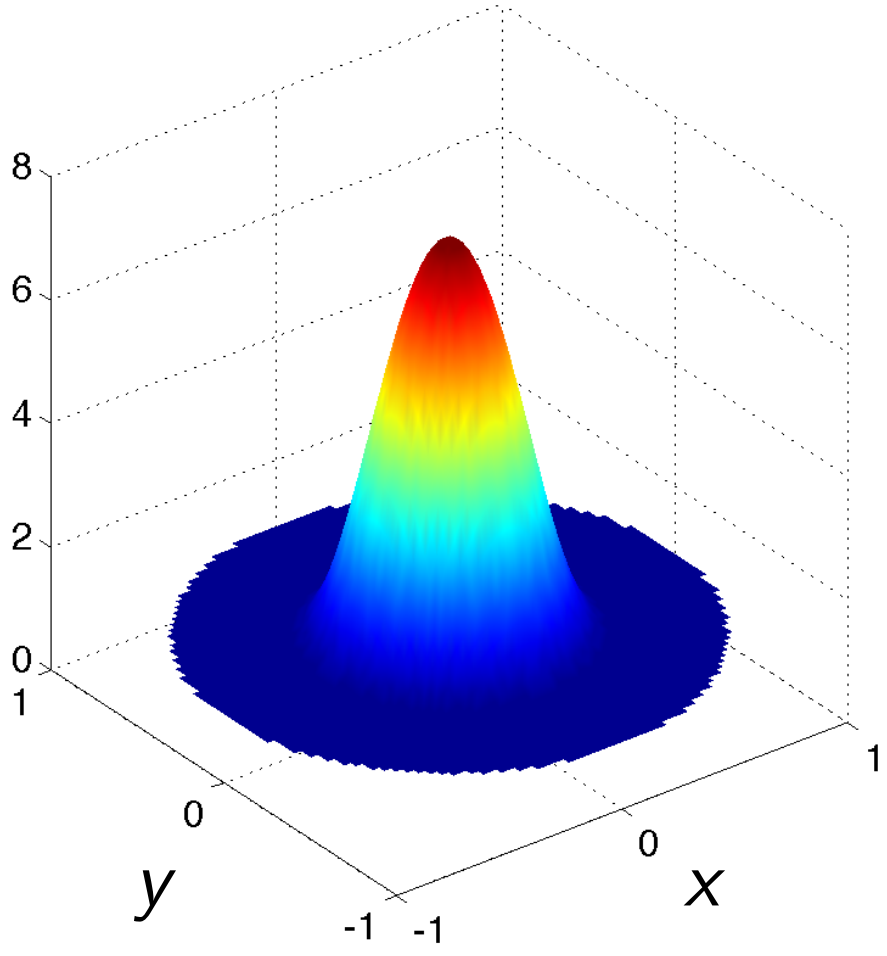

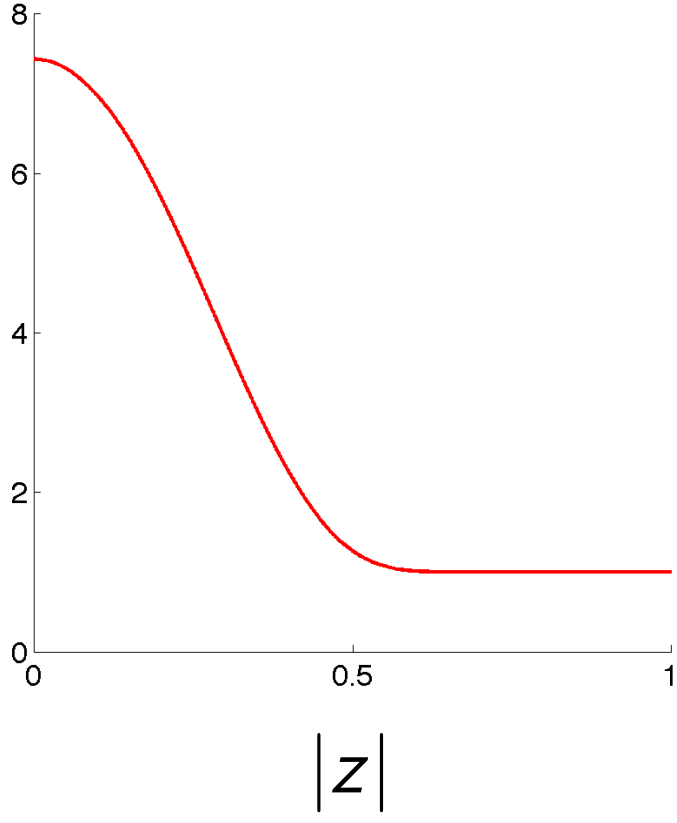

This is the initial potential $q_0(z) = \sigma^{-1/2}(z)\Delta\sigma^{1/2}(z)$

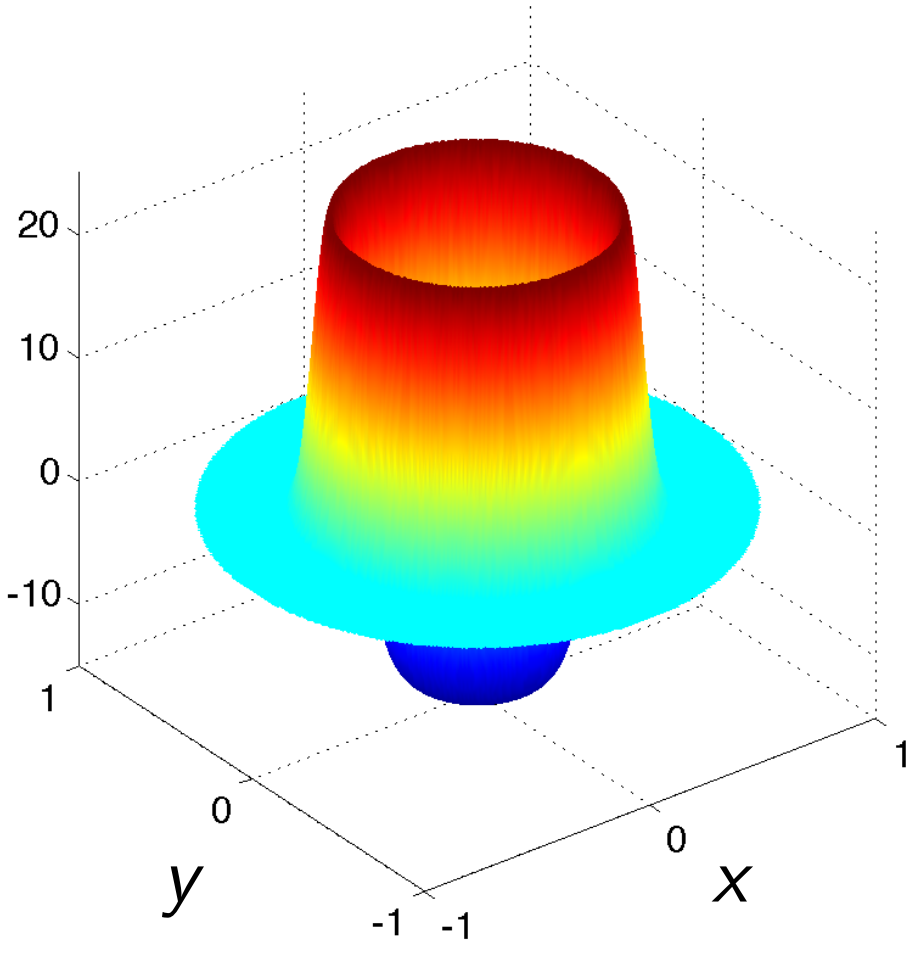

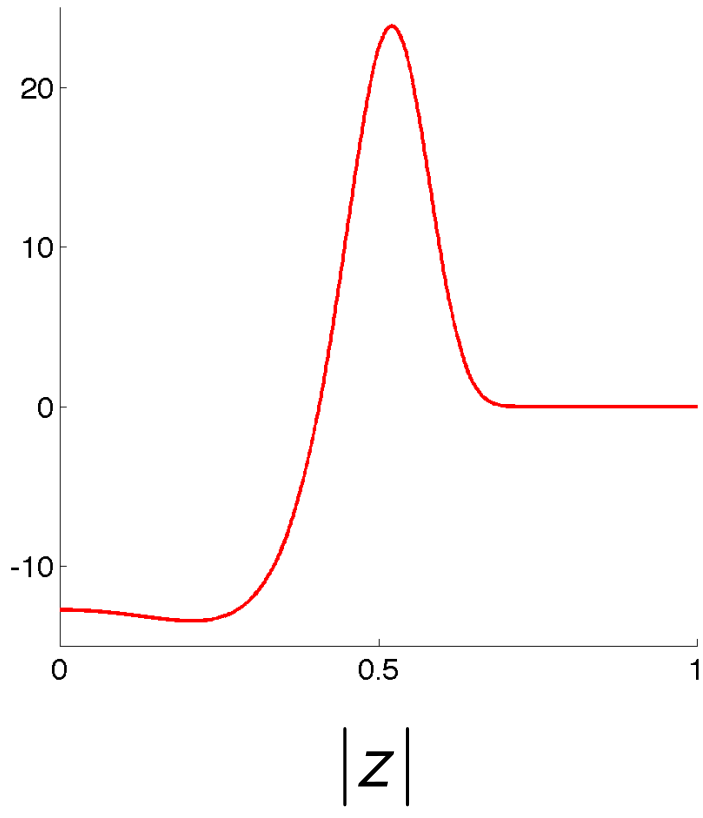

This is the initial scattering transform $\mathbf{t}_0(k)$

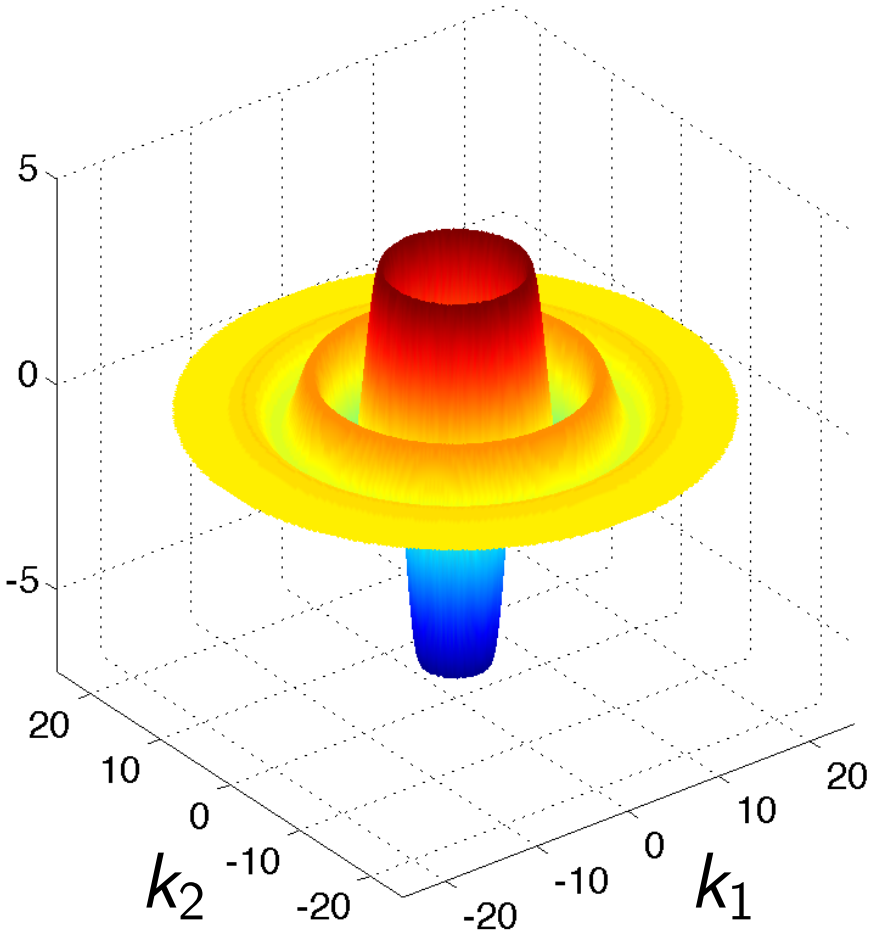

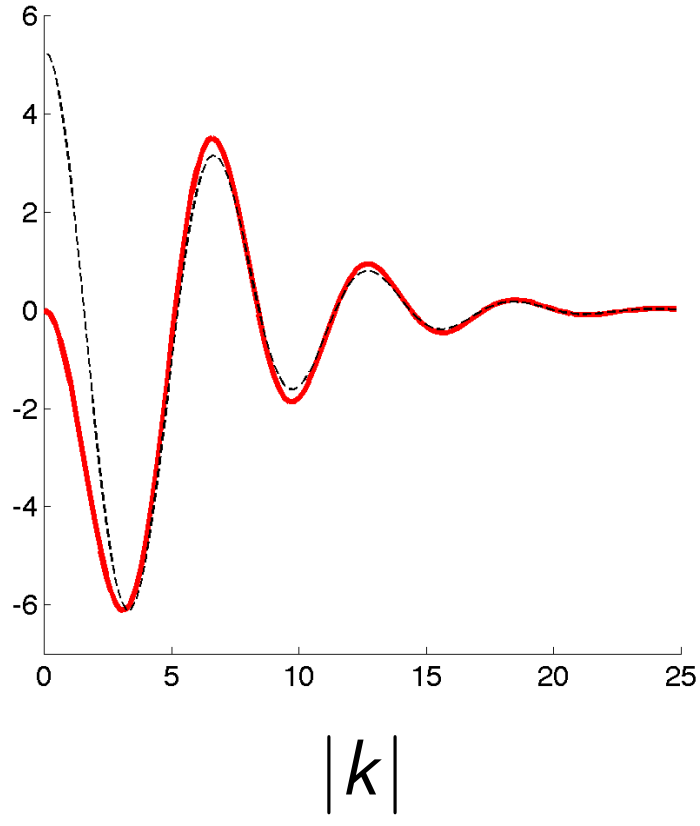

This is the Novikov-Veselov evolution

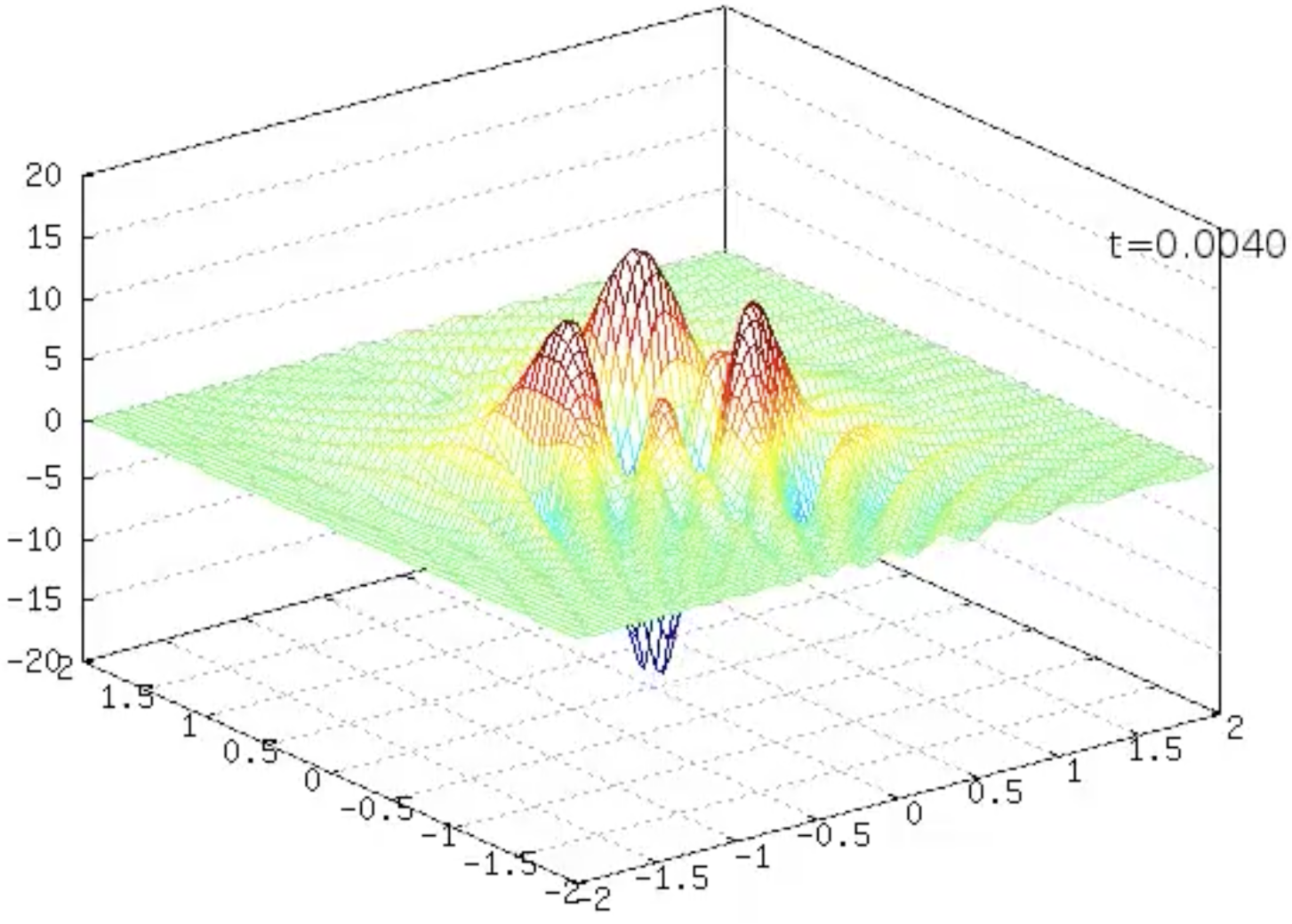

Dynamics of NV solutions for $\lambda > 0$ (A. Stahel); no apparent singularities

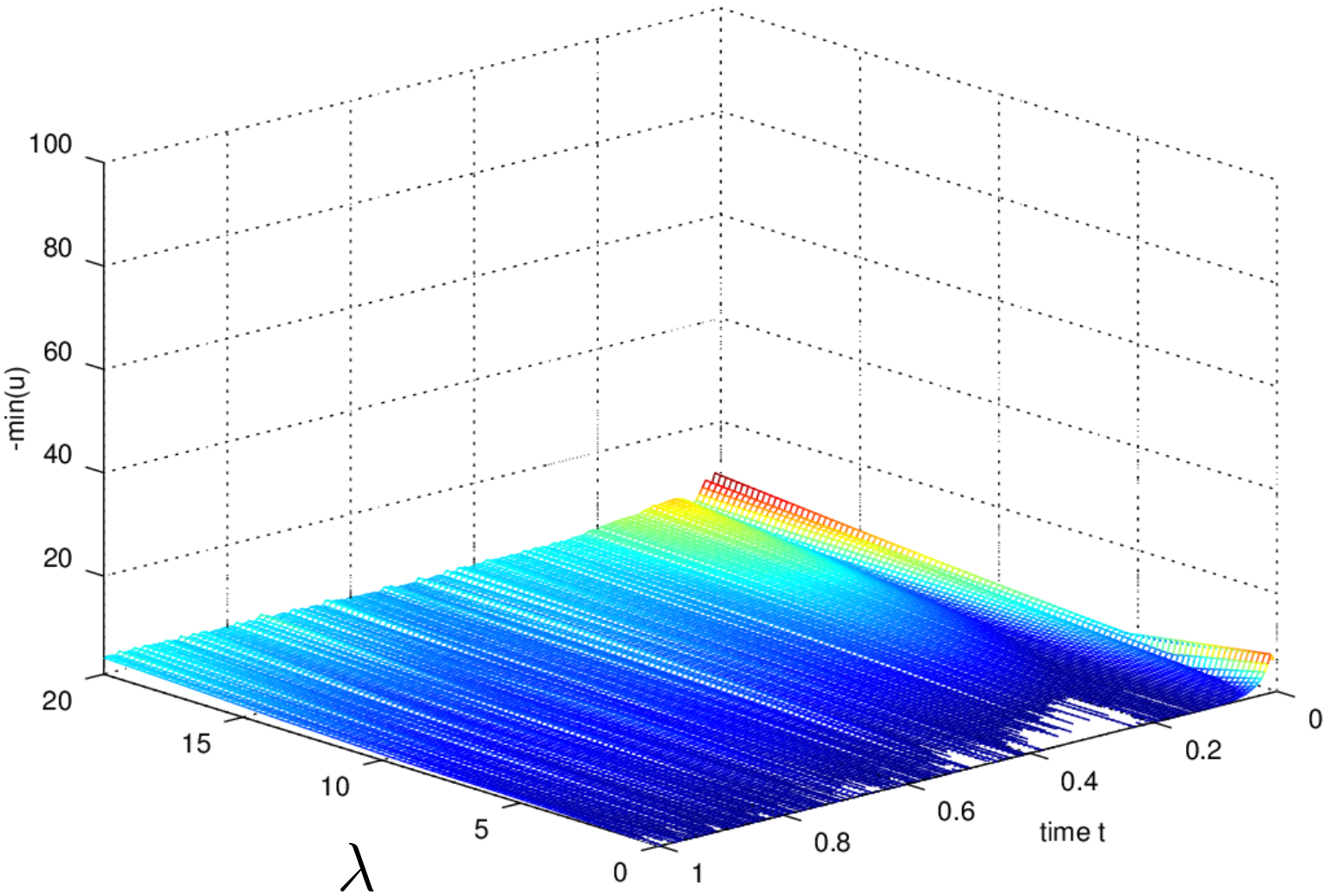

This is in accordance with [Music and Perry 2015]

Dynamics of NV solutions for $\lambda < 0$ (A. Stahel), seemingly with blowup in finite time

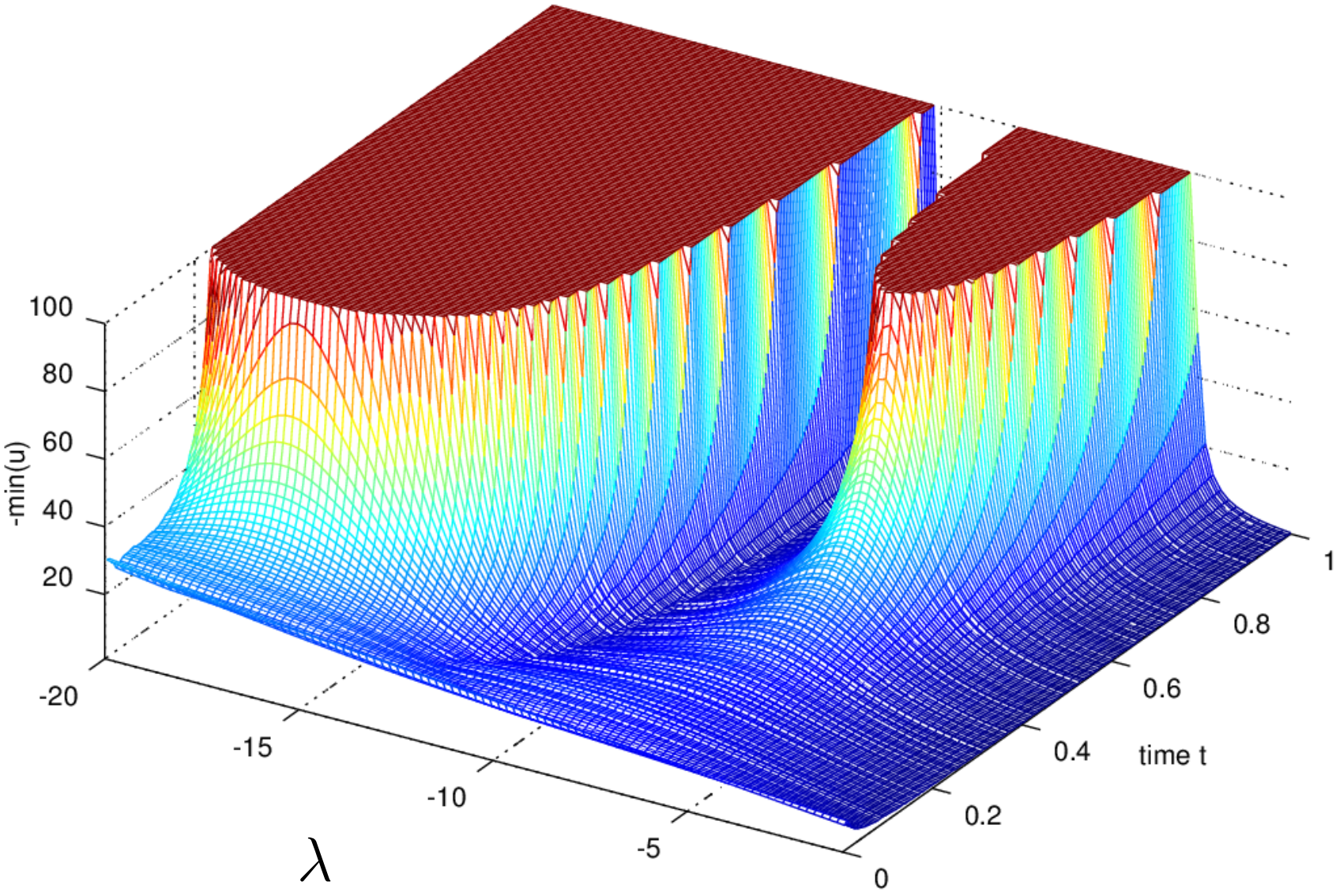

Outline

EIT is the zero-energy CGO case; positive and negative energies have applications as well

1986, 1988, 1992, 1999 R. G. Novikov

1988 Nachman

2013 R. G. Novikov and Santacesaria

2013 Santacesaria

2016 Kazeykina and Munõz

Computational studies:

2016 Tamminen, Tarvainen and S:
Negative-energy D-bar method for diffuse optical tomography

2016 de Hoop, Lassas, Santacesaria, S and Tamminen:
Positive-energy D-bar method for acoustic tomography

Challenges for young mathematicians

Nonlinear Fourier transforms hold enormous promise for many practical applications. There is a lot of delightfully nonlinear research work to be done both in the theoretical and computational aspects.

Exceptional points for potentials seem to correspond to finite-time blowup for Novikov-Veselov evolutions. There is yet no theoretical understanding of this.

Links to open computational resources

Open EIT datasets:

- Finnish Inverse Problems Society (FIPS) dataset page

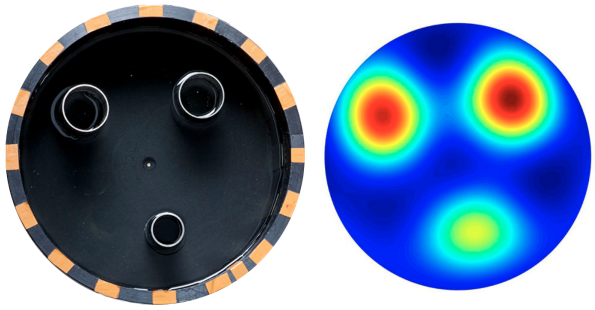

Reconstruction algorithms: FIPS Computational Blog

- The D-bar Method for EIT—Simulated Data
- The D-bar Method for EIT—Experimental Data

For these slides see: http://www.siltanen-research.net/talks.html


Thank you for your attention!

Negative-energy NV by Kazeykina and Klein 2017

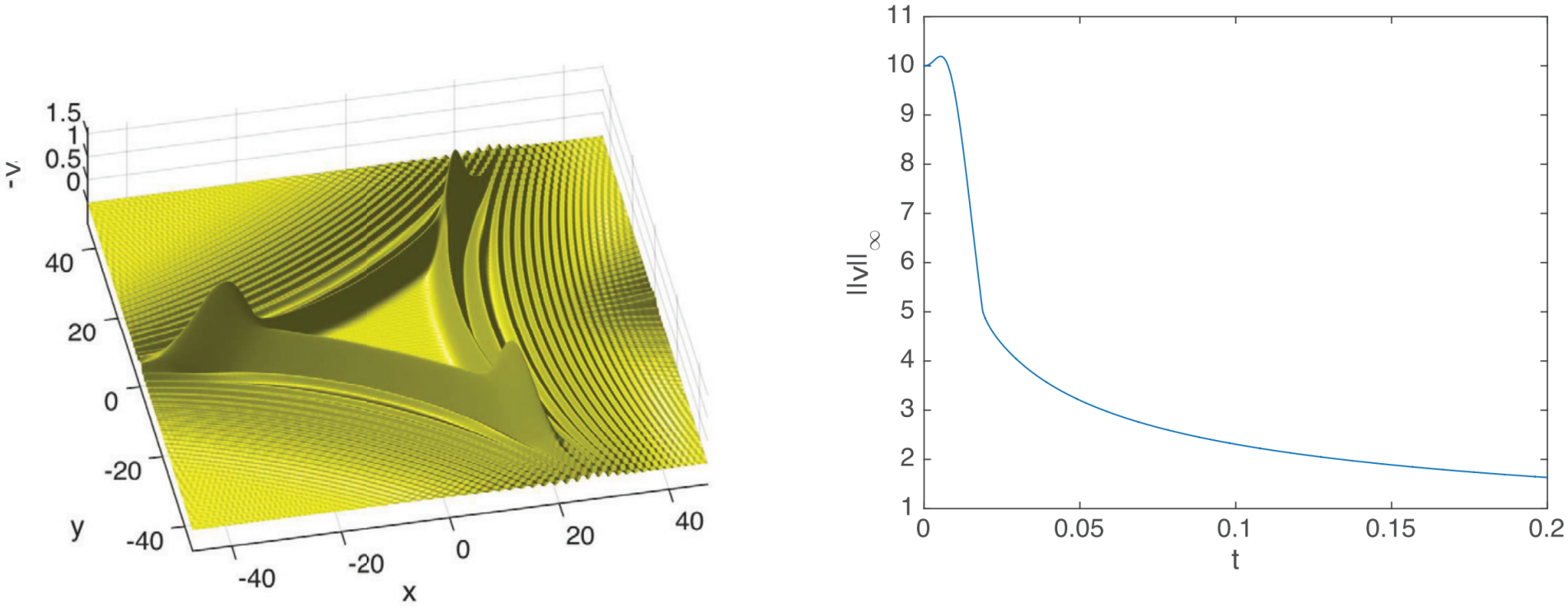

Figure 16. Solution of the NV equation (1a) with $E = -10$ for the initial data (41) and $\beta = -10$; on the left the solution for $t = 0.2$, on the right the L^∞ norm of the solution in dependence of time.

Initial data $v(x, y, 0) = \beta \exp(-x^2 - y^2)$